On the anatomy of nearshore sandbars

A systematic exposition of inter-annual sandbar dynamics

Walstra, Dirkjan

DOI
10.4233/uuid:3f86bf04-c6af-486f-b972-bd228d84ebed

Publication date
2016

Document Version
Final published version

Citation (APA)
Walstra, D. (2016). *On the anatomy of nearshore sandbars: A systematic exposition of inter-annual sandbar dynamics*. [Dissertation (TU Delft), Delft University of Technology]. https://doi.org/10.4233/uuid:3f86bf04-c6af-486f-b972-bd228d84ebed

On the anatomy of nearshore sandbars

On the anatomy of nearshore sandbars

A systematic exposition of inter-annual sandbar dynamics

DISSERTATION

for the purpose of obtaining the degree of doctor
at Delft University of Technology
by the authority of the Rector Magnificus Prof. Ir. K.Ch.A.M. Luyben;
Chair of the Board for Doctorates
to be defended publicly on

Friday 17 June 2016 at 15:00 hours

by

Dirk Jan Roelof WALSTRA

Civil Engineer, Delft University of Technology
born in Sneek

This dissertation has been approved by the promotors:
Prof. dr. ir. M.J.F. Stive and Prof. dr. B.G. Ruessink

Composition of the doctoral committee:

Rector Magnificus	chairperson
Prof. dr. ir. M.J.F. Stive	Promotor, Delft University of Technology
Prof. dr. B.G. Ruessink	Promotor, Utrecht University
Prof. dr. ir. A.J.H.M. Reniers	Delft University of Technology
Independent members:	
Prof. dr. ir. Z.B. Wang	Delft University of Technology
Prof. dr. ir. L.C. van Rijn	Independent Researcher
Dr. P. Ruggiero	Oregon State University, USA
Prof. dr. H. Hanson	Lund University, Sweden
Prof. dr. ir. A.W. Heemink	Delft University of Technology, reserve member

Cover: time stack of the 10 year simulation of the Noordwijk profile subjected to the Egmond wave climate (Scenario NE in Chapter 4 of this thesis)

ISBN 978-94-6186-647-9

Printed by Gildeprint – The Netherlands

An electronic version of this thesis is available at
https://repository.tudelft.nl

Contents

Abstract

Nearshore sandbars have a lifetime of many years, during which they exhibit cyclic, offshore directed behaviour with strong alongshore coherence. A bar is generated near the shoreline and grows in height and width while migrating offshore, before finally decaying at the seaward limit of the surf zone. It may take 10 to 15 years for a bar to exhibit this cycle. Four to five bars may occur simultaneously within a cross-shore bed profile. Alongshore variations in cross-shore bar position and bar amplitude are commonly observed. A strong or abrupt alongshore variability is referred to as a bar switch. At large spatial scales, the inter-annual bar dynamics may vary considerably across sites with very similar environmental settings. In particular, the bar cycle return period (T_r, i.e. the duration between two successive bar decay events) may differ by a factor of three to four. This type of change in T_r appears to be always present in time and is characterized as a persistent bar switch. At smaller (kilometer) scales, bar switches typically occur in areas with similar T_r-values on both sides of a bar switch and occasionally disappear when the bars re-attach. These are characterized as non-persistent bar switches.

The assimilation of shoreface nourishments into the coastal system involves a strong interaction with the pre-existing sandbar system. Typically the placement of a shoreface nourishment just seaward of an outer bar reverses the bar cycle temporalily, inducing a landward migration of the bar system. The shoreface nourishment becomes absorbed in the coastal system as the new outer bar. At the distal ends of the shoreface nourishment bar switches often manifest, owing to a distinct difference in the bar migration cycle phase that is induced. Given the importance of the bar-nourishment interaction, an improved understanding of the nearshore bar dynamics is expected to improve the efficacy of shoreface nourishments. Furthermore, the long-term evolution of the nearshore barred profiles is generally considered indicative of the quality of the modelling for the response of the entire nearshore coastal system. Therefore, the ability to perform reliable and robust a-priori, long-term predictions has broad societal relevance in view of anticipated adverse impacts of climate change and sea level rise on the stability of coasts worldwide. Until now the anatomy of the nearshore sandbars has primarily been studied using field data. Although these studies have provided insight into how the geometric bar parameters respond to the external forcings, no comprehensive conceptual framework is available that explains the full life cycle of a sandbar and its associated characteristics. The overarching objective of this study is to

elucidate the anatomy of the inter-annual bar morphology using a combined data and model approach. This overarching objective is in turn devolved into three objectives aiming to understand key features of bar morphology and a further objective to enable a comprehensive modelling approach based on the acquired insights. The latter objective involves the development of an input-reduction framework for advanced process-based forward modelling of the inter-annual bar morphology.

1) To elucidate the morphodynamic processes that result in cross-shore transient sandbar amplitude responses (i.e. the transition from bar growth in the intertidal and across surf zone to sandbar decay at the seaward edge of the surf zone).
2) To establish the role of cross-shore processes in non-persistent bar switches.
3) To identify the dominant environmental variables and the associated mechanisms that govern the bar cycle return period.
4) To develop an input-reduction framework to enable the application of state-of-the-art process based forward area models to simulate the multi-annual bar behaviour and nearshore morphology.

A comprehensive study approach is adopted in which observations of the nearshore morphology are combined with detailed forward modeling of the bar dynamics at Noordwijk (The Netherlands) utilizing wave and waterlevel observations as boundary conditions. The Noordwijk model acts as a reference for additional simulations at Egmond (The Netherland) and at Hasaki (Japan) to address the specific characteristics of the nearshore sandbar morphodynamics as outlined above.

The transient cross-shore bar amplitude response

Based on a three-year hindcast of a bar cycle at Noordwijk (Netherlands) and on additional synthetic runs using a wave-averaged cross-shore process model, the dominant mechanisms that govern the bar amplitude growth and decay during net inter-annual offshore migration are identified. The bar amplitude response is particularly sensitive to the water depth above the bar crest, h_{Xb}, and the angle of wave incidence, θ. These variables largely control the amount of waves breaking on the bar and the strength and cross-shore distribution of the associated longshore current. The longshore current has its maximum landward of the bar crest, inducing additional stirring of sediment on the landward bar slope and trough. The enhanced sediment concentration in the trough region shifts the cross-shore transport peak landward of the bar crest, forcing bar amplitude growth during offshore migration. For increased h_{Xb}-values wave breaking becomes less frequent, reducing the influence of the longshore current on sediment stirring. Therefore, the resulting dominance of the cross-shore current results in a sediment transport peak at, or just seaward of, the bar crest causing bar amplitude decay. All four types of bar response (viz. all combinations of

onshore/offshore migration and bar amplitude growth/decay) can occur for a single wave height and wave period combination, depending on h_{Xb} and θ. Additional hindcast runs in which the wave direction was assumed time-invariant confirmed that h_{Xb} and θ largely control the transient bar amplitude response.

The mechanics of non-persistent bar switches
Intra-site alongshore variability is greatest when bars display km-scale disruptions, indicative of a distinct alongshore phase shift in the bar cycle. An outer bar is then, for example, attached to an inner bar, referred to as a non-persistent bar switch. This large-scale alongshore variability is investigated by applying the reference model at 24 transects along a 6 km section of the barred beach at Noordwijk (The Netherlands). When alongshore variability is limited, the model predicts that the bars migrate offshore at approximately the same rate (i.e. the bars remain in phase). Only under specific bar configurations with high wave-energy levels is an increase in the alongshore variability predicted. This suggests that cross-shore processes may trigger a switch in the case of specific antecedent morphological configurations combined with storm conditions. It is expected that three-dimensional (3D) flow patterns augment the alongshore variability in such instances. In contrast to the observed bar behaviour, predicted bar morphologies on either side of a switch remain in different phases, even though the bars are occasionally located at a similar cross-shore position. In short, the 1D profile model is not able to remove a bar switch. This data-model mismatch suggests that 3D flow patterns are key to the dissipation of bar switches.

The mechanics of persistent bar switches and the bar cycle return period
To date, data-analytic studies have had only partial success in explaining differences in T_r, establishing at best weak correlations to local environmental characteristics. In the present approach the process-based profile reference model is utilized to investigate the non-linear interactions between the hydrodynamic forcing and the morphodynamic profile response for two sites. Despite strong similarity in environmental conditions, the sites at Noordwijk and Egmond on the Holland coast exhibit distinctly different T_r values. The detailed comparison of modelling results enables a consistent investigation of the role of specific parameters at a level of detail that could not have been achieved from observations alone, and provides insights into the mechanisms that govern T_r. The results reveal that the bed slope at the barred zone is the most important parameter governing T_r. As a bar migrates further offshore, a steeper slope results in a stronger relative increase in h_{Xb} which reduces wave breaking and in turn reduces the offshore migration rate. The deceleration of the offshore migration rate as the bar moves to deeper water - the morphodynamic feedback loop - contrasts with the initial enhanced offshore migration behaviour of the bar. The initial behaviour is determined by the intense wave breaking associated with the steeper profile slope. These mechanisms explain the counter-intuitive observations at Egmond where T_r is significantly longer

than at Noordwijk despite Egmond having the more energetic wave climate which typically reduces T_r.

Input reduction for inter-annual advanced forward model applications
In order to avoid excessively long computation times, input reduction is imperative for the application of advanced forward morphodynamic area models to consider long-term (>years) predictions. Here, an input reduction framework for wave-dominated coastal settings is introduced. The framework comprises 4 steps, viz. (1) the selection of the duration of the original (full) time series of wave forcing, (2) the selection of the representative wave conditions, (3) the sequencing of these conditions, and (4) the time span after which the sequence is repeated. In step (2), the chronology of the original series is retained, while that is no longer the case in steps (3) and (4). We apply the framework to two different sites (Noordwijk, The Netherlands and Hasaki, Japan) with multiple nearshore sandbars but contrasting long-term offshore-directed behaviour: at Noordwijk the offshore migration is gradual and not coupled to individual storms, while at Hasaki the offshore migration is more episodic, and wave chronology appears to control the long-term evolution. The performance of the model with reduced wave climates is compared with a simulation with the actual (full) wave-forcing series. It is demonstrated that input reduction can dramatically affect long-term predictions, to such an extent that the main characteristics of the offshore bar cycle are no longer reproduced. This was the case at Hasaki, in particular, where all synthetic series that no longer retain the initial chronology (steps 3 and 4) lead to rather unrealistic long-term simulations. At Noordwijk, synthetic series can result in realistic behaviour, provided that the time span after which the sequence is repeated is not too large; the reduction of this time span has the same positive effect on the simulation as increasing the number of selected conditions in step 2. It is further demonstrated that, although storms result in the largest morphological change, conditions with low to intermediate wave energy must be retained to obtain realistic long-term sandbar behaviour. The input-reduction framework must be applied in an iterative fashion to obtain a reduced wave climate that is able to simulate long-term sandbar behaviour sufficiently accurately within an acceptable computation time. These results imply that it is essential to consider input reduction as an intrinsic part of any model set-up, calibration and validation effort.

The study outcomes indicate clearly that a relatively simple model can be utilized to study the highly non-linear interaction between the nearshore hydrodynamics and morphology in great detail. This was achieved through carefully designed numerical experiments in which the influence of a specific process or environmental variable was isolated and identified. Although the model only considers cross-shore processes, the numerical experiments generated new insights into the importance of 3D processes under particular morphological conditions of the nearshore barred profiles. Even though the model was successfully calibrated at Noordwijk, the application at Egmond

showed a significantly reduced predictive capacity. The model was able to reproduce the main characteristics of the inter-annual bar morphodynamics, but the bar cycle return period was under-estimated by about 30%. This suggests that the model can capture trends fairly well, but is unable to produce accurate absolute predictions - a finding that has broader implications. As stated earlier, accurate predictions of the long-term evolution of the nearshore barred profiles are generally considered indicative of the quality of the modelling of the entire nearshore coastal system. Consequently, further improvement of morphodynamic process-based models, particularly for the nearshore zone, constitutes a major research priority.

Samenvatting

Zandbanken in de brandingszone hebben in het algemeen een meerjarige levensduur. Ze vertonen een cyclisch zeewaarts gerichte migratie en hebben meestal een aanzienlijke kustlangse coherentie. Over het algemeen worden banken gegenereerd rond de waterlijn en groeien geleidelijk terwijl ze zeewaarts migreren. Rond de zeewaartse grens van de brandingszone neemt de migratiesnelheid geleidelijk af tot nul en slaat de bankgroei om in een afname waarna de bank geleidelijk verdwijnt. Het doorlopen van de gehele cyclus kan wel 10 tot 15 jaar duren. In een dwarsprofiel kunnen maximaal vier tot vijf banken tegelijkertijd voorkomen. Alhoewel banken over een aantal kilometers een coherent kustlangs gedrag kunnen vertonen, treden er regelmatig ook aanzienlijke kustlangse variaties op. Dit fenomeen, waarbij in zijn meest extreme vorm banken kustlangs volledig zijn losgekoppeld, wordt een bankovergang genoemd. Op grotere kustlangse schalen kan het meerjarige bankgedrag ook aanzienlijk variëren terwijl er op het eerste gezicht geen in het oog springende verschillen in de omgevingscondities zijn. Vooral de bank cyclus periode (T_r), gedefinieerd als de tijd tussen twee opeenvolgende bankverval momenten, kan met wel een factor drie tot vier verschillen. Dit type grootschalige langsvariatie in bankgedrag wordt een persistente bankovergang genoemd omdat de locatie over het algemeen vastligt en ze continu aanwezig zijn. De eerder genoemde bankovergangen, voorkomend in gebieden met dezelfde T_r, kunnen kustlangs over meer dan 100 m migreren en verdwijnen als banken aan weerszijden van een overgang in dezelfde fase zitten worden daarom niet-persistente bankovergangen genoemd.

Op basis van observaties is vastgesteld dat de opname van een onderwater-suppletie in het kustsysteem gepaard gaat met een sterke interactie met het al aanwezige bankensysteem. De plaatsing van een onderwatersuppletie is meestal net zeewaarts van de buitenste bank wat resulteert in een omkering van de bankcyclus welke tot uiting komt in een tijdelijke netto landwaartse migratie van de banken. Het resultaat van deze response is dat de onderwatersuppletie de plaats van de oorspronkelijke buitenste bank na ongeveer 6-12 maanden na de aanleg heeft ingenomen. Vervolgens hervat de natuurlijke cyclus zich en zal de onderwatersuppletie geleidelijk verdwijnen terwijl de landwaartse banken netto weer zeewaarts migreren. Aan de kustlangse uiteinden van een suppletie komen vaak niet-persistente bankovergangen voor vanwege het faseverschil in de bankcyclus tussen het gesuppleerde en de aanliggende kustvakken. Gezien de sterke bank-suppletie interactie is het de verwachting dat de werkzaamheid

van onderwatersuppleties kan profiteren van een verbeterd begrip van het meerjarige bankgedrag.

Behalve het belang voor onderwatersuppleties wordt de lange-termijn ontwikkeling van de bankprofielen over het algemeen ook gezien als een indicatie van de kwaliteit van modelvoorspellingen voor de gehele kustnabije zone. Vandaar dat nauwkeurige en robuuste lange-termijn voorspellingen een brede maatschappelijke relevantie hebben. Temeer, gezien de verwachte negatieve invloed van klimaatverandering en zeespiegelstijging op de stabiliteit en weerbaarheid van kusten wereldwijd. Tot nu toe is de bankmorfologie en de onderliggende processen vooral onderzocht op basis van observaties in het veld. Hoewel deze studies een waardevolle bijdrage hebben geleverd aan het huidige inzicht hoe bepaalde geometrische bankkarakteristieken beïnvloedt worden door de externe forcering, is er geen alomvattend conceptueel kader welke de volledige levenscyclus van een bank en de bijbehorende karakteristieken beschrijft. Vandaar dat het overkoepelende doel van dit onderzoek is om de anatomie en werking van het langjarig bankgedrag te doorgronden. Dit doel is opgesplitst in drie doelstellingen gericht op het begrijpen van specifieke onderdelen van het bankgedrag en een doelstelling om geavanceerde lange-termijn modellering mogelijk te maken. De laatste doelstelling wordt bereikt door het ontwikkelen van een invoer-reductie kader wat de toepassing van proces gebaseerde gebiedsmodellen in de kustnabije zone mogelijk maakt. De doelstellingen worden hieronder samengevat en vervolgens successievelijk verder uitgewerkt.

1) Begrijpen waarom de kustdwars veranderende bank amplitude response optreedt (i.e. de overgang van bankgroei nabij de waterlijn en brandingszone naar bank verval aan de zeewaartse grens van de brandingszone).
2) Vaststellen welke rol kustdwarse processen spelen bij het ontstaan en verdwijnen van de kustlangse variabiliteit in bankpositie en amplitude aan weerszijden van niet-persistente bankovergangen.
3) Het identificeren van de belangrijkste omgevingsfactoren en de onderliggende fysische processen welke de kustlangse variabiliteit in de bank cyclus periode (T_r), behorende bij persistente bankovergangen, veroorzaken.
4) Het ontwikkelen van een generiek invoer-reductie kader wat de lange termijn modellering van het meerjarig bankgedrag en de kustnabije zone mogelijk maakt.

Om de bovenstaande doelstellingen te adresseren is een uitgebreide aanpak opgezet waarin observaties van de kustzone morfologie gecombineerd worden met gedetailleerde voorwaartse modellering van het temporele bankgedrag bij Noordwijk (Nederland) op basis van gemeten golfcondities en waterstanden. Het model voor Noordwijk dient als referentie voor vergelijkbare modellen bij Egmond (Nederland) en

Hasaki (Japan) waarmee specifieke aspecten van het bankgedrag onderzocht en verklaard worden.

De kustdwars veranderende bank amplitude response
Op basis van een voorspelling van een geobserveerde bank cyclus en synthetische simulaties met een golf-gemiddeld kustdwars proces-gebaseerd model worden de dominante processen dat bankgroei en bankverval veroorzaken geïdentificeerd. De bankamplitude response is vooral gevoelig voor de waterdiepte boven de banktop (h_{Xb}) en de hoek van de inkomende golven met de kustnormaal (θ). Deze parameters bepalen grotendeels de mate van golfbreking op de bank en de daaruitvolgende kustdwarse verdeling van de golfgedreven langsstroming. De langsstroming is maximaal net landwaarts van de banktop waardoor extra zand wordt opgewoeld op de landwaartse bankhelling en trog. De toegenomen sedimentconcentratie in de zone landwaarts van de banktop verschuift het kustdwarse transportmaximum ook landwaarts waardoor de bank groeit gedurende zeewaartse migratie. Bij toenemende h_{Xb}-waarden treedt gemiddeld genomen minder golfbreking op waardoor de kustlangse golfgedreven stroming en de additionele sedimentopwoeling ook reduceert. Hierdoor wordt de dwarsstroming dominant waardoor het kustdwarse transportmaximum bij de banktop optreedt (of net landwaarts daarvan) waardoor de bankamplitude afneemt. Alle vier typen bankgedrag (viz. alle combinaties van landwaarte/zeewaartse migratie en bankamplitude groei/afname) kunnen voorkomen bij dezelfde golfconditie waarbij de lokale waarden van h_{Xb} en θ de bankamplitude response bepalen.

De mechanismen van een niet-persistente bankovergang
Variabiliteit op km-schaal is maximaal wanneer banken kustlangs volledig zijn losgekoppeld. Dit is meestal het gevolg van een duidelijke kustlangse faseverschuiving in de bankcyclus. De buitenste bank loopt dan bijvoorbeeld over in de binnenste bank en wordt gekarakteriseerd als een niet-persistente bankovergang. Deze grootschalige kustlangse variabiliteit wordt onderzocht door het referentiemodel toegepast op 24 omliggende gemeten profielen waarmee in totaal 6 km van de kust bij Noordwijk wordt beschouwd. Wanneer de langsvariabiliteit beperkt is, voorspeld het model dat de banken in de beschouwde bodemprofielen ongeveer met dezelfde snelheid netto zeewaarts migreren (i.e. de banken blijven dus in dezelfde fase). Uitsluitend voor specifieke bankconfiguraties en hoog energetische golfcondities wordt een toename in de langsvariabiliteit voorspeld. Deze voorspelling suggereert dat kustdwarse processen een niet-persistente bankovergang kunnen genereren onder specifieke bankconfiguraties en stormcondities. Daarbij is het de verwachting dat 3-Dimensionale stroom- en transportpatronen de langsvariabiliteit van de bankontwikkeling versterken. In tegenstelling tot de observaties wordt het verdwijnen van bankovergangen niet voorspeld. De banken blijven in verschillende fasen, ook als de banken incidenteel dezelfde kustdwarse positie innemen. Het toegepaste 1D profielmodel is dus niet in

staat een bankovergang te verwijderen. Deze afwijking tussen observaties en de modelvoorspellingen suggereren dat 3D stroompatronen essentieel zijn voor het verwijderen van een niet-persistente bankovergang.

De mechanismen van een persistente bankovergang en bank cyclus periode
Data-analyse studies zijn slechts ten dele in staat geweest om de verschillen in T_r te verklaren, veelal zijn er slechts beperkte correlaties gevonden met lokale omgevingsvariabelen. In de huidige benadering wordt het procesmodel ingezet om de niet-lineaire interacties tussen de hydrodynamische forcering en morfologische profielresponse te onderzoeken voor twee locaties langs de Hollandse kust (Noordwijk en Egmond). Deze locaties zijn gekozen omdat, ondanks het vergelijkbare golf- en getij klimaat, er aanzienlijke verschillen in T_r zijn. De gedetailleerde vergelijking van modelresultaten maakt het mogelijk om op een consistente manier de rol van specifieke parameters te onderzoeken in een mate van detail wat niet mogelijk is op basis van observatiedata. Op deze wijze wordt inzicht verkregen in welke mechanismen T_r primair beïnvloeden. Het blijkt dat de profielhelling in de kustdwarse zone van het bankengebied de grootste invloed heeft op T_r. Dit wordt vooral veroorzaakt door de grote gevoeligheid van het bankengedrag voor h_{Xb}. Als een bank zeewaarts migreert over een steil profiel neemt h_{Xb} sneller toe, met als gevolg dat er minder golven breken op de bank waardoor de zeewaartse migratie aanzienlijk reduceert. De afname van de zeewaartse migratiesnelheid terwijl de bank in dieper water terechtkomt door morfologische terugkoppeling is tegengesteld aan de initieel relatief grotere zeewaartse migratie. Deze initiële sterkere response wordt veroorzaakt door een relatieve toename van golfbreking omdat bij een steil profiel hogere golven de bank kunnen bereiken. De morfologische terugkoppeling verklaard dus ook de contra-intuïtieve observatie van de veel grotere T_r bij Egmond ondanks het enigszins hogere energetisch golfklimaat vergeleken bij Noordwijk wat normaal gesproken zou resulteren in een lagere T_r waarde.

Reductie van de invoer voor langjarige geavanceerde modeltoepassingen
Reductie van het aantal forceringscondities is essentieel om de rekentijden van geavanceerde langjarige morfologische gebiedsmodeltoepassingen hanteerbaar te houden. Daartoe is een invoer-reductie kader ontwikkelt voor golfgedomineerde kusten. Het invoer-reductie kader bestaat uit 4 stappen, viz. (1) de bepaling van de lengte van de tijdserie van de golfcondities waarop de reductie toegepast dient te worden, (2) de selectie van de representatieve golfcondities, (3) de volgorde waarin de geselecteerde golfcondities worden opgelegd, (4) de herhalingsduur van de opgelegde tijdserie. In de eerste twee stappen wordt de chronologie van de originele tijdserie behouden, terwijl dit bij stappen 3 en 4 niet langer het geval is. Het invoer-reductie kader wordt toegepast op twee locaties (Noordwijk en Hasaki in Japan) waar meerdere zandbanken tegelijkertijd voorkomen de kustnabije zone maar met afwijkend langjarig

bankgedrag. Bij Noordwijk is het verloop van de zeewaartse migratie geleidelijk en niet direct gekoppeld aan individuele stormen, terwijl bij Hasaki de zeewaartse migratie een episodisch karakter heeft waarbij de chronologie van stormen in de golftijdserie de meerjarige bankontwikkeling aanstuurt. De kwaliteit van de modelvoorspellingen op basis van gereduceerde invoercondities wordt bepaald door deze te vergelijken met voorspellingen waarbij de volledige golftijdserie als forcering is gebruikt. Uit de vergelijking blijkt dat het reduceren van het aantal beschouwde condities de kwaliteit van de meerjarige voorspellingen van het bankgedrag significant kan beïnvloeden. Reductie van het aantal invoercondities kan er zelfs toe leiden dat de specifieke karakteristieken van het bankgedrag niet langer worden voorspeld. Dit was specifiek het geval voor Hasaki voor alle beschouwde synthetische tijdseries waarin de gemeten golfchronologie niet in is opgenomen (resulterend uit stappen 3 en 4) omdat al deze forcerings tijdseries leidden tot onrealistische voorspellingen van het bankgedrag. Voor Noordwijk kon het bankgedrag wel nauwkeurig worden gereproduceerd met synthetische tijdseries indien de herhalingsduur (bepaald in stap 4) van de opgelegde tijdserie niet te groot gekozen was. Het reduceren van de herhalingsduur had een vergelijkbaar positief effect op de kwaliteit van de voorspellingen als het opnemen van een groter aantal representatieve condities (bepaald in stap 2). Voorts blijkt dat, alhoewel stormcondities de grootste morfologische response veroorzaken, de gemiddelde en lage golfcondities ook dienen te worden opgenomen in de selectie van representatieve condities om het langjarige bankgedrag goed te kunnen voorspellen. Iteratieve toepassing van het invoer-reductiekader is vereist om gereduceerd golfklimaat af te leiden om tot een betrouwbare voorspelling van het langjarige bankgedrag te komen. Gezien het feit dat de reductie van het aantal beschouwde condities een significante invloed kan hebben op de kwaliteit van de daarop gebaseerde voorspellingen, is het essentieel om invoerreductie een intrinsiek onderdeel te maken van iedere model opzet, kalibratie en validatie.

De studieresultaten hebben duidelijk aangetoond dat met een relatief simpel model vergaande inzichten in de complexe niet-lineaire interacties tussen hydrodynamische en morfologische processen verkregen zijn. Dit is bereikt middels het opzetten van zorgvuldig ontworpen numerieke experimenten waarin de invloed van een specifiek proces of omgevingsvariabele kon worden geïsoleerd en geïdentificeerd. Hoewel het model uitsluitend kustdwarse processen beschouwd, hebben de numerieke experimenten ook nieuwe inzichten opgeleverd over het belang van 3-dimensionale processen in geval van een specifieke morfologische staat van de gebankte bodemprofielen. Ondanks het feit dat het model succesvol was gekalibreerd op een profiel bij Noordwijk resulteerde de toepassing bij Egmond in aanzienlijke afwijkingen ten opzichte van de gemeten morfologische ontwikkeling. Het model was in staat om de algemene trends in bankontwikkeling goed weer te geven, maar de bankcyclus periode werd met 30% onderschat. Dit wijst erop dat het model de trends goed kan

voorspellen maar dat het voldoende nauwkeurig voorspellen van absolute veranderingen niet goed mogelijk is zonder een locatie-specifieke kalibratie. Deze bevinding heeft een bredere implicatie omdat het modelleren van het lange termijn gedrag van gebankte profielen in het algemeen wordt gezien als een indicator voor de kwaliteit van de modellering van de gehele kustzone. Het vermogen om betrouwbare en robuuste a priori lange termijn voorspellingen te maken van het kustsysteem dient daarom een breder maatschappelijk belang. Verdere verbetering van morfologische procesmodellen specifiek voor toepassingen in de kustzone dient daarom met hoge prioriteit te worden opgepakt.

1 Introduction

1.1 Motivation

Nearshore sandbars are present along most of the wave dominated sandy coasts wordwide. As sand bars are sub-aerial features predominantly present across and just seaward of the surf zone (up to water depths of about 10 m), many studies have highlighted their importance. For example, the alongshore variability of the bar height or its cross-shore location may have a profound impact on nearshore hydrodynamics, resulting in rip currents that affect swimmer safety and beach width. Bars may dissipate as much as 80% of the incident wave energy and consequently act as a natural barrier for the beach and dune regions. This, for example, implies that the influence of bars should be included in flood risks assessments.

In general, up to 5 nearshore bars are found simultaneously in a cross-shore profile. They typically have a multi-annual lifetime, during which they most often behave in a cyclic, offshore directed manner with often a strong longshore coherence (Wijnberg and Terwindt, 1995; Shand et al., 1999, Kuriyama, 2002; Ruessink and Kroon, 1994). As the most seaward (outer) bar limits the amount of wave energy by enforcing waves to break, it controls the evolution of the shoreward located (inner) bars (Ruessink et al., 2007; Ruessink and Terwindt. 2000). Decay of the outer bar typically initiates a cascaded response in which the next (shoreward) bar experiences amplitude growth and net seaward migration. This in turn creates accommodation space for its shoreward neighbour and so on, eventually resulting in the generation of a new bar near the shoreline. This offshore directed cyclic character is typically measured by the period between two bar decay events. This so-called bar cycle return period (T_r) has been reported to vary worldwide between approximately 1 and 15 years (Shand et al., 1999; Ruessink et al., 2003). The net offshore bar migration is the result of gradual onshore movement during calm periods and episodic strong offshore movement during storms. As a bar migrates offshore it increases in height and width before finally decaying in the outer surf zone region.

Although bars often show a strong longshore coherence over several km's, this does not imply that bars along the coast are all in the same phase of the bar migration cycle. Distinct shifts are observed in which for example the outer bar is attached to an inner bar. This is often referred to as bar switching (Wijnberg and Terwindt, 1995). It is

defined as bars being alongshore discontinuous, either in a different phase of the bar cycle or with a completely different T_r (Plant et al., 1999; Wijnberg and Terwindt, 1995). For the latter case differences in T_r can be substantial (exceeding a factor 4) and appear to be continuously present in time (Wijnberg and Terwindt, 1995). This is here referred to as a persistent bar switch. Bar switches that separate sections with similar T_r are usually less persistent, as alongshore interactions cause bar switches to disappear when the adjacent bars are temporarily in a similar phase, here referred to as a non-persistent bar switch.

Detailed studies (e.g., Van Duin et al., 2004; Grunnet and Ruessink, 2005; Ojeda et al., 2008) revealed that bars strongly interact with shoreface nourishments placed at the seaward limit of the surf zone in water depths from 5 to 8 m. This interaction may also influence the efficacy of both shoreface and beach nourishments (e.g. Walstra et al., 2014). Design guidelines for shoreface nourishments even suggest to use the observed bar volume as an estimate for the nourishment volume (van der Spek et al., 2007). Observations (Van Duin et al., 2004; Grunnet and Ruessink, 2005; Ojeda et al., 2008; Sonneville and van der Spek, 2012; van der Spek and Elias, 2013; Walstra et al., 2014) clearly showed that bars immediately react to the placement of a shoreface nourishment. As a shoreface nourishment is usually placed just seaward of the outer bar (van Duin et al., 2004; de Sonneville and van der Spek, 2012) it affects all landward bars. The shoreface nourishment becomes the outer bar and causes a temporary reverse in the bar migration (i.e. from seaward to landward). This initiates a reverse cascaded response in which the former outer bar becomes the new middle bar and so on. Consequently, bars in the nourished section are now in a different phase than the adjacent sections, which causes discontinuities at the distal ends of the nourishment. These are interpreted as non-persistent bar switches as they have a very similar appearance as the naturally observed bar switches in areas with similar T_r values (e.g. van Duin et al., 2004, de Sonneville and van der Spek, 2012, Walstra et al., 2014). Typically within 6 months after placement of a shoreface nourishment it is absorbed in the nearshore bar system; i.e. the shoreface nourishment has become the outer bar and the landward bars have completed the above described response (Van Duin et al., 2003; Walstra et al., 2014; Ojeda et al., 2008). The time scales on which the dissipation of shoreface nourishments occurs is comparable to that of bars in natural settings. As a consequence shoreface nourishments can be distinguished in the nearshore morphology for several years after placement.

Besides the relevance for shoreface nourishments, the long-term evolution of the nearshore barred profiles is also generally considered indicative of the quality of the modelling for the response of the entire nearshore coastal system. Therefore, the ability to perform reliable and robust a-priori, long-term predictions has broad societal

relevance in view of anticipated adverse impacts of climate change and sea level rise on the stability of coasts worldwide.

Although field-based quantitative descriptions of inter-annual bar behaviour are now available (e.g. Ruessink et al., 2003; Shand et al., 1999; Ruggiero et al., 2009), attempts to correlate environmental parameters to key morphological bar indicators have only been partially successful (Ruessink et al., 2003; Shand et al., 1999). Consequently, the physical reasons underlying the main features of the inter-annual bar behaviour are still poorly understood.

The development of process-based morphodynamic forward models in which the hydrodynamics, sediment transport and bed level change closely interact (e.g. Roelvink et al., 1994; Christensen et al., 2004; Lesser et al., 2004; Ruessink et al., 2007; Van Rijn et al., 2013; Dubarbier et al., 2015) has created the opportunity for more comprehensive analyses of morphodynamic systems in which insights from observational data are combined with model predictions. Roelvink et al. (1995) and Ruessink et al. (2007) were among the first to show that a process based model was able to reproduce the weekly to multi-annual nearshore bar behaviour with reasonable accuracy.

The present study investigates inter-annual sandbar behavior with the overarching aim to identify the main underlying governing physical processes. The following features that together encompass the main characteristics of the inter-annual bar morphology ('sandbar anatomy') are considered:

1) The cross-shore transient bar amplitude response, that is, the transition from bar growth in the intertidal and across surf zone to bar decay at the seaward edge of the surf zone.
2) The intra-site alongshore variability in cross-shore bar position, bar amplitude and the occurrence of non-persistent bar switches.
3) The inter-site variability in the bar cycle return period which is typically accompanied by a persistent bar switch that separates two sections with different bar cycle return periods.

A comprehensive study approach is adopted in which observations of the nearshore morphology are combined with detailed forward model simulations in which the measured wave and waterlevel conditions are used to force the model (referred to as brute forcing). Since the utilized model only considers cross-shore profile evolution, brute forcing does not cause unpractically long calculation times. However, application of more comprehensive models in which both the cross-shore and longshore dimensions are considered (e.g. Lesser et al., 2004 or Roelvink et al., 2009) would lead to calculation times in the same range as the simulation times (e.g. a prediction of 1

year could take as much as 1 year to run). Application of these so-called depth-averaged or 3-dimensional area models is usually achieved by considering a limited set of input conditions which together represent the complete forcing signal as accurately as possible. Tidal schematizations in which for example a full spring-neap tidal cycle is reduced to a single so-called morphological tide are now available (e.g. Latteux, 1995; Van Rijn, 2003; Lesser, 2009). However, wave climate input reduction techniques have not yet been evaluated to study the multi-annual evolution of nearshore sandbars. Therefore, a comprehensive input reduction framework is developed which utilizes a relatively simple input reduction method (Benedet et al., 2016). The framework is evaluated for two sites with distinctly different bar response characteristics by comparing the predictions with the reduced forcing condition to the brute forcing predictions. This not only provides insight into the efficacy of reduced forcing signals to predict inter-annual bar morphology, it also provides an indication of the minimal required number of forcing conditions that need to be considered.

The study focuses on a coastal section at Noordwijk located along the Holland coast. In the next section the objectives and the research questions are formulated that address the identified characteristics listed above.

1.2 Objectives and Research Questions

The overarching objective of this study is to elucidate the anatomy of the inter-annual bar morphology, that is, to identify the main underlying governing physical processes and explain the features that together encompass the main characteristics. This overarching objective is in turn devolved into three objectives aiming to understand key features of bar morphology as outlined in the previous section. A further objective is defined to enable a comprehensive modelling approach based on the acquired insights. The latter objective involves the development of an input-reduction framework for advanced process-based forward modelling of the inter-annual bar morphology. This leads to the objectives and associated research questions outlined below.

Objective I:

To elucidate the morphodynamic processes that result in cross-shore transient bar amplitude response, that is, the transition from bar growth in the intertidal and across surf zone to bar decay at the seaward edge of the surf zone.

Research Questions:

1) Why does a bar experience amplitude growth when it migrates from the inner to the middle surf zone regions?

2) Why does a bar decay at the seaward boundary of the surf zone and does the offshore migration stop?

Objective II:

To establish the role of cross-shore processes in non-persistent bar switches.

Research Questions:

3) To what extent can cross-shore processes initiate, amplify or dampen the km-scale alongshore sandbar variability?
4) What is the relative importance of the wave forcing and the antecedent morphology on the predicted alongshore bar variability?

Objective III:

To identify the dominant environmental variables and the associated physical mechanisms that govern inter-site variability in the bar cycle return period.

Research Questions:

5) Which environmental parameters (e.g. wave forcing, sediment size, profile slope) primarily influence the bar cycle return period?
6) What are the dominant mechanisms that govern inter-site variability in the bar cycle return period?

Objective IV:

To develop an input-reduction framework to enable the application of state-of-the-art process based forward area models to simulate the multi-annual bar behaviour and nearshore morphology.

Research Questions:

7) Can the inter-annual bar evolution be predicted with a reduced set of wave conditions?
8) Which aspects influence the predictability of the bar evolution?

1.3 Approach and thesis outline

To achieve the overarching aim to elucidate the anatomy of the inter-annual bar morphology, it is not only imperative to consider the detailed hydrodynamic and sediment transport processes at the bar, but also to include the interaction with the evolving bar morphology as it responds to the subjected forcing. It is especially this interaction between the forcing and the morphology in the so-called morphological feedback loop which is practically impossible to study in the field or experimentally. Therefore, central in this study is the utilization of a wave-averaged process-based

numerical forward model in conjunction with abundant field measurements acquired along the Dutch coast.

Prior to addressing the objectives, a reference model was constructed, calibrated and validated. The reference model was applied to a single bar cycle return period at Noordwijk (The Netherlands) to calibrate the model's free parameters. This reference model forms the basis of the study as it is combined with a range of schematic cases or compared to predictions at other sites to address the research questions. The objectives are addressed in four separate chapters which, in turn, are largely based on published peer-reviewed manuscripts. These manuscripts have been reformatted, but have undergone only limited editing.

Objective I (and Research Questions 1 and 2) is addressed in Chapter 2 through a detailed analysis in which a reference model hindcast is combined with a range of schematic cases. This approach enables a detailed analysis of the dependency of bar amplitude growth and decay on the offshore wave conditions (height, period and angle) and the cross-shore bar location. Subsequently, the identified dominant processes that govern bar amplitude change are related to the observations to explain the transient bar amplitude change during the inter-annual net offshore bar migration.

To address Objective II (and Research Questions 3 and 4) the reference model is applied on 24 transects with an alongshore spacing of 250 m at a 6 km coastal section near Noordwijk in The Netherlands (Chapter 3). During the considered period, continuous alongshore bars are followed by natural bar switching events which in time transform back to continuous alongshore bars. To identify the importance of cross-shore processes, model predictions initialized with a relatively alongshore uniform set of profiles are compared with predictions starting in a year when a bar switch was present. Comparison of the predicted and observed alongshore variability in cross-shore bar location and bar amplitude for the for both cases provides insight into the relevance of cross-shore processes. Next, the relative importance of the wave forcing and the initial morphology are investigated for nine simulation periods. For each period, hindcast simulations act as a reference for simulations in which either the wave forcing or the initial profiles were modified.

Since one of the most prominent differences in the bar cycle return period was found between the area north and south of the IJmuiden harbor moles (Wijnberg and Terwindt, 1995; Ruessink et al., 2003), reference model predictions at Noordwijk (located south of IJmuiden) are compared with predictions made at Egmond (located North of IJmuiden) for Objective III (and Research Questions 5 and 6; see Chapter 4). The predicted bar cycle return periods are compared for various combinations of environmental variables from the Noordwijk and Egmond sites to identify their

relevance. The considered variables comprise the wave forcing (viz. wave height and incident wave angle), sediment size, and various geometric profile properties (viz. bar size, bar location and profile steepness). Subsequently, the underlying processes that predominantly govern T_r are identified by considering a range of synthetic profiles combined with different forcing combinations and sediment size.

In Chapter 5 the influence of a reduced set of wave forcing conditions on the wave-driven morphological evolution of nearshore sandbars on the time scale of years, i.e. on the time scale of their quasi-cyclic offshore-directed behavior is investigated to address Objective IV (and Research Questions 7 and 8). To investigate the predictability of the bar morphology with a set of reduced input conditions, two sites with distinctly different environmental settings and bar cycle return periods are considered: the reference model (Noordwijk) as well as a model at Hasaki (Japan) are utilized. For both models long-term brute force models are available that have been calibrated according to the same optimization method.

The answers to the research questions formulated in this chapter, and additional remarks on the broader relevance on the findings from this study, conclude the thesis in Chapter 6.

1.4 References

Benedet, L., Dobrochinski, J.P.F., Walstra, D.J.R., Klein, A.H.F., Ranasinghe, R., 2016. A morphological modeling study to compare different methods of wave climate schematization and evaluate strategies to reduce erosion losses from a beach nourishment project. *Coastal Engineering*, 112, pp 69–86. doi:10.1016/j.coastaleng.2016.02.005

Christensen, E., Walstra, D.J.R., Emarat, N., 2002. Vertical variation of the flow across the surf zone. *Coastal Engineering*, 45, pp 169–198. doi:10.1016/S0378-3839(02)00033-9.

De Sonneville, B., van der Spek, A., 2012 . Sediment- and morphodynamics of shoreface nourishments along the North-Holland coast. *Coastal Engineering Proceedings*, 33. doi: dx.doi.org/10.9753/icce.v33.sediment.44

Dubarbier, B., Castelle, B., Marieu, V., Ruessink, B.G., 2015. Process-based modeling of cross-shore sandbar behavior. *Coastal Engineering*, 95, 35–50. doi:10.1016/j.coastaleng.2014.09.004.

Kuriyama, Y., 2002. Medium-term bar behavior and associated sediment transport at Hasaki, Japan. Journal of Geophysical Research 107 (C9), 3132. doi:10.1029/2001JC000899.

Latteux, A., 1995. Techniques for long-term morphological simulation under tidal action. *Marine Geology*, 126, 129–141. doi:10.1016/0025-3227(95)00069-B.

Lesser, G.R., Roelvink, J.A., van Kester, J.A.T.M., Stelling, G.S., 2004. Development and validation of a three-dimensional morphological model. *Coastal Engineering*, 51, 883–915. doi:10.1016/j.coastaleng.2004.07.014.

Lesser, G.R., 2009. An approach to medium-term coastal morphological modeling. *Phd-thesis*, Delft University of Technology, CRC Press/Balkema. ISBN 978-0-415-55668-2.

Ojeda E., Ruessink B.G., Guillen J., 2008. Morphodynamic response of a two-barred beach to a shoreface nourishment. *Coastal Engineering*, 55, 1185–1196. doi: 10.1016/j.coastaleng.2008.05.006.

Plant, N.G.; Holman, R.A.; Freilich, M.H.; Birkemeier, W.A., 1999. A simple model for inter-annual sandbar behavior, *Journal of Geophysical Research – Oceans*, 104-C7,15.755–15.776.

Roelvink, J.A., Walstra, D.J.R., Chen, Z., 1994. Morphological modelling of Keta Lagoon case. *Coastal Engineering Proceedings*. 24. doi:dx.doi.org/10.9753/icce.v24.

Roelvink, J.A., Meijer, T.J.G.P., Houwman, K., Bakker, R., Spanhoff, R., 1995. Field validation and application of a coastal profile model. *Proc. Coastal Dynamics 95 Conference*, Gdansk, Poland.

Roelvink, J.A., Reniers, A.J.H.M, van Dongeren, A., van Thiel de Vries, J., McCall, R., Lescinski, J., 2009. Modelling storm impacts on beaches, dunes and barrier islands. *Coastal Engineering*, 56, 1133–1152. doi:10.1016/j.coastaleng.2009.08.006.

Shand, R.D., Bailey, D.G., Shephard, M.J., 1999. An inter-site comparison of net offshore bar migration characteristics and environmental conditions. *Journal of Coastal Research*,15, 750–765.

Ruessink, B.G., Kroon, A., 1994. The behaviour of a multiple bar system in the nearshore zone of Terschelling: 1965–1993. *Marine Geology*, 121, 187–197. doi:10.1016/0025-3227(94)90030-2.

Ruessink, B.G., Terwindt, J.H.J., 2000. The behaviour of nearshore bars on the time scale of years: a conceptual model. *Marine Geology*, 163, 289 – 302. doi:10.1016/S0025-3227(99)00094-8.

Ruessink, B.G., Wijnberg, K.M., Holman, R.A., Kuriyama, Y., van Enckevort, I.M.J., 2003. Intersite comparison of inter-annual nearshore bar behavior. *Journal of Geophysical Research*, 108 (C8), 3249. doi:10.1029/2002JC001505.

Ruessink, B.G., Kuriyama, Y., Reniers, A.J.H.M., Roelvink, J.A., Walstra, D.J.R., 2007. Modeling cross-shore sandbar behavior on the timescale of weeks. *Journal of Geophysical Research-Earth Surface*, 112 (F3), 1–15. doi:10.1029/2006JF000730.

Ruggiero, P., Walstra, D.J.R., Gelfenbaum, G., van Ormondt, M., 2009. Seasonal-scale nearshore morphological evolution: Field observations and numerical modeling. *Coastal Engineering*, 56, 1153–1172. doi:10.1016/j.coastaleng.2009.08.003.

Van der Spek, A.J.F., de Kruif, A.C., Spanhoff, R., 2007. Guidelines for shoreface nourishments (in Dutch). *Rijkswaterstaat*, RIKZ-rapport 2007.012, ISBN 978 90 369 5764 9.

Van der Spek, A.J.F., Elias, E.P.L., 2013. The effects of nourishments on autonomous coastal behaviour. *Proc. Coastal Dynamics Conference*. Archachon, France.

Van Duin, M.J.P., Wiersma, N.R., Walstra, D.J.R., van Rijn, L.C., Stive, M.J.F., 2004. Nourishing the shoreface: observations and hindcasting of the Egmond case, The Netherlands. *Coastal Engineering*, 51, 813-837. doi:10.1016/j.coastaleng.2004.07.011.

Rijn, L.C. van, 1993. Principles of sediment transport in rivers, estuaries and coastal seas. *Aqua Publications*, The Netherlands.

Van Rijn, L.C., Ribberink, J.S., van der Werf, J., Walstra, D.J.R., 2013. Coastal sediment dynamics: recent advances and future research needs. *Journal of Hydraulic Research*, 51, No. 5, 475–493. doi:dx.doi.org/10.1080/00221686.2013.849297.

Walstra. D.J.R., Brière, C.D.E., Vonhögen-Peeters. L.M., 2014. Evaluating the PEM passive beach drainage system in a 4-year field experiment at Egmond (The Netherlands). *Coastal Engineering*, 93, 1–14. doi:10.1016/j.coastaleng.2014.07.002.

Wijnberg, K.M., Terwindt, J.H.J., 1995. Extracting decadal morphological behavior from high-resolution, long-term bathymetric surveys along the Holland coast using eigen function analysis. *Marine Geology*, 126 (1–4), 301–330. doi: 10.1016/0025-3227(95)00084-C.

2 On bar growth and decay during inter-annual net offshore migration

This chapter is largely based on the article:

Walstra, D.J.R., Reniers, A.J.H.M., Ranasinghe, R., Roelvink, J.A., Ruessink, B.G., 2012. On bar growth and decay during inter-annual net offshore migration. *Coastal Engineering*, 60, 190–200. doi:10.1016/j.coastaleng.2011.10.002.

2.1 Introduction

Nearshore sand bars often have a multi-annual lifetime, during which they can behave in a cyclic, offshore directed manner with a strong longshore uniformity (Kuriyama, 2002; Ruessink and Kroon, 1994; Shand et al., 1999; Wijnberg and Terwindt, 1995). The cyclic behavior, with periods between 1 and 15 years (Shand et al., 1999) begins with an initially nearshore bar moving net offshore. The net offshore bar migration is the result of gradual onshore movement during calm periods and episodic strong offshore movement during storms (Van Enckevort and Ruessink, 2003). As the bar moves net offshore, it increases in height and width before finally decaying in the outer surf zone (Kuriyama, 2002; Ruessink et al., 2003b; Wijnberg and Terwindt, 1995). Bar decay promotes enhanced net offshore migration of shoreward located inner bars and new inner bar generation near the shoreline, perpetuating the cycle. Observations to date indicate that the net offshore bar migration appears not to be related to alongshore propagating shore oblique bars (Ruessink et al., 2003a). Although, the net offshore bar migration phenomenon has major implications for beach/dune behavior (Guillen et al., 1999) and the efficacy of shoreface nourishments (Grunnet and Ruessink, 2005; Ojeda et al., 2008; van Duin et al., 2004), the physical mechanisms underlying inter-annual net bar migration are not yet fully understood. In particular, the cross-shore variability in bar amplitude during the net offshore migration has received very little attention to date. A bar cycle comprises the combined effect of transient bar amplitude response to forcing and net offshore bar migration. Several previous studies have shown that bar amplitude change is governed by the spatial shift between the sediment transport pattern and the underlying bottom profile (e.g. Hulscher, 1996; Plant and Holman, 1997; Roelvink and Reniers, 2011; van Rijn et al., 2003), see Figure 2.1. A positive

shift, i.e. the transport peak is landward of the bar crest X_b, forces bars to grow while propagating offshore. A zero shift results in propagation only, whereas a negative shift leads to damping during offshore migration (Figure 2.1a and c). The opposite relation holds for the spatial shift and the bar amplitude response during onshore migration (Figure 2.1b and d).

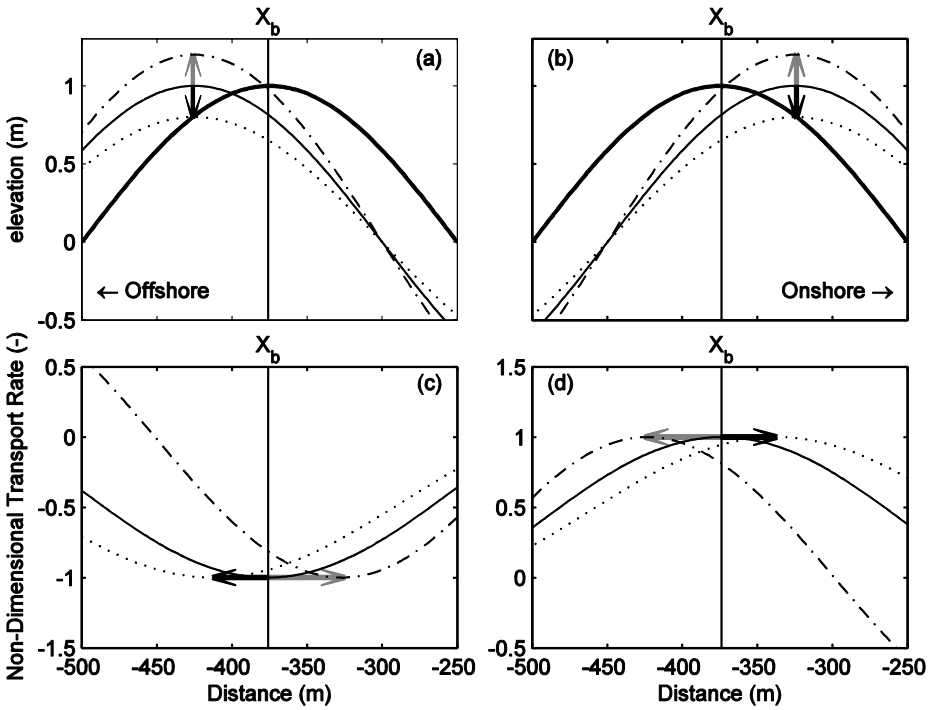

Figure 2.1 *Overview of bar response types (a, b) and the initial non-dimensional sediment transport distributions (c, d). Thick solid lines (a, b): initial bar profiles; thin solid lines (a, b): seaward or landward bar migration with constant bar amplitude; dotted lines (a, b): bar amplitude decay during seaward (SD) and landward migration (LD); dash-dotted lines (a, b): bar amplitude growth during seaward (SG) and landward migration (LG). Initial non-dimensional transports (c, d) according to definitions for the bar response types in (a, b). Vertical line indicates the bar crest position, X_b. Arrows (a, b) indicate bar amplitude growth (gray) or decay (black). Arrows (c, d) indicate the associated shift of the transport peaks relative to the initial bar crest position of both types of amplitude response.*

The aim of this paper is to investigate bar amplitude growth and decay within the bar cycle using a wave-averaged cross-shore process model in conjunction with abundant

field measurements acquired along the Dutch coast. We commence by applying the model to a single cycle at Noordwijk (Netherlands) to calibrate the model's free parameters. A detailed analysis, in which the hindcast is combined with a range of schematic cases, is subsequently undertaken with the aim of determining the dependency of bar amplitude growth and decay on the offshore wave conditions (height, period and angle) and cross-shore bar location. Finally, the identified dominant processes that govern bar amplitude change are related to the observations to explain the transient bar amplitude change during the inter-annual net offshore bar migration.

2.2 Model Description

The Unibest-TC model which comprises coupled, wave-averaged equations of hydrodynamics (waves and mean currents), sediment transport, and bed level evolution is used throughout this study. Straight, parallel depth contours are assumed in all simulations undertaken herein. Starting with an initial, measured cross-shore depth profile and boundary conditions offshore, the cross-shore distribution of the hydrodynamics and sediment transport are computed. Transport divergence yields bathymetric changes, which feed back to the hydrodynamic model at the subsequent time step, forming a coupled model for bed level evolution. Only the main model equations are described below, including those containing the free model parameters. The model is described in detail in Ruessink et al. (2007). The Unibest-TC model was chosen here because earlier research (e.g., Pape et al., 2010; Ruessink and Kuriyama, 2008) has demonstrated that it may produce realistic results on seasonal to multi-annual time scales. In the following we reiterate its main equations to aid in the interpretation of the model results in Sections 2.4 and 2.5.

2.2.1 Waves

The phase-averaged wave model is based on the balance of the short wave energy:

$$\frac{\partial}{\partial x}\left(E_w c_g \cos\theta\right) = -D_b - D_w \tag{2.1}$$

where E_w is the wave energy, x the cross-shore coordinate, c_g is the group velocity, θ is the wave angle to shore normal and D_b and D_w are the dissipations due to bed friction and breaking, respectively. The latter term, which in the surf zone dominates over the dissipation by bed friction, is based on Battjes and Janssen (1978)

$$D_w = \frac{1}{4}\rho g \alpha_w f_p H_{\max}^2 Q_b \tag{2.2}$$

in which ρ = 1025 kg/m^3 is the water density, g = 9.81 m/s^2 is gravitational acceleration, α_w = 1 is a dissipation parameter, f_p is the peak wave frequency, H_{max} is the maximum wave height and Q_b is the fraction of breaking waves. The model applies a so-called clipped Rayleigh distribution through the surf zone, assuming that the waves smaller than H_{max} are not breaking and are Rayleigh distributed, and that all waves larger than H_{max} are breaking. This maximum wave height H_{max} is given by:

$$H_{\max} = \frac{0.88}{k_p}\tanh\left(\frac{\gamma k_p h_r}{0.88}\right) \tag{2.3}$$

where k_p is the local wave number related to f_p, γ is the wave height to depth ratio, for which the expression by Ruessink et al. (2003a) was used and h_r is the water depth obtained from a local linear weighting function applied on the water depth in the seaward direction (Roelvink et al., 1995). This function is governed by the averaging window, x_{bd}, and the weighting function, W. The averaging window is expressed as a function of the local wave length, $L_p=2\pi/k_p$, $x_{bd}=\lambda L_p$ in which λ is the breaker-delay parameter (a user-defined free parameter). The weighting function is given by

$$W(x') = (x_{bd} - x')^p \tag{2.4}$$

where x' is the local grid-coordinate ($x'=x_{bd}-x$ positive in the seaward direction) and p is a user defined parameter which determines the shape of the weighting function. The expression for h_r now becomes

$$h_r(x) = \frac{\int_{x-x_{bd}(x)}^{x} W(x-x')h(x)\,dx}{\int_{x-x_{bd}(x)}^{x} W(x-x')\,dx} \tag{2.5}$$

This so-called breaker delay concept, which accounts for the fact that short waves require some time to react to the local changes in the bathymetry, is critical to obtain an accurate cross-shore distribution of the wave forcing (Reniers et al., 2004b).

The wave energy balance is extended with the roller model according to Nairn et al. (1990) to have an improved estimation of the cross-shore distribution of the wave forcing

$$\frac{\partial}{\partial x}\left(2E_r c\cos\theta\right) = -D_w - D_r \tag{2.6}$$

where E_r is the roller energy, c is the phase speed and D_r is the roller dissipation (Svendsen, 1984)

$$D_r = 2\beta g\frac{E_r}{c} \tag{2.7}$$

in which the front of the wave slope, β, is set to 0.1 (Nairn et al., 1990). The two energy balances are completed by the depth-integrated and time-averaged cross-shore momentum equation to yield the wave setdown/setup.

2.2.2 Currents

The vertical distribution of the cross-shore and alongshore current velocities are calculated with the Reniers et al. (2004a) analytical 1DV-model. Currents are driven by the local wave forcing, mass flux, large scale O(km) surface gradients, and wind. The effects of wave breaking on the vertical current distribution are accounted for by considering a surface shear stress due to wave breaking derived from D_r (Deigaard, 1993; Stive and Wind, 1986; Svendsen, 1984)

$$\begin{aligned}\tau_{sw,x} &= \frac{D_r}{c}\cos\theta \\ \tau_{sw,y} &= \frac{D_r}{c}\sin\theta\end{aligned} \tag{2.8}$$

Streaming effects (Longuet-Higgins, 1953) are included as a time-averaged shear stress, based on Db, assumed to decrease linearly to zero across the wave boundary layer, δ. In the surf zone wave breaking is the dominant source of turbulence which is included in the depth-averaged eddy viscosity, $\overline{\upsilon}_w$, as (Battjes, 1975)

$$\overline{\upsilon}_w = \alpha_w H_{rms}\left(\frac{D_r}{\rho}\right) \tag{2.9}$$

where αw=0.1 and Hrms is the root-mean-square wave height. A parabolic shape function is scaled with Eq. (2.9) to derive a vertical distribution of the eddy viscosity, see Reniers et al. (2004a) for details. The onshore directed wave-induced mass flux above the wave trough level is compensated by a seaward flow below the wave trough (e.g. Phillips, 1977) in which also the roller contribution is included. The cross-shore, depth-averaged, currents, u, are governed by the wave-induced mass flux

$$u = \frac{\left(E_w + E_r\right)\cos\theta}{\rho g h} \tag{2.10}$$

2.2.3 Sediment transport and bed change

The transport formulations distinguish between bed load, S_{bed}, and suspended load, S_{sus}, transport, $S_{tot} = S_{bed} + S_{sus}$. The bed load formulation (Ribberink, 1998; Van Rijn, 1995) is driven by instantaneous (i.e. intra-wave) shear stresses near the bed

$$S_{bed} = \left\langle 9.1\beta_s \left(\left|\phi'(t)\right| - \phi_{c,s}\right)^{1.8} \frac{\phi'(t)}{\left|\phi'(t)\right|} \sqrt{\Delta g D_{50}^3} \right\rangle \tag{2.11}$$

in which ⟨⟩ indicates averaging over many waves, βs is the Bagnold parameter, Δ = 1.65 is the relative density, D_{50} the mean grain size diameter, t is time and $\phi'(t)$ is the instantaneous (intra-wave) time series of the dimensionless effective shear stress due to currents and waves

$$\phi'(t) = \frac{f_{cw}' \left|u_b(t)\right| u_b(t)}{2\Delta g D_{50}} \tag{2.12}$$

where f'_{cw} is the friction coefficient for currents and waves as given in van Rijn (1993). $S_{bed} = 0$ if $|\phi'(t)| \leq \phi_{c,s}$ ($\phi_{c,s}$ is the ϕ at incipient motion). The time series of the near-bed intrawave near-bottom horizontal velocity of the combined wave-current motion, $u_b(t)$, comprises three components (Roelvink and Stive, 1989)

$$u_b(t) = u_{sw}(t) + u_{lw}(t) + u_c \tag{2.13}$$

The time series of nonlinear near-bed short-wave orbital motion $u_{sw}(t)$ is modeled according to Rienecker and Fenton (1981). The resulting time series has nonzero velocity skewness but zero acceleration skewness. The computation of the bound-infragravity series $u_{lw}(t)$ is based on the method of Sand (1982). The mean-flow component in Eq. (2.13), u_c, is the time-averaged horizontal velocity at 1 cm above the bed in the (phase-averaged) flow model. With this term, the contribution of the mean flow in the wave boundary layer to the bed shear stress (and bed load transport) is considered. The cross-shore component, $u_{c,x}$, is typically onshore directed under non-breaking waves owing to streaming and offshore directed in breaking wave conditions when the mass-flux compensation (undertow) is dominant.

The Bagnold parameter reads

$$\beta_s = \frac{\tan\varphi}{\tan\varphi + \frac{u_{b,x}(t)}{u_b}\frac{dz}{dx}} \tag{2.14}$$

The parameter tanφ is the tangent of the angle of repose (a user-defined free parameter), $u_{b,x}(t)$ is the cross-shore component of $u_b(t)$ and dz/dx is the local bed slope.

The suspended transport, S_{sus}, is based on the integration over the water column of the current-related suspended sediment flux. The wave-averaged near-bed sediment reference concentration, c_a, prescribed at the reference height z_a according to van Rijn (1993) serves as the bed boundary condition for a the 1D vertical advection diffusion equation which is used to determine the distribution of the sediment concentration across the water column. The computation of c_a requires the specification of the wave-related roughness, k_w, for which we take
$2.5D_{50}$ (Soulsby, 1997). Following van Rijn (1993), the reference height z_a equals the current-related roughness k_c, a free model parameter.

Finally, temporal bed changes are calculated based on the spatial divergence of the cross-shore sediment transport using a 4-point Preismann implicit scheme.

2.3 Noordwijk application

2.3.1 Model set-up

The model is first used to simulate a complete bar cycle at Noordwijk from 1984 to 1987 (Figure 2.2). The simulation period was selected as the sand bars showed the highest measured alongshore coherence during this period. The initial profile is based on a single transect which was measured in 1984 and was interpolated onto a computational grid with a resolution of 200 m offshore, gradually decreasing to 2 m across the active part of the profile (above −10m water depth). The model was forced with wave time series (H_{rms}, peak period T_p, and θ) measured 5 km offshore, in about 18m of water (Figure 2.3a–c) and measured water level time series (η) covering the entire period with a 3-hour resolution. The tide at Noordwijk is semi-diurnal with a 1 m and a 1.8 m range at neap and spring tide, respectively. Storm surges occasionally raised the water level by more than 1 m above the astronomical tide level during the considered period. D_{50} was taken as 180 μm (Van Enckevort et al., 2004).

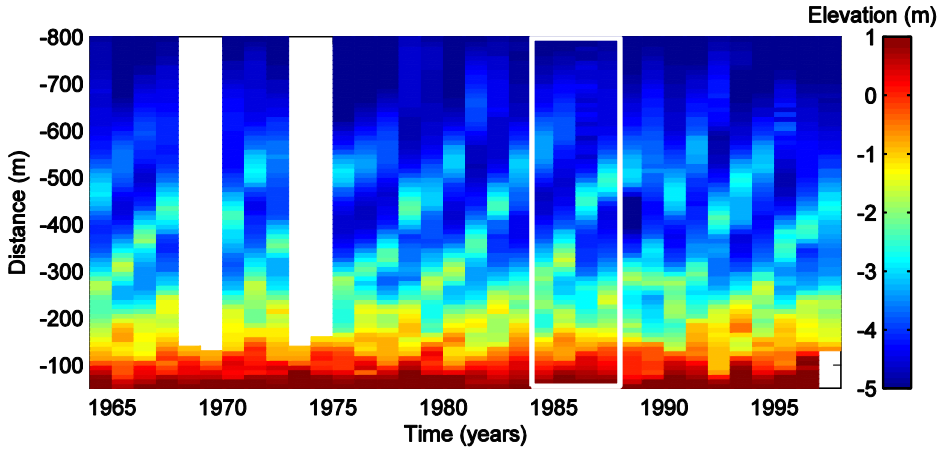

Figure 2.2 *Space-time map of the measured profiles at Noordwijk (box: hindcast period). The profiles are part of the Jarkus database (Wijnberg and Terwindt, 1995), which comprises annual cross-shore soundings of the nearshore zone along the entire Dutch coast with a typical profile spacing of 250 m. The data shown here correspond to local beachpole number 80. Distance=0 is a local, time-invariant position dating back to the mid-19th century (Ruessink and Jeuken, 2002).*

2.3.2 Model calibration

The model contains a number of free parameters that were tuned against the available 1985–1987 profile data. In particular, we focused on the breaker-delay parameter λ, the angle of repose $\tan\varphi$, and the current-related roughness k_c, which were suggested by Roelvink et al. (1995) to be of paramount importance in accurately modeling inter-annual sandbar evolution. First, 1000 parameter sets (λ, $\tan\varphi$, k_c) were randomly sampled from user-specified ranges (based on our earlier experience) and the cumulative mean-squared error between the 1985–1987 observed and predicted bed profiles were computed for each parameter set. The best parameter set was then further fine-tuned using the downhill-simplex approach of Nelder and Mead (1965). The resulting optimum set was λ = 2.76, $\tan\varphi$ = 0.157, and k_c = 0.0056 m, values that are comparable to earlier applications (Ruessink et al., 2007). The Brier Skill Score (Sutherland et al., 2004), defined with respect to a no-change model, of the bed profile predictions with the optimum parameter set was 0.38, 0.49 and 0.65 after respectively 1, 2 and 3 years. According to van Rijn et al. (2003) this classifies these predictions as 'reasonable' (years 1, 2) and 'good' (year 3). Remarkably, the model performance after 3 years was comparable to the performance on weekly time scales (Ruessink et al., 2007).

2.3.3 Results

With the optimum parameter set the net offshore bar migration was reasonably well represented after 377 days (Figure 2.4a), but the bar amplitude was under-estimated. This is especially true for the inner bar. After about 3 years, in 1987, the offshore bar migration was well predicted, but again the bar amplitude was under-estimated (Figure 2.1b). Detailed model-output reveals that this bar has migrated offshore and decayed (see Figure 2.3d, which shows the perturbation determined by subtracting the time-averaged profile from the instantaneous profiles). The final outer bar is the initial inner bar (green line in Figure 2.3d, indicating the bar crest position X_b). In the following discussion, the bars are numbered in the landward direction (bar 1 is the most offshore bar). In view of the fact that there are only 3 observations of the cross-shore profile within the 3 year time span, the model predictions are qualitatively evaluated using measured multi-annual bar amplitude characteristics.

The temporal evolution of the profile is characterized by relatively short (1 to 5 days) offshore migration periods, during wave events with offshore H_{rms} larger than about 2 m; however, not all high wave events resulted in offshore bar migration. For example, one of the largest wave events (offshore H_{rms} = 3.6 m) at t = 195 days (Figure 2.3a) did not induce a noticeable profile response (Figure 2.3d). Onshore migration was gradual and occurred during periods of moderately energetic, but just or non-breaking wave conditions (typically offshore H_{rms} < 1.5 m), which can last for several weeks to months at the study site. The temporal development of the bar amplitudes, A_b, (Figure 2.3e) clearly shows the decay of the two outer bars (bars 1 and 2). Notably, the amplitude of both outer bars responds only to major storm events. The inner bar amplitudes (bars 3 and 4) are more dynamic and show periods of bar growth not present for the two outer bars. All bars generally have a comparable migration response, dX_b/dt, but the associated amplitude change, dA_b/dt, is less consistent as individual bars may grow and decay simultaneously. For example, at t=550days, the largest profile response event with the largest simultaneous offshore bar migration, bar 2 decayed whereas bars 3 and 4 became more pronounced. In accordance with Ruggiero et al. (2009), dA_b/dt is sensitive to the water depth above the bar crest, h_{Xb}. In Figure 2.5 the predicted cross-shore distribution of the bar amplitude is compared to field data. Annually observed A_b were derived for the same transect, but covering the entire period for which data was available (1964–2003; Figure 2.2). As the bars show a net inter-annual offshore migration (Figs. 2 and 3), the cross-shore change in A_b also implies that the transient bar amplitude response is captured by the model (i.e. the residual transition from $dA_b/dt > 0$ to $dA_b/dt < 0$ at about x= −500 m).

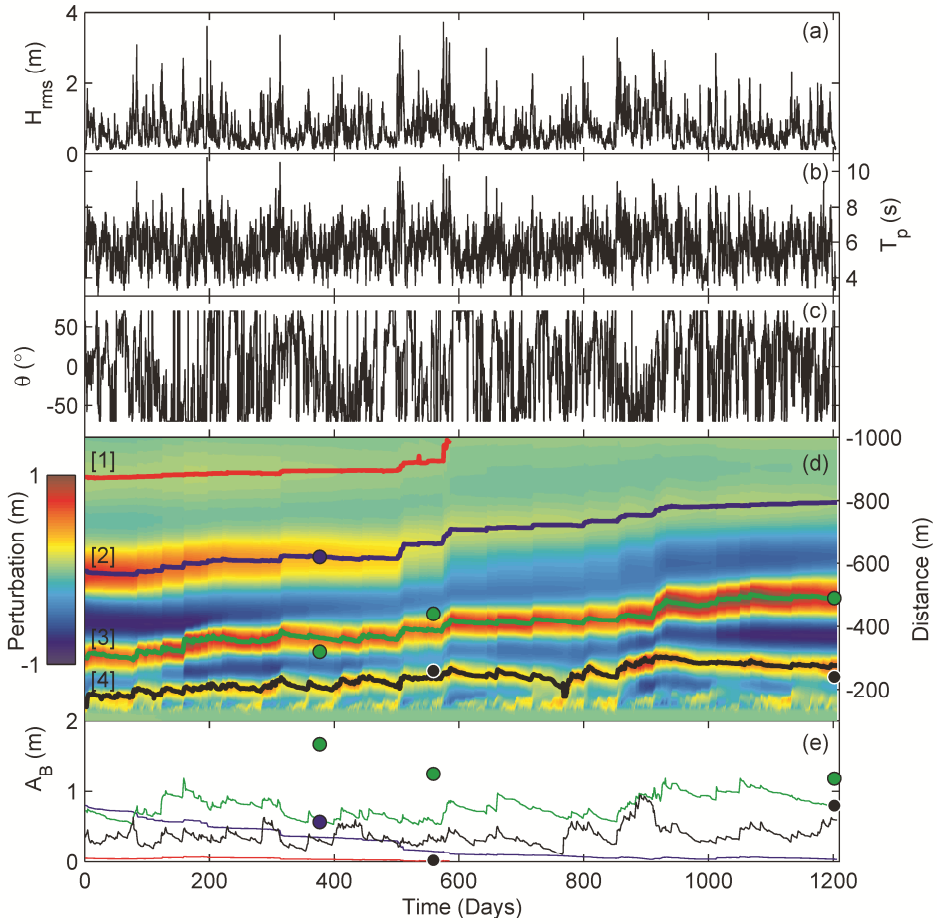

Figure 2.3 *Time series of (a) offshore root-mean-square wave height H_{rms}, (b) offshore peak wave period T_p, (c) offshore incident wave angle θ, (d) time stack of predicted profile perturbation and indication of bar crests ([1], [2], [3], [4]) , and (e) predicted bar amplitudes A_b, line colors indicate bar crest position in (d). Circles indicate the measured crest positions (d) or bar amplitudes (e). T=0 days corresponds to 19 June 1984 00:00 hh:mm.*

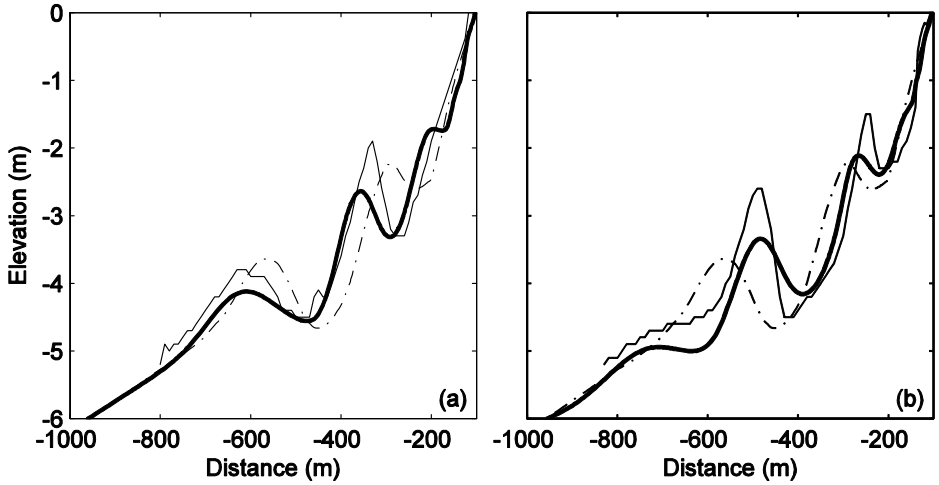

Figure 2.4 *Predicted (thick solid line) and measured (thin solid line) elevation versus cross-shore distance after (a) 377 days (1985) and (b) 1207 days (1987) with optimum parameter set. Initial (1984) elevation: dash-dot.*

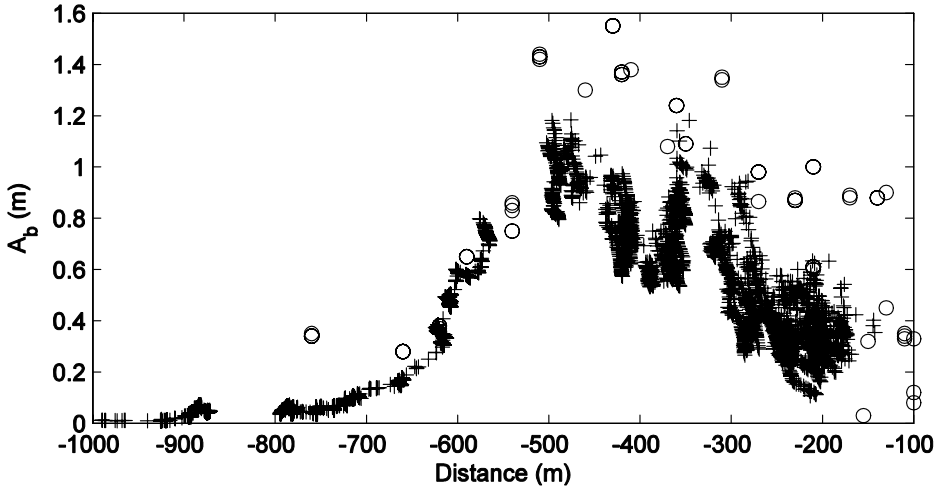

Figure 2.5 *Predicted (1984–1987,+) and observed (1964–1998, o) cross-shore distribution of bar amplitude.*

Table 2.1 presents several statistics quantifying the predicted bar migration and amplitude change. Onshore migration is more common for the bars 2–4, on average 70% of the simulation period. In contrast, the outer bar (bar 1) migrates offshore more

frequently. Both the gross onshore and offshore averaged migration rates are noticeably larger for the two inner bars (bars 3 and 4), but the net offshore migration is surprisingly consistent for all bars at −0.1 to −0.2 m/day. The net offshore migration seems to be directly correlated to the position of the bar in the profile as the inner bar has the lowest and the outer bar has the highest offshore net migration rates. Although the periods of bar amplitude decay are larger for the outer bars, the variation between the bars is small. This is not the case if the average growth and decay rates are compared: the inner bars (bars 3 and 4) have significantly higher growth and decay rates, as was already obvious from Figure 2.3e. Over the entire simulation period the two inner bars grow in amplitude, while the two outer bars (bars 1 and 2) decay.

2.4 Mechanisms underlying bar amplitude change

2.4.1 Analysis of hindcast simulations

As a first step to determine when bars grow and decay, dA_b/dt, extracted from Figure 2.3e, was correlated with offshore and local (i.e. at the bar crest) wave parameters. Figure 2.6 demonstrates that the correlation coefficients are relatively low (yet statistically significant at the 95% confidence level), generally not exceeding 0.5. The offshore wave height and the wave height at the bar crest result in similar correlations. Interestingly, the sign of the correlation changes from bar 1 toward bar 4. This indicates the opposite response to similar wave conditions, also observed in Figure 2.3e. The correlation for the absolute offshore and local wave angle is generally smaller than for the wave height, but is always positive. The correlation for the local surface shear stress due to wave breaking ($|\tau_{sw}|$, Eq. (2.8)) and its cross-shore, $|\tau_{sw,x}|$, and longshore components, $|\tau_{sw,y}|$, are significantly larger for all bars. Especially the large correlation with $\tau_{sw,y}$ for bars 3 and 4 indicates that longshore forcing may play a significant role in the bar growth in the inner surf zone. However, this relation is not present for bar 1 and opposite for bar 2. The correlation with the offshore water level and wave period was significantly lower than with the wave height and is not shown here. These correlations are qualitatively comparable to those found by Ruessink et al. (2003b).

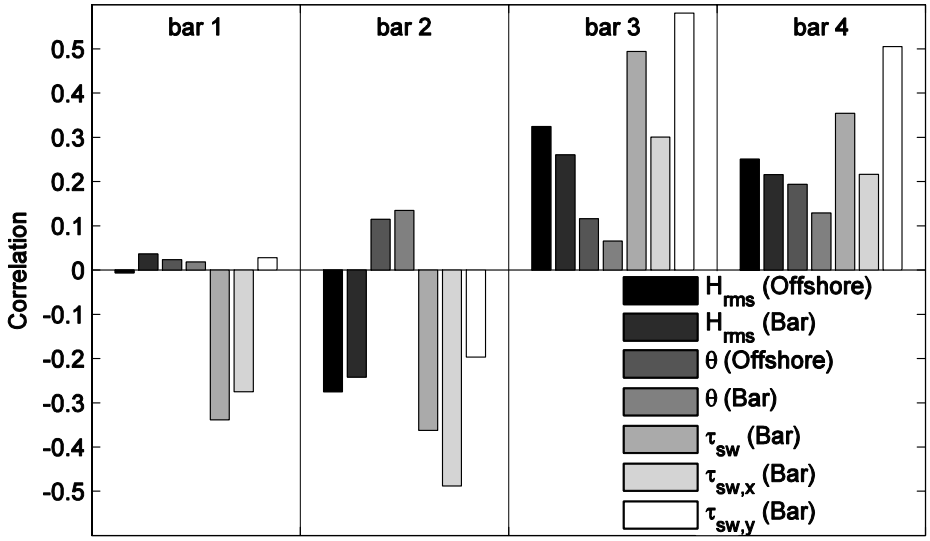

Figure 2.6 *Correlation coefficients between wave parameters and dA_b/dt.*

2.4.2 Influence of individual forcing conditions

The relatively low correlations between dA_b/dt and the wave parameters (H_{rms}, θ, τ_{sw}) may be due to (the combined effect) variations in wave period, tide and wave setup related water level variations, and profile change, or due to the non-linear dependency between dA_b/dt and (H_{rms}, θ, τ_{sw}). To investigate this further, 2240 additional simulations were undertaken (Table 2.2) to separate the interaction between the forcing parameters and the bar morphology by considering a range of wave conditions and water level combinations (H_{rms}, T_p, θ, η). For each forcing combination a one day morphodynamic simulation was undertaken to investigate bar response using the same initial Noordwijk profile as applied in the full hindcast with the optimum parameter settings. The results are analyzed by evaluating dA_b/dt for bars 2 and 3 for all forcing conditions. dA_b/dt is shown in Figure 2.7a-d (bar 2) and Figure 2.7e-h (bar 3) as a function of the wave height at the bar crest for each of the considered incident wave angles. The colors indicate the different water levels imposed: no distinction was made for the wave period as dA_b/dt appeared to be relatively insensitive to variations inwave period. The results indicate that the incident wave angle has a major impact on dA_b/dt. For normally incident waves (Figure 2.7a,e) the bars decay for nearly all (H_{rms}, T_p, θ, η) combinations. As the incident wave angle increases, bar growth is predicted for an increasing number of (H_{rms}, T_p, θ, η) conditions (Figure 2.7b–d for bar 2 and f–h for bar 3). Although the response of both bars is qualitatively similar, the growth rates ($dA_b/dt > 0$) are more frequent and significantly higher for the more shoreward inner bar 3

(notice the different scaling of Figure 2.7a–d and e–h). This also explains the transient bar response in the hindcast simulation (i.e. net decay of bars 1 and 2 and net growth of bars 3 and 4). As a whole, the results in Figure 2.7 show that the bars grow only for specific wave conditions and that the angle of wave incidence controls whether a specific (H_{rms}, T_p, θ, η) condition results in bar growth or decay (i.e. the same wave height and period can result in either bar decay or growth depending on the wave angle).

The question now arises as to why the angle of wave incidence is so important to bar growth and decay. Conceptually, obliquely incident waves induce longshore wave-driven currents which will influence the magnitude of bed shear stresses and subsequently the cross-shore distribution of the sediment transport via enhanced sediment stirring. This is illustrated in Figure 2.8a–f by comparing the distribution of relevant model outputs across bar 3 for two conditions with identical water level, offshore wave height and period (H_{rms} = 1.7 m, T_p = 8 s, η = 0 m), but different wave angles (θ = 0° versus θ = 60°). The two conditions induce an opposite dA_b/dt response during offshore bar migration. Figure 2.8f shows the initial and final perturbations from which it is clear that the oblique waves induce a growth of bar 3, whereas for the shore-normal waves the bar decays. As shown conceptually in Figure 2.1, observed morphological response is clearly linked to the distribution of the total cross-shore transports, S_x, tot (Figure 2.8e). The shore-normal wave condition results in a maximum offshore $S_{x,tot}$, $S_{x,max}$, just seaward of the bar crest while for the oblique wave condition $S_{x,max}$ is located about 20 m landward of the bar crest. So θ has considerable influence on the distribution of $S_{x,tot}$.

Table 2.1 *Summary of bar migration and amplitude change statistics. Bar response types defined in Figure 2.1.*

	Bar 1	Bar 2	Bar 3	Bar 4
Relative period LD type bar response %*	13	61	71	60
Relative period LG type bar response %*	5	1	7	10
Relative period SD type bar response %*	29	30	11	13
Relative period SG type bar response %*	4	6	11	17
$\langle dX_b / dt \rangle > 0$ (m/day)	0.25	0.13	0.39	0.88
$\langle dX_b / dt \rangle < 0$ (m/day)	-0.41	-0.73	-2.15	-2.47
$\langle dX_b / dt \rangle$ (m/day)	-0.19	-0.18	-0.16	-0.11
$\langle dA_b / dt \rangle > 0$ (m/day)	1	2	23	22
$\langle dA_b / dt \rangle < 0$ (m/day)	-0.2	-0.9	-5.1	-8.1
$\left(A_b^{t=T_s} - A_b^{t=0} \right) / A_b^{t=0}$ (m/day) %*	-76	-95	10	69

* % are relative to total simulation period.

This is investigated further by analyzing cross-shore distributions of the predicted hydrodynamics from which $S_{x,tot}$ is determined. The cross-shore wave height distributions (Figure 2.8a) show a reduced wave height for the oblique wave due to refraction, but for both conditions waves break on the bar. The cross-shore wave forcing, $\tau_{sw,x}$, has a similar distribution for both wave angles (Figure 2.8d), but is about 30% smaller for the oblique-wave case. The longshore component, $\tau_{sw,y}$, is on average about 50% smaller (notice the different vertical axes scales), its maximum lies slightly more landward than the maximum $\tau_{sw,x}$ location but the maxima of both $\tau_{sw,x}$ and $\tau_{sw,y}$ are landward of the bar crest. As waves break they do not instantaneously dissipate energy, it is first transferred to the surface rollers in which the energy is dissipated: this results in a landward shift of D_r from which τ_{sw} is calculated according to Eq. (2.8). The longshore currents, however, are considerably larger than the cross-shore currents (Figure 2.8e).

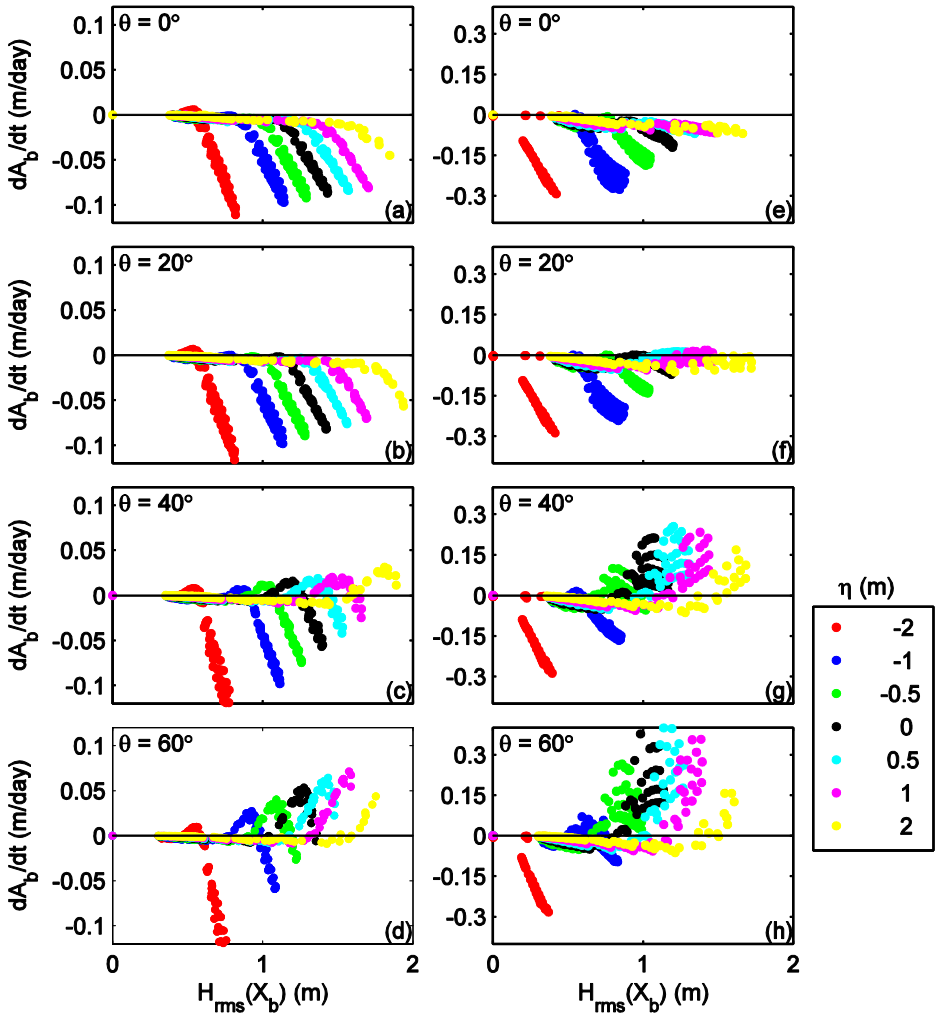

Figure 2.7 *Bar amplitude response at bar 2 (a–d) and bar 3 (e–h) as a function of the wave height at the bar crest for a range of (H_{rms}, T_p, θ, η) conditions (see Table 2.2).*

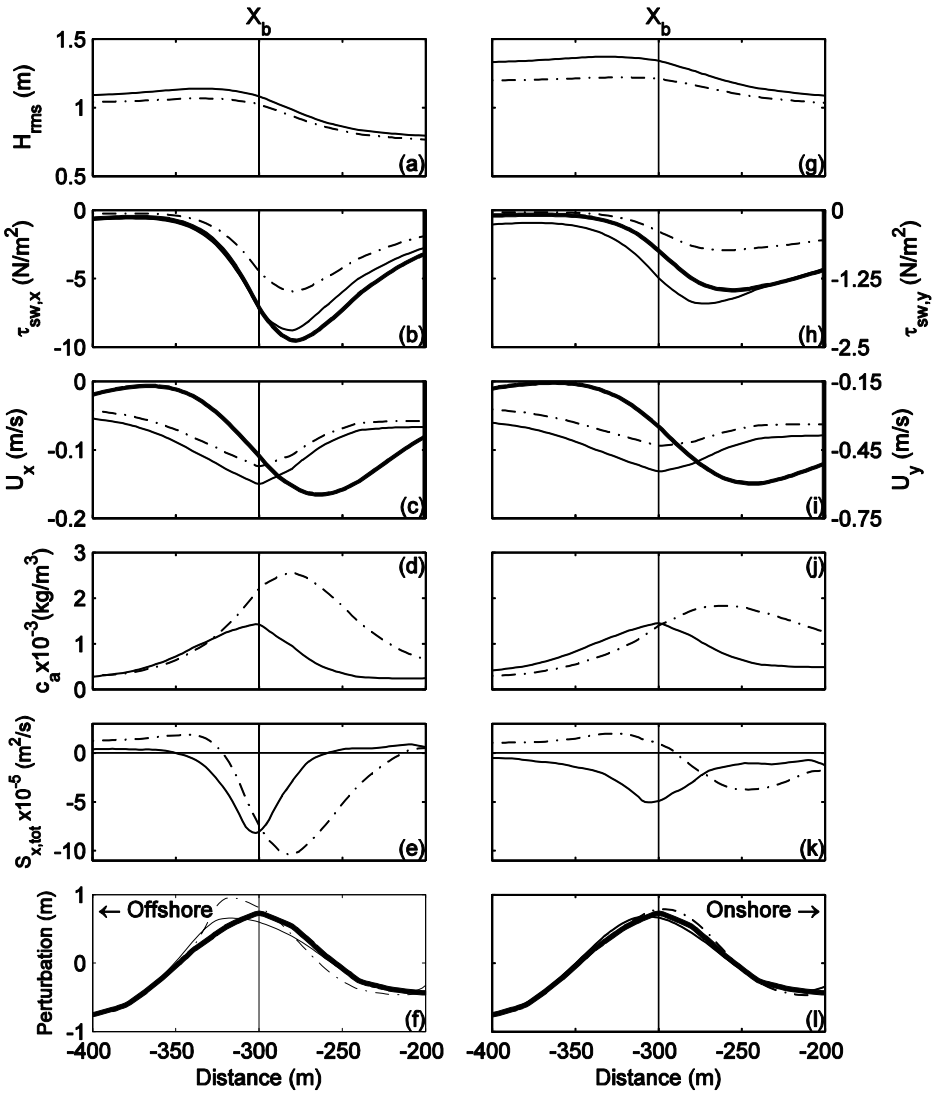

Figure 2.8 *Comparison predictions with oblique (θ = 60°, dash-dotted lines) and shore normal (θ = 0°, solid lines) incident wave angles for η = 0 m (a–f) and η = 1 m (g–l) for H_{rms} = 1.7 m and T_p = 8 s (vertical lines indicate bar crest). Cross-shore distribution of: (a, g) wave height, (b, h) cross-shore wave forcing and longshore wave forcing (thick line), (c, i) cross-shore velocities and longshore velocities (thick line), (d, j) near-bed reference concentration, (e, k) cross-shore sediment transport, and (f, l) initial profile (thick solid line) and predicted profiles after 1 day.*

This difference is caused by the different forcing mechanisms that drive the cross-shore and longshore currents. The local distribution of the cross-shore currents over the bar is particularly sensitive to variations in the local water depth as the cross-shore variation in wave height is limited. This causes the location of the maximum cross-shore currents to coincide with the bar crest location. As the wave-driven longshore current originates from $\tau_{sw,y}$, it has a very similar distribution resulting in a concomitant landward shift of the longshore current (Reniers and Battjes, 1997; Ruessink et al., 2001) which is much larger than the cross-shore current for the oblique wave-case. The sediment concentration is based on the current magnitude to approximately the 4th power resulting in a cross-shore distribution similar to the longshore current for the oblique-wave case (Figure 2.8d). So in case of oblique incident waves, longshore currentswill have a considerable influence on the distribution of the cross-shore sediment transports. If the offshore transport peak is shifted landward of the bar crest, bar amplitude growth instead of decay is predicted (bar response type SG, Figure 2.1).

Table 2.2 *Imposed forcing conditions.*

Parameter	Range	Step
H_{rms} (m)	0.4 to 2.5	0.05 (from 0.4 to 0.7 m) and 0.2
T_p (s)	6, 7, 8, 9, 10	
θ (°)	0, 20, 40, 60	
η (m)	-2, -1, -0.5, 0, 0.5, 1, 2	

A similar analysis is performed for a second set of conditions which concerns onshore bar migration (Figure 2.8g–l). The wave conditions were the same as used for the offshore migration case of Figure 2.8a–f, the only difference being an increased water level of η = 1 m. The increased η results in an opposite bar migration for the θ = 0° and θ = 60° cases. For θ = 0° a small offshore migration and bar decay, $dA_b/dt < 0$ is predicted, while θ = 60° induces onshore bar migration and bar growth, $dA_b/dt > 0$. The morphological response to the (θ = 0°, η = 1 m) and (θ = 0°, η = 0 m) conditions is very similar (compare Figure 2.8f and l) and is not further discussed. The onshore migration for θ = 60° is caused by positive $S_{x,tot}$ values on the seaward bar slope and bar crest (Figure 2.8k). Landward of the bar $S_{x,tot}$ is offshore directed. So sediment is transported toward the bar crest from both sides. Landward migration is dominant because the zero crossing of $S_{x,tot}$ is just landward of X_b. The onshore $S_{x,tot}$ values are caused by the onshore directed oscillatory wave bed load transports becoming dominant over the offshore directed suspended transport, $S_{x,sus}$. Compared to the η = 0 m case, the increased water level results in an increase in the onshore directed $S_{x,bed}$ by about 15% and a decrease in the offshore directed $S_{x,sus}$ by about 40% at X_b. The former is a direct result of the increased wave heights, the latter is caused by reduced wave breaking (Figure 2.8h,i) which primarily affects the vertical distribution of the offshore currents. Reduced wave breaking results in lower offshore directed currents in the

lower part of the water column where the suspended sediment concentration is high. Similar to the η = 0 m case, the longshore currents are again much larger than the cross-shore velocities (Figure 2.8i). On the landward bar slope and adjacent trough region the increased longshore currents caused increased suspended sediment concentrations (Figure 2.8j) resulting in enhanced offshore directed transports in this region (Figure 2.8k) compared to the θ = 0° case. Thus, for onshore bar migration also, the incident wave angle and the associated longshore currents are very important as sand is eroded from the troughs and deposited on the bar enhancing bar growth and onshore migration.

Consistent with Thornton et al. (1996), both oblique wave conditions result in sand being eroded from the landward bar slope and adjacent trough. The sand is deposited on or near the landward side of the bar crest, further enhancing the bar amplitude growth during onshore bar migration for the η = 1 m case (Figure 2.8l) and during offshore bar migration for the η = 0 m case (Figure 2.8f).

2.4.3 Synthetic model runs

In addition to the incident wave angle, the bar response is also influenced by the water level. This was investigated further using schematic single barred bed profiles in which the water depth at the bar crest, h_{Xb}, was varied for a range of cross-shore bar locations, while the initial bar amplitude and shape were kept constant. Following the approach of de Vroeg (1987), the synthetic bars are described as

$$z_{bar} = A_b \exp\left(-\left(\frac{x - X_b}{R_b}\right)^2\right)\cos\left(\frac{2\pi}{L_b}\left(x - X_b\right) + \varphi_b\right) \tag{2.15}$$

which is combined with the profile composed from the Noordwijk profile below a depth of −6m and extended with a Dean profile (Dean, 1977) for the upper part. The parameters in Eq. (2.15) were determined by finding the optimal fit to bar 3 of the initial profile (Figure 2.4). This resulted in a bar amplitude, A_b, of 1.5 m, a bar width, L_b, of 475 m with a phase shift, φ_b, of $-\pi/4$ and a damping width, R_b, of 71.3 m. In total 25 bar positions (Figure 2.9) were forced with the same (H_{rms} = 1.7 m,T_p = 8 s) wave condition as considered in Figure 2.8, combined with a range of wave angles (θ = 0° to 70°, $\Delta\theta$ = 2.5°), again using the hindcast model settings.

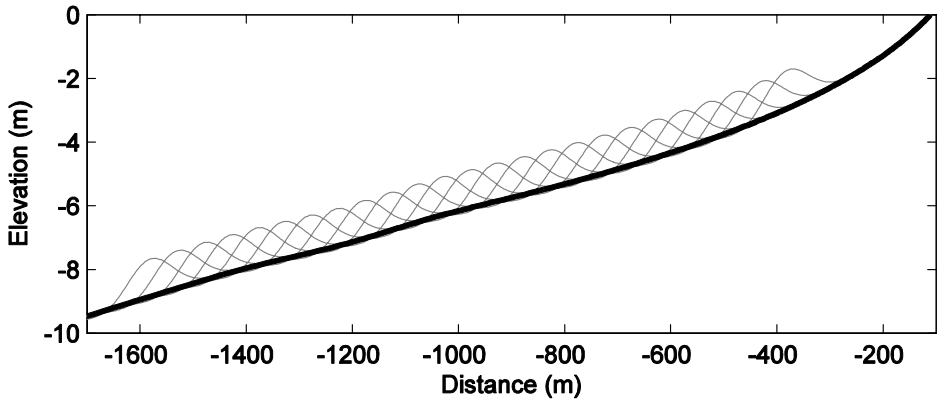

Figure 2.9 *Averaged profile (black) and bottom profiles with the schematic bars (gray).*

For the considered wave condition, dA_b/dt is clearly influenced by both the wave direction and the position of the bar in the profile (Figure 2.10a). If the water depth at the bar crest, h_{Xb}, is larger than 5m, $dA_b/dt < 0$ irrespective of θ_{Xb}. When located in shallower water, the bar responds more strongly and is also sensitive to θ_{Xb}. For oblique waves, θ_{Xb} >15∘, the bar amplitude grows or is showing a small decay for larger h_{Xb} values, whereas for smaller angles the bar generally decays ($\theta_{Xb} < 12°$ always results in $dA_b/dt < 0$). If $\theta_{Xb} < 15°$ the bar migrates offshore for smaller values of h_{Xb} and is stable for larger values of h_{Xb} (Figure 2.10b). In case $\theta_{Xb} > 15°$ there is a transition from $dX_b/dt < 0$ for small h_{Xb} values to $dX_b/dt > 0$ with intermediate h_{Xb} values to $dX_b/dt = 0$ for $h_{Xb} > 6$ m. Consequently, h_{Xb} is an important parameter as it determines dX_b/dt for a given wave condition. This finding is consistent with Ruggiero et al. (2009) which concluded that h_{Xb} was the most important of the investigated parameters. By combining the transitions from $dA_b/dt > 0$ to $dA_b/dt < 0$ (indicated by gray line in Figure 2.10a,b) with the transition from $dX_b/dt > 0$ to $dX_b/dt < 0$ (black line Figure 2.10a,b) it is clear that dX_b/dt is uncorrelated to dA_b/dt as all combinations of bar response (LD, LG, SD and SG, see Figure 2.10) are possible for the same wave condition. It is noteworthy that in deeper water (h_{Xb} >6m) bars decay but do not migrate anymore. Furthermore, onshore migration rates are usually lower than offshore migration rates and are associated with lower dA_b/dt rates. The largest bar amplitude change (growth and decay) takes place during offshore migration.

2.5 Discussion

The schematic cases, discussed in the previous section, have clearly identified the importance of θ and h_{Xb} on bar growth and decay. The forcing of the Noordwijk profile with a range of (H_{rms}, T_p, θ, η) conditions (Figure 2.7) revealed that only specific conditions resulted in bar growth.

For θ = 0∘ and 20° only 5% of the considered wave conditions resulted in bar growth, whereas for θ = 40° and θ = 60° this was the case for over 25%. The influence of the bar position was separately addressed by considering one (H_{rms}, T_p, η) condition for a range of h_{Xb} -values (Figs. 9 and 10). In contrast to van Rijn et al. (2003), the present analysis showed that all four bar response types (LD, LG, SD and SG) are predicted for one (H_{rms}, T_p) condition. Furthermore, the predicted bar response due to variations in h_{Xb} and θ has a general qualitative validity as it was found for other (H_{rms}, T_p) conditions as well (not shown).The analysis has unequivocally shown that wave-driven longshore currents play a key role in the bar amplitude response during both onshore and offshore bar migration. In case of low or absent longshore currents, bars will generally decay as sediment transports are dominated by the cross-shore velocities (bar response types LD and SD). In case of oblique waves, longshore velocities are considerably larger than the cross-shore velocities. The longshore velocity has its maximum landward of the bar crest (Reniers and Battjes, 1997; Ruessink et al., 2001) shifting the offshore transport peak landward of the bar crest resulting in bar growth in case of offshore bar migration (bar response type SG). During onshore bar migration a similar increase in the transports at the bar trough is combined with onshore migration on the seaward bar slope (bar response type LG). Wave-driven longshore currents develop when oblique incident waves break on a bar. For the considered wave condition, this is only the case for bars in relatively shallow water (e.g. bar response types LG/SG, $dA_b/dt > 0$, $\theta > 10°$ and $h_{Xb} < 5$ m, Figure 2.10a). When bars are in located in deeper water or waves are shore-normal, longshore currents are negligible due to the absence of the longshore wave forcing (bar response types LD/SD, $dA_b/dt < 0$, $\theta < 10°$ or $h_{Xb} > 5$ m, Figure 2.10a).

The use of synthetic single-barred profiles to investigate multi-barred dynamics may, at first, seems odd, but is justified as the model estimates sand transport rates based on local forcing. The interaction between bars is thus limited to the influence a seaward bar may have on the local wave characteristics at the adjacent shoreward bar. Additional simulations using a synthetic double-barred profile (not shown here) confirmed that, although the magnitudes of the inner-bar response changed, the trends in the type of bar response remained unchanged.

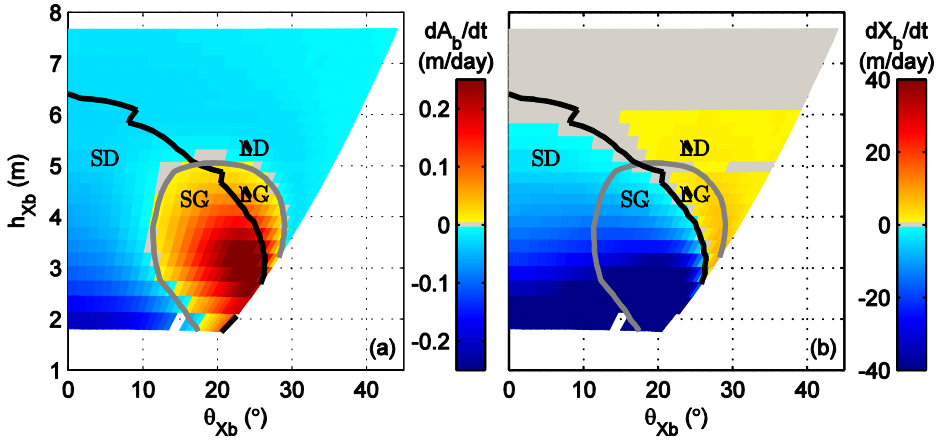

Figure 2.10 *Predicted bar amplitude change (a) and bar migration (b) as a function of the water depth and the wave angle at the bar crest. Black line indicates dX_b/dt = 0 contour line, gray line indicates dA_b/dt = 0 contour line. Identified bar response (SD, SG, LD and LG) as defined in Figure 2.1.*

The relatively low correlations between dA_b/dt and the wave parameters for the hindcast simulation (Figure 2.6) seem to contrast the evident findings derived from the schematic cases. The schematic cases showed that, given a certain wave condition, h_{Xb} determines the type of bar response. As the profile evolves in the hindcast simulation (see e.g. Figure 2.3 and Figure 2.4), the correlations between the wave parameters and dA_b/dt were consequently determined for bars with varying h_{Xb} values. The low correlation values indicate that h_{Xb} is relatively important. Instead of performing a detailed analysis in which these variations are eliminated, we have performed a number of sensitivity simulations for the hindcast that demonstrate the importance of the incident wave angle (and the associated longshore currents). In five additional hindcast simulations some of the forcing conditions were modified: the wave height time series were scaled, the incident wave angle and water level were set to constant values (Table 2.3). Only one parameter was varied per simulation, the duration and other model settings were identical to the hindcast.

Table 2.3 *Imposed forcing conditions.*

Parameter	Scale factor (SF) / Constant value (CV)
η (m)	0 (CV)
H_{rms} (m)	0.8 to 1.2 (SF)
θ (°)	0, 40 (CV)

The use of a constant water level has no noticeable impact on the response of the bars, only near the water line small deviations are predicted. Scaling of the wave height primarily influences the bar migration rate, but also impacts bar amplitude change (Figure 2.11a). Increased wave heights result in larger bars and an enhanced net offshore migration. A reduced wave height has the opposite effect as almost no net offshore bar migration is predicted and bars are now much less pronounced. With θ = 0° the bars have almost completely disappeared at the end of the simulation (Figure 2.11b). The opposite is the case for θ = 40°. The net offshore migration of bar 3 is hardly influenced, but the bar amplitudes have increased considerably. Interestingly, the bar 2 migrated much further offshore and continued to grow instead of to decay, consistent with earlier model runs with time-invariant offshore angle of incidence (Ruessink and Kuriyama, 2008).

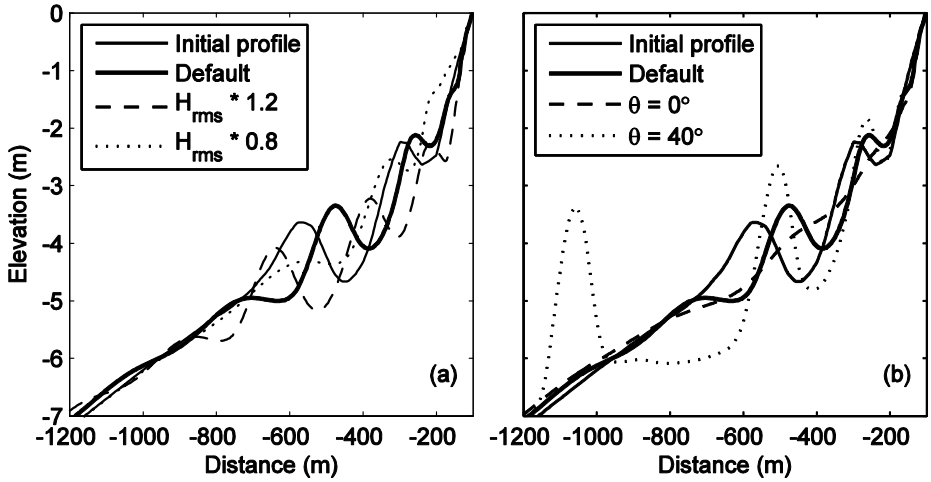

Figure 2.11 *Initial and predicted profile development for the Noordwijk hindcast (a) scaled wave height, (b) different time-invariant incident wave angle.*

The constant water level has limited influence because the net bar migration and amplitude change result in time varying h_{Xb} values that are dominant over the (micro) tidal water level variations at Noordwijk. Besides the obvious effect the scaled wave heights have on the cross-shore currents and associated cross-shore transports, the longshore velocities are also of paramount importance. Reduced wave heights result in lower longshore currents causing more conditions that promote bar amplitude decay, whereas increased wave height enhances longshore currents that augment bar amplitude growth. By varying the incident wave angle, the longshore current is directly affected and these simulations consequently have the highest impact on the bar response. The sensitivity simulations indicate a similar type of bar response to

variations in wave height and wave angle. While the latter directly impacts the longshore currents which results in a strong bar response, the former influences both the longshore and cross-shore current and transport components resulting in a clear but more moderate bar response.

These findings are of particular relevance for investigations of nearshore bar morphology using advanced process area (2DH or 3D) models that require a reduced set of forcing conditions to avoid excessive run times. Generally the forcing reduction for such model applications is justified by ensuring that the longshore gross transports are reproduced (e.g. Grunnet et al., 2004; van Duin et al., 2004). However, the large dependency of the bar response on the angle of wave incidence that has been identified in the present study implies that consideration of the directional distribution of the wave induced transport maybe of crucial importance for the accurate simulation of nearshore bar behavior.

2.6 Conclusions

With a relatively simple wave-averaged cross-shore profile model the observed bar growth and decay during inter-annual net offshore bar migration at Noordwijk (Netherlands) could be reproduced by tuning three free model parameters. A linear regression analysis between the bar amplitude response and wave characteristics (both offshore and at the bar crest) resulted in relatively low correlations ($r < 0.5$). Model results indicate that the enhanced sediment stirring on the landward bar slope and trough by the breaking wave induced longshore current can shift the cross-shore transport peak landward of the bar crest which forces bar amplitude growth during offshore migration. During onshore bar migration the enhanced sediment stirring by the longshore current results in increased transport from the landward trough toward the bar crest promoting bar amplitude growth. The water depth at the bar crest, h_{Xb}, and the angle of wave incidence, θ, control the generation of the longshore current. For bars in shallow water the bar amplitude response and θ are strongly related, due to the relatively strong longshore current that waves breaking under an angle generate. The absence of breaking waves and the associated longshore current at bars in deeper water result in the dominance of cross-shore currents on sediment transport. This results in transport peaks that coincide with the bar crest location forcing bar amplitude decay at larger water depths.

The strong dependency on the longshore current also explains the observed transient bar amplitude response during the net inter-annual offshore migration. For bars in relatively shallow water wave breaking is more frequent, promoting net bar amplitude growth in case of oblique wave incidence, whereas in deeper water wave breaking on the bars is limited, leading to net bar amplitude decay.

2.7 References

Battjes, J.A., 1975. Modelling of turbulence in the surf zone. *Proceedings and Symposium on Modelling Techniques* 1, 1050–1061.

Battjes, J.A., Janssen, J.P.F.M., 1978. Energy loss and set-up due to breaking of random waves. *Proc. 16th Int. Conf. on Coastal Engineering*. ASCE, New York, pp. 570–587.

de Vroeg, J. H., 1987. Schematisering brandingsruggen met behulp van jaarlijkse kustmetingen. *Master's thesis*, Delft University of Technology

Dean, R.G., 1977. Equilibrium Beach Profiles: U.S. Atlantic and Gulf Coasts. *Department of Civil Engineering*, Ocean Engineering. University of Delaware, Newark, Delaware. Report No. 12, 45 pp.

Deigaard, R., 1993. A note on the three-dimensional shear stress distribution in a surf zone. *Coastal Engineering* 20, 157–171. doi:10.1016/0378-3839(93)90059.

Grunnet, N.M., Walstra, D.J.R., Ruessink, B.G., 2004. Process-based modelling of a shoreface nourishment. *Coastal Engineering* 51 (7), 581–607. doi:10.1016/j.coastaleng.2004.07.016.

Grunnet, N.M., Ruessink, B.G., 2005. Morphodynamic response of nearshore bars to a shoreface nourishment. *Coastal Engineering* 52, 119–137. doi:10.1016/j. coastaleng.2004.09.006.

Guillen, J., Stive,M.J.F., Capobianco,M., 1999. Shoreline evolution of the Holland coast on a decadal scale. *Earth Surface Processes and Landforms* 24, 517–536. doi:10.1002/(SICI)1096-9837(199906).

Hulscher, S., 1996. Formation and migration of large-scale, rhythmic sea-bed patterns: a stability approach. *Ph.D. thesis*, University of Utrecht.

Kuriyama, Y., 2002. Medium-term bar behavior and associated sediment transport at Hasaki, Japan. *Journal of Geophysical Research* 107 (C9), 3132. doi:10.1029/2001JC000899.

Longuet-Higgins, M.S., 1953. Mass transport in water waves. *Philosophical Transactions of the Royal Society of London*, Series A 535–581.

Nairn, R.B., Roelvink, J.A., Southgate, H.N., 1990. Transition zone width and implications for modelling surfzone hydrodynamics. *Proc. 22nd International Conference on Coastal Engineering*. ASCE, pp. 68–91.

Nelder, J.A., Mead, R., 1965. A simplex method for function minimization. *The Computer Journal* 4, 308–313.

Ojeda, E., Ruessink, B.G., Guillen, J., 2008. Morphodynamic response a two-barred beach to a shoreface nourishment. *Coastal Engineering* 55, 1185–1196. doi:10.1016/j.coastaleng.2008.05.006.

Pape, L., Kuriyama, Y., Ruessink, B.G., 2010. Models and scales for nearshore sandbar behavior. *Journal of Geophysical Research — Earth Surface* 115, F03043. doi:10.1029/2009JF001644.

Phillips, O.M., 1977. The dynamics of the upper ocean. *Cambridge Univ. Press*.

Plant, N.G., Holman, R.A., 1997. Strange kinematics of nearshore sandbars. *Proc. Coastal Dynamics*, Plymouth, UK. ASCE, New York, pp. 355–364.

Reniers, A.J.H.M., Battjes, J.A., 1997. A laboratory study of longshore currents over barred and non-barred beaches. *Coastal Engineering* 30, 1–22. doi:10.1016/S0378-3839(97)00017-3.

Reniers, A.J.H.M., Thornton, E.B., Stanton, T.P., Roelvink, J.A., 2004a. Vertical flow structure during sandy duck: observations and modeling. *Coastal Engineering* 51, 237–260. doi:10.1016/j.coastaleng.2004.02.001.

Reniers, A.J.H.M., Roelvink, J.A., Thornton, E.B., 2004b. Morphodynamic modeling of an embayed beach under wave group forcing. *Journal of Geophysical Research* 109, 1–22. doi:10.1029/2002JC001586.

Ribberink, J., 1998. Bed-load transport for steady flows and unsteady oscillatory flows. *Coastal Engineering* 34, 52–82. doi:10.1016/S0378-3839(98)00013-1.

Rienecker, M.M., Fenton, J.D., 1981. A fourier approximation method for steady water waves. *Journal of Fluid Mechanics* 104, 119–137.

Roelvink, J.A., Meijer, T.J.G.P., Houwman, K., Bakker, R., Spanhoff, R., 1995. Field validation and application of a coastal profile model. *Proc. Coastal Dynamics 95 Conference*.

Roelvink, J.A., Reniers, A.J.H.M., 2011. A guide to modelling coastal morphology. Advances in Coastal and Ocean Engineering. *World Scientific Pub. Co. Inc*.

Roelvink, J.A., Stive, M.J.F., 1989. Bar-generating cross-shore flow mechanisms on a beach. *Journal of Geophysical Research* 94 (C4), 4785–4800.

Ruessink, B.G., Jeuken, M.C.J.L., 2002. Dunefoot dynamics along the Dutch coast. *Earth Surface Processes and Landforms* 27, 1043–1056. doi:10.1002/esp. 391.

Ruessink, B.G., Kroon, A., 1994. The behaviour of a multiple bar system in the nearshore zone of Terschelling: 1965–1993. *Marine Geology* 121, 187–197. doi:10.1016/0025-3227(94)90030-2.

Ruessink, B.G., Kuriyama, Y., 2008. Numerical predictability experiments of cross-shore sandbar migration. *Geophyiscal Research Letters* 35, L01603. doi:10.1029/2007GL032530.

Ruessink, B.G., Kuriyama, Y., Reniers, A.J.H.M., Roelvink, J.A., Walstra, D.J.R., 2007. Modeling cross-shore sandbar behavior on the timescale of weeks. *Journal of Geophysical Research-Earth Surface* 112 (F3), 1–15. doi:10.1029/2006JF000730.

Ruessink, B.G., Miles, J.R., Feddersen, F., Guza, R.T., Elgar, S., 2001. Modeling the alongshore current on barred beaches. *Journal of Geophysical Research* 106, 22451–22463. doi:10.1029/2002JC001505.

Ruessink, B.G., Walstra, D.J.R., Southgate, H.N., 2003a. Calibration and verification of a parametric wave model on barred beaches. *Coastal Engineering* 48 (3), 139–149. doi:10.1016/S0378-3839(03)00023-1.

Ruessink, B.G., Wijnberg, K.M., Holman, R.A., Kuriyama, Y., van Enckevort, I.M.J., 2003b. Intersite comparison of inter-annual nearshore bar behavior. *Journal of Geophysical Research* 108 (C8), 3249. doi:10.1029/2002JC001505.

Ruggiero, P.,Walstra, D.J.R., Gelfenbaum, G., van Ormondt, M., 2009. Seasonal-scale nearshore morphological evolution: field observations and numerical modeling. *Coastal Engineering* 56 (11–12), 1153–1172. doi:10.1016/j.coastaleng.2009.08.003.

Sand, S.E., 1982. Long wave problems in laboratory models. *Journal of Waterway, Port, Coastal, and Ocean Engineering* 108, 492–503.

Shand, R.D., Bailey, D.G., Shephard, M.J., 1999. An inter-site comparison of net offshore bar migration characteristics and environmental conditions. *Journal of Coastal Research* 15, 750–765.

Soulsby, R.L., 1997. Dynamics of Marine Sands. *Thomas Telford*, London.

Stive, M.J.F., Wind, H.G., 1986. Cross-shore mean flow in the surf zone. *Coastal Engineering* 10, 235–340. doi:10.1016/0378-3839(86)90019-0.

Sutherland, J., Peet, A.H., Soulsby, R.L., 2004. Evaluating the performance of morphological models. *Coastal Engineering* 51 (8–9), 917–939. doi:10.1016/j.coastaleng.2004.07.015.

Svendsen, I.A., 1984. Wave heights and set-up in a surf zone. *Coastal Engineering* 8 (4), 303–330. doi:10.1016/0378-3839(84)90028-0.

Thornton, E.B., Humiston, R.T., Birkemeier, W.A., 1996. Bar/trough generation on a natural beach. *Journal of Geophysical Research* 101, 12097–12110.

van Duin, M.J.P.,Wiersma, N.R.,Walstra, D.J.R., van Rijn, L.C., Stive, M.J.F., 2004. Nourishing the shoreface: observations and hindcasting of the Egmond case, The Netherlands. *Coastal Engineering* 51 (8–9), 813–837. doi:10.1016/j.coastaleng.2004.07.011.

Van Enckevort, I.M.J., Ruessink, B.G., 2003. Video observations of nearshore bar behavior. Part 1: alongshore uniform variability. *Continental Shelf Research* 23, 501–512. doi:10.1016/S0278-4343(02)00234-0.

Van Enckevort, I.M.J., Ruessink, B.G., Coco, G., Suzuki, K., Turner, I.L., Plant, N.G., Holman, R. A., 2004. Observations of nearshore crescentic sandbars. *Journal of Geophyiscal Research* 109, C06028. doi:10.1029/2003JC002214.

van Rijn, L.C., 1993. Principles of Sediment Transport in Rivers, Estuaries and Coastal Seas. *Aqua Publications*, Amsterdam.

Van Rijn, L.C., 1995. Yearly averaged sand transport at the 20mand 8mnap depth contours of the jarkus profiles 14, 40, 76 and 103. *Report H1887*. Delft Hydraulics, Delft, The Netherlands.

van Rijn, L.C., Walstra, D.J.R., Grasmeijer, B., Sutherland, J., Pan, S., Sierra, J.P., 2003. The predictability of cross-shore bed evolution of sandy beaches at the time scale of storms and seasons using process-based profile models. *Coastal Engineering* 47 (3), 295–327. doi:10.1016/S0378-3839(02)00120-5.

Wijnberg, K.M., Terwindt, J.H.J., 1995. Extracting decadal morphological behavior from high-resolution, long-term bathymetric surveys along the Holland coast using eigenfunction analysis. *Marine Geology* 126 (1–4), 301–330.

3 Process-based modeling of kilometer-scale alongshore sandbar variability

This chapter is largely based on the article:

Walstra, D.J.R., Ruessink, B.G., Reniers, A.J.H.M. and Ranasinghe, R., 2015. Process-based modeling of kilometer-scale alongshore sandbar variability. *Earth Surface Processes and Landforms*, 40, 995–1005. doi:10.1002/esp.3676.

3.1 Introduction

Subtidal sandbars are ubiquitous features in the nearshore zone; their number can range from 1 (Lippmann and Holman, 1990), mostly on swell-dominated coasts, to 3 or 4 on storm-dominated coasts (e.g., Van Enckevort and Ruessink, 2003a; Ruggiero et al., 2009; Castelle et al., 2007). In general, the individual bars in a multiple-barred system have a multi-annual lifetime, during which they can behave in a gradual cyclic, offshore directed manner (Ruessink and Kroon, 1994; Plant et al., 1999; Shand et al., 1999; Kuriyama, 2002; Ruessink et al., 2003; Ruggiero et al. 2009; Aagaard et al., 2010). Bars have also been observed to migrate offshore in a rather abrupt manner in response to extreme storm events (e.g., Ruessink et al., 2009) as well as net onshore (e.g., Aagaard et al., 2004). Here, we focus on the more typical gradual offshore migration. Offshore cycle periods vary worldwide between approximately 1 and 15 years (Shand et al., 1999). The net offshore bar migration is the result of gradual onshore movement during calm periods combined with episodic strong offshore movement during storms (Van Enckevort and Ruessink, 2003a; Walstra et al., 2012). Bars are generated in the intertidal or uppermost subtidal zone. Storm events typically cause the bars to grow, whereas calm conditions lead to bar decay, especially when waves are shore-normally incident (Ruessink et al., 2007; Pape et al., 2010). However, the net bar amplitude response depends on the cross-shore position (Walstra et al., 2012). As a bar moves offshore towards the middle of the surf zone, it increases in height and width. Bar decay sets in when it approaches the seaward limits of the surf zone. Due to the larger water depth the net offshore migration rate gradually decreases and also causes a reduction in the strength of the breaking wave induced longshore

currents. As demonstrated in Walstra et al. (2012), this results in cross-shore sediment transport gradients that promote bar decay.

Cyclic bar behavior often shows strong alongshore coherence (Wijnberg and Terwindt, 1995; Shand et al., 1999; Kuriyama, 2002; Ruessink and Kroon, 1994), indicating that this phenomenon is not the result of alongshore propagating shore oblique bars (Ruessink et al., 2003, Walstra et al., 2012). This implies that transport gradients induced by cross-shore hydrodynamics are dominant over gradients originating from longshore processes where this cyclic bar behavior is concerned. Using a process-based profile model (i.e. assuming alongshore uniformity), Walstra et al. (2012) showed that the transient inter-annual bar amplitude response is primarily governed by the water depth above the bar crest, h_{Xb}, and the incident wave angle, θ.

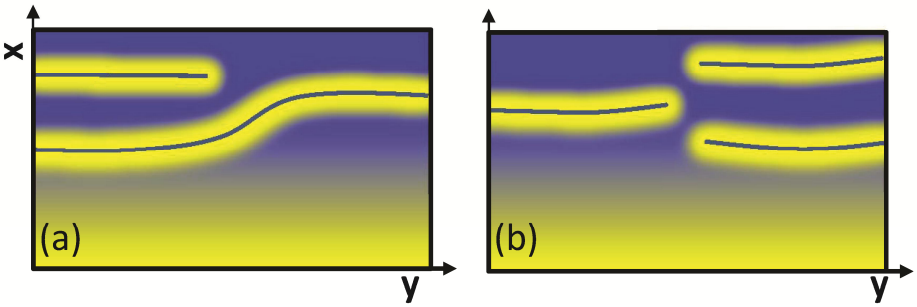

Figure 3.1 *Schematic overview of two bar switch configurations: (a) bar switch where the outer bar is attached to the inner bar of alongshore uniform bars and (b) fork like bar switch configuration with a complete alongshore separation of the bars. The colors specify depth in a relative sense; the thin blue lines in the yellow bands indicate the bar crests.*

Although the alongshore coherent net offshore migration dominates bar behavior at inter-annual time scales, bars also display alongshore non-uniformities on temporal scales of days to years and spatial scales of 100 m to 2 km (e.g. Shand and Bailey, 1999). Processes governing the initiation and evolution of small-scale alongshore non-uniformities such as rip cells and crescentic plan shapes, O(100 m, days to weeks) are now quite well understood (Reniers et al., 2004; Ranasinghe et al., 2004; Holman et al., 2006; Garnier et al., 2013). On the other hand, the physics governing larger scale alongshore non-uniformities, such as bar switching, are less well known. Bar switching is typically an indication of a distinct phase shift in the bar cycle (Wijnberg and Wolf, 1994; Wijnberg and Terwindt, 1995; Shand, 2003) where an outer bar is attached to an inner bar (Figure 3.1a) or where bars are detached completely, resulting in a fork-like configuration (Figure 3.1b). Although bars can switch under natural conditions, shoreface nourishments may also trigger switches. For example at Noordwijk, The

Netherlands, the net offshore bar migration was delayed immediately landward of a shoreface nourishment, while elsewhere net offshore bar migration continued. This spatially discontinuous offshore migration resulted in bar switches that lasted about one year (Ojeda et al., 2008). Under natural conditions bar switching has a relatively large inter-site variation in the associated temporal scales (months to years; Shand et al., 2001) while the alongshore length of the transition zones can differ at least one order of magnitude (100's of m versus km's). Bar switches initiate at the seaward limit of the surf zone, and once established, show limited cross-shore migration (e.g. Shand et al., 2001). However, their alongshore migration can be several kilometers during their lifetime (e.g. Wijnberg and Terwindt, 1995; Ruessink and Kroon, 1994).

Although natural and nourishment-induced bar switching events are largely similar, little is known about the physical processes that govern this type of morphological response under natural conditions. Shand et al. (2001) found that only shore oblique energetic wave conditions triggered bar switching events. However, as not all high energy events resulted in bar switching, Shand et al. (2001) concluded that other factors such as the antecedent morphology could play a controlling role too. Furthermore, Shand et al. (2001) suggested that the observed regularity in the alongshore bar switching locations (both at Wanganui and the Dutch coast) could be an indication of regional hydrodynamic controls or a link to alongshore changes in cross-shore slope or the number of bars.

Because cross-shore processes dominate the cyclic bar behavior (e.g. Walstra et al., 2012), it is likely that this also applies to the local bar morphology on either side of a bar switch. For example, small variability in water depth along an initially coherent bar could trigger different migration rates that ultimately result in a switch. Therefore, the objective of the present paper is 1) to establish to what extent cross-shore processes can initiate, amplify or dampen alongshore sandbar variability on km-scale and 2) to identify the relative importance of wave forcing and antecedent morphology on the predicted large scale alongshore variability. This study focusses on a double barred beach located along the storm dominated Dutch coast during a time it was unaffected by nourishments.

To reach our aims, we apply a process based cross shore profile model (Ruessink et al., 2007; Walstra et al., 2012) on 24 transects with an alongshore spacing of 250 m at a 6 km coastal section near Noordwijk in The Netherlands (Figure 3.2). During the considered period, continuous alongshore bars are followed by natural bar switching events which in time transform back to continuous alongshore bars. In the model the (bar) morphology evolves because of the cross-shore feedback between the hydrodynamics (waves and currents), sediment transport and the morphology itself (Van Rijn et al., 2013). We selected this model for two reasons: 1) to our knowledge

process-based area models have not been able to predict accurately inter-annual bar morphology behavior (e.g. Van Duin et al., 2004; Grunnet et al., 2004; Ruggiero et al., 2009) and 2) detailed evaluation of the wave forcing would not be possible as acceptable run times require a significant reduction of the number of wave conditions (e.g. Walstra et al., 2013).

To identify the importance of cross-shore processes, model predictions initialized with a relatively alongshore uniform set of profiles are compared with predictions starting in a year when a bar switch was present. Next, the relative importance of the wave forcing and the initial morphology are investigated for nine simulation periods. For each period, hindcast simulations act as a reference for simulations in which either the wave forcing or the initial profiles were modified.

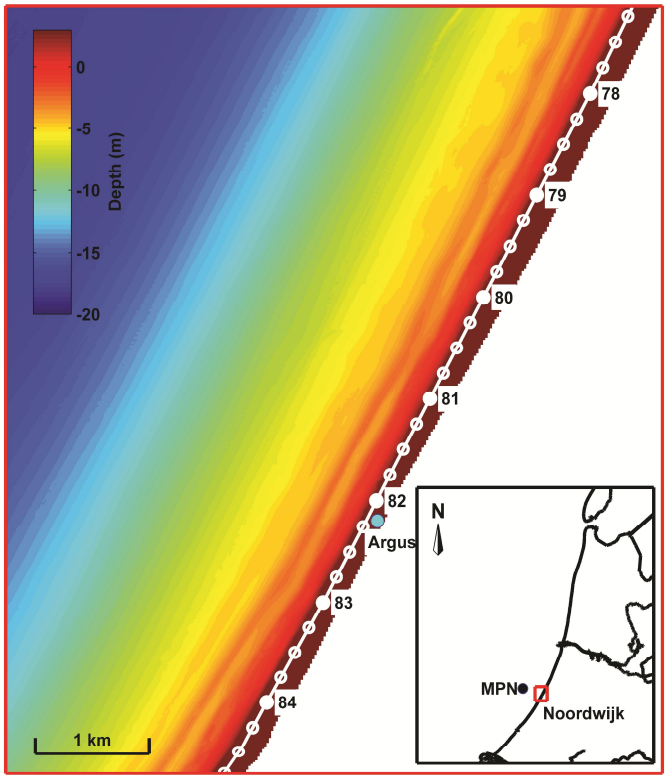

Figure 3.2 *The Noordwijk coast with the beachpoles representing the alongshore coordinate system. The location of the ARGUS video system and the wave station MPN are also indicated.*

3.2 Observations

3.2.1 Study site

Noordwijk is located within the central part of the 120-km long uninterrupted Dutch coast, faces northwest (298°N) and is more than 20 km away from the most nearby harbor moles (see Figure 3.2). Offshore wave recordings, available from 1979 to 2002 in 18 m water depth (Meetpost Noordwijk –MPN– about 5 km offshore, see Figure 3.2), indicate an average offshore root-mean-square wave height (H_{rms}) of 0.7 m and a corresponding peak wave period of 6 s. Waves are mainly incident from south-west to north-west. Storm waves are primarily obliquely incident and occur throughout the year, although autumn and winter are usually slightly more energetic (storms with offshore wave heights of about 3 – 4 m typically occur 2 to 3 times in the autumn-winter season). The tide at Noordwijk is semi-diurnal with a 1 m and a 1.8 m range at neap and spring tide, respectively. Storm surges can raise the water level by more than 1 m above the astronomical tide level. Because bar dynamics are, in part, governed by the water depth above the bar, h_{Xb}, measured water levels at IJmuiden are directly imposed as boundary conditions.

Using annual depth surveys with a 250m longshore resolution spanning nearly 3 decades, Wijnberg and Terwindt (1995) showed that the site is characterized by a shore-parallel double subtidal bar system that experiences inter-annual net offshore migration with occasional bar switches. The bar cycle, marked by the period between two bar decay events, takes about 3 to 4 years to complete. During storms, the outer bar decays and the inner bar migrates offshore to become the new outer bar. Also an intertidal bar is usually present, but with a substantial shorter lifetime (weeks to one month), which at first glance suggests no correlation with the subtidal bar cycle (Quartel et al., 2007). However, the decay of the outer bar initiates a cascaded response which also causes the intertidal bar to migrate offshore towards the subtidal region and to become the new inner bar, thus perpetuating the cycle (Walstra et al., 2012). The residual inter-annual offshore bar migration at Noordwijk was confirmed by Van Enckevort and Ruessink (2003a,b) based on daily observations of the inner and outer bar crest positions from 1995 to 1998 derived from video imagery between y=79 km to y=81.75 km (distances are defined in a local longshore coordinate system, see also Figure 3.2). Although on shorter time scales small alongshore non-uniform features such as rip channels were observed, these did not appear to affect the inner and outer bar behavior on inter-annual time scales. Detailed comparisons of the alongshore variability of the bar crest locations based on the annual Jarkus surveys and the daily Argus surveys clearly showed that the annual surveys were sufficient to capture the inter-annual bar morphology (not shown). In the following, we consider a 6 km section at the coast of Noordwijk from y=78 km to y=84 km.

3.2.2 Site-averaged sandbar behaviour

Following Plant et al. (1999), we summarize the observed development of the 6 km coastal section at Noordwijk in Figure 3.3a with a time stack of the alongshore averaged profile perturbations, $Z_y'(x,t)$, from the start of the surveys in 1965 to 2010,

$$Z_y'(x,t) = \sum_{y=78}^{y=83.75} Z_t'(x,y,t) / N_Y \tag{3.1}$$

The perturbations $Z_t'(x,y,t)$ were determined by subtracting the time-averaged bathymetry from the surveyed bathymetries, *Z*, as:

$$Z_t'(x,y,t) = Z(x,y,t) - \sum_{t=1965}^{t=1998} Z(x,y,t) / N_t \tag{3.2}$$

Here N_Y is the number of cross-shore profile locations, N_t is the number survey dates between 1965 and 1998, *x* is the (equidistant) cross-shore coordinate, *y* the longshore coordinate and *t* denotes time. The surveys from 1999 onwards were not considered in the time-averaged bathymetry as the shoreface at Noordwijk was regularly nourished since that time (e.g. Ojeda et al., 2008).

The distinct signature of the alongshore averaged cyclic offshore bar migration visible in Figure 3.3a confirms previous observations (e.g. Wijnberg and Terwindt, 1995; Walstra et al., 2012) and highlights that the bar migration is alongshore coherent and dominates the long-term morphology throughout the considered 1965 to 1998 period. The nourishments have a profound impact on the bar morphology from 1999 onwards. Consistent with observations elsewhere along the Dutch coast (Van Duin et al., 2004; Grunnet and Ruessink, 2005), the bars have migrated somewhat shoreward and the net offshore migration has been absent since 1999 (see also Ojeda et al., 2008).

Cross-shore averaging of $Z_y'(x,t)$ allows us to determine the degree to which mass was conserved in the study area (Figure 3.3b). Although a small increasing trend is present, changes in mean elevation are limited and seem to be within, or close to, the ranges of the measurement accuracy (Wijnberg and Terwindt, 1995) until 1998. From 1999 onwards, the nourishments clearly induce an increasing mean elevation. The local mean elevation minima in 1975-1976 and 1994-1996 (Figure 3.3b) are correlated to periods when the outer bar had migrated beyond the seaward limit of the surveys (approximately at 8 m water depth) and the new outer bar had not yet reached its maximum amplitude. The local maxima in mean elevations (e.g. 1979, 1981, 1984,

1987 and 1992) coincided primarily with periods when the middle bar was most pronounced and the outer bar not yet had decayed and/or migrated offshore. Therefore, the inter-annual fluctuations of the mean elevation within the survey area are correlated to the alongshore averaged phase of the bar cycle. The life cycle (i.e. bar initiation near the water line followed by gradual growth and offshore migration and finally the decay at the seaward limit of the surf zone) of 7 bars was fully captured. As can be seen in Figure 3.3a, each bar life cycle was approximately 10 years. Overall, prior to the nourishments, the bars had fairly similar amplitude response and migration characteristics. The bar crest, indicated by the gray lines, run more or less parallel in Figure 3.3a and the bars amplitude grow and decay in approximately the same cross-shore regions.

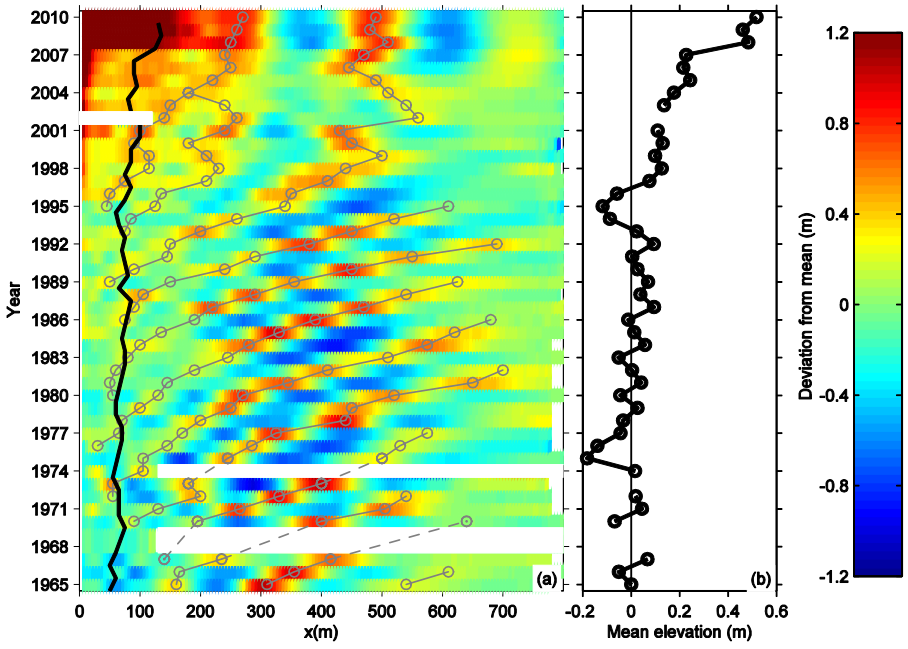

Figure 3.3 *a) Time stack of alongshore-averaged depth deviations (y=[78:84] km) from the 25-year mean profile. Black line indicates the alongshore averaged shoreline (z=0 m) position (x=0 m is at the 2005 dune foot positions z=+3 m), the gray lines indicate alongshore averaged bar crest positions; b) Time series of cross-shore averaged profile perturbations from Figure 3.3a.*

3.2.3 Intra-site variability in sandbar behaviour

From here onwards, only the period from 1987 to 1998 is considered in detail as this period encompassed the full life cycle of the two most recent bars unaffected by nourishments (i.e. bars that were present in the years 1986 – 1995 and 1989 – 1998, respectively, see also Figure 3). Furthermore, this period encompassed two distinct episodes of bar switching alternating with periods of more alongshore coherent behavior (Figure 3.4). The first bar switch occurred from 1988 to 1989. Because the outer bar in 1987 was fairly alongshore uniform, this bar switch originated from a distinct alongshore difference in net offshore migration rates or bar amplitude response between 1987 and 1988. The outer bar in the southern section (y= 82 km to y=84 km) experienced a relatively large bar amplitude decay compared to the northern section (y= 78 km to y=82 km, Figure 3.4b). In 1988 some remains of the outer bar can still be distinguished in the northern section, which suggests that the offshore migration was approximately similar for the entire section. However, when considering the bar crest location, the 1988 morphology resembles the schematic bar switch configuration in Figure 3.1a. The outer bar amplitude decay at the southern section enhanced the offshore migration of the inner bar, which by 1989 (Figure 3.4c) resulted in a breakup of the 1988 inner bar that resembles fork-like bar switch configuration as shown schematically in Figure 3.1b. One year later a similar kind of response can be observed for the northern section (y= 78 km to y=81.25 km, Figure 3.4d): the decay of the outer bar caused a rapid offshore migration of the inner bar in this region. As a consequence it attached to the outer bar in the southern section, which marked the end of the bar switch period.

The 1988-1989 bar switch period resulted in an outer bar with a relatively large alongshore variation in bar amplitude (and h_{Xb}) in 1990 (Figure 3.4d). As a consequence there was a substantial alongshore variation in offshore bar migration from 1990 to 1991. By 1992 this enhanced alongshore outer bar variability caused a similar response to the inner bar causing it to break up at y = 83 km (Figure 3.4f). We did not specifically consider this bar switch because it was less pronounced and did not seem to indicate a clear shift in the bar cycle. However, during both bar switching periods, the outer bar response clearly controlled the inner bar development to a large extent.

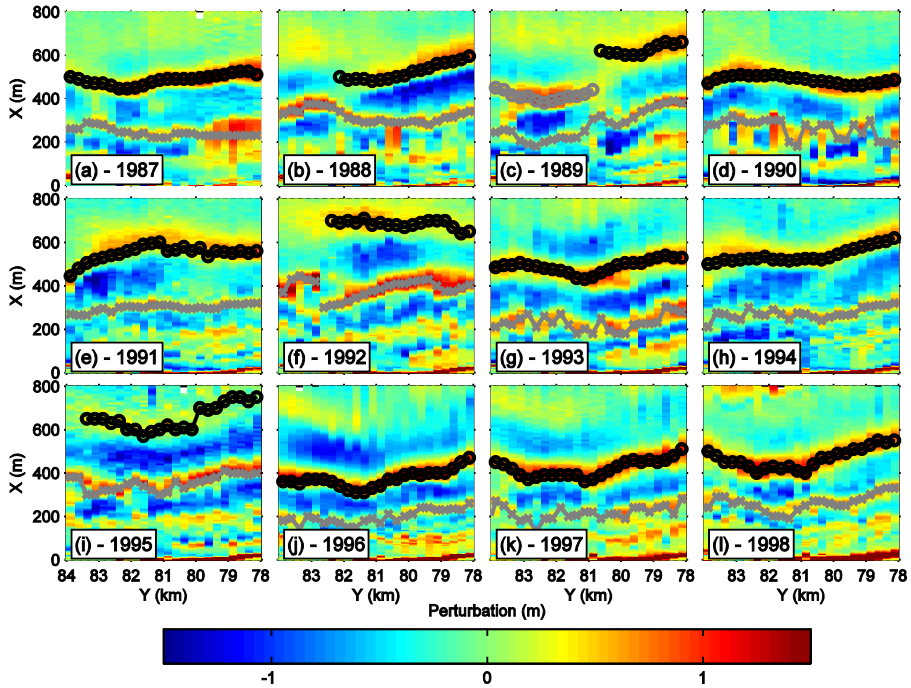

Figure 3.4 *Observed profile perturbations from 1987 to 1998; black circles and grey crosses indicate the outer and inner bar respectively. In 1989 (plot c) the grey circles indicate the alongshore part of the outer bar that was the inner bar in the previous year.*

From 1994 to 1998 the outer bars were relatively alongshore uniform or coherent (Figure 3.4h-l). By 1995 a new cycle was initiated as the outer bar by this time had decayed considerably, the new outer bar migrated gradually offshore and was still present in 1998. No bar switching events on intra-annual time scales were observed in the daily video images collected between 1995 and 1998 (Van Enckevort and Ruessink, 2003b).

3.3 Model Approach

The first objective (can cross-shore processes initiate, amplify and dampen alongshore sandbar variability on km scale?) was addressed by considering two analysis periods. As the lifespan of the bar switches at Noordwijk were less than the bar cycle period of about 3 years, the analysis interval (and model period) was restricted to this period. The first period comprised the 1987 to 1990 period which is characterized by an

initially alongshore uniform morphology from which in the two following years a distinct bar switch evolved, but by 1990 the bar switch had decayed resulting in a relatively alongshore uniform morphology again (see also Figure 3.4). The second period started in 1989 when the bar switch was most pronounced, followed by two years when the bars were alongshore continuous, but in the last year (1992) a bar switch was present again in the middle bar. The first period was used to investigate whether the model was able to develop a bar switch from relatively alongshore uniform profiles. The second period is primarily used to test the ability of the model to dampen a bar switch.

The second objective (establish the relative importance of the wave forcing and the antecedent morphology on the predicted alongshore variability) was addressed by considering nine periods of 3-year hindcast predictions that started with the annually surveyed profiles between 1987 and 1995. These acted as a reference for sets of 3-year simulations in which either the wave forcing or the initial profiles were modified.

The model was forced with wave data measured in about 18 m depth, 5 km offshore. The initial profiles were taken from the Jarkus database (Wijnberg and Terwindt, 1995) and interpolated onto the computational grid with a resolution of 200 m offshore, gradually decreasing to 2 m across the active part of the profile (above 10 m water depth) without any alongshore averaging.

3.3.1 Model Simulations

The objectives are addressed through a combined analysis of the observed and the predicted barred cross-shore profile development at the surveyed transects within the 6 km study area. The exact period was defined by the survey dates of the Jarkus profiles 3 years apart. The measured wave and water level data corresponding to the simulation periods were directly imposed on the seaward model boundary. Given the alongshore uniform offshore bathymetry (Figure 3.2), we assumed no alongshore variation in the wave conditions. This allowed us to force the models at the considered transects with identical wave forcing time series. These reference simulations were carried out for all (24) survey transects within the 6 km study area.

The effect of modified initial profiles and wave forcing was investigated for three periods in which again all 24 survey transects were included:

A. 1987-1990: besides the presence of the bar switch, it was also selected because it was the most energetic period (see Figure 3.5);
B. 1989-1992: because of the bar switch that was present in the 1989 morphology;
C. 1995-1998: during this period no bar switch was present and it had the least energetic wave forcing (see Figure 3.5).

For each of these periods we performed simulations in which either 1) the starting profiles were kept at 1987 or 1989, but forced with the time series of all the considered periods of the reference simulations or 2) the wave forcing time series was kept at the 1987-1990, 1989-1991 or 1995-1998 periods, but the profiles from 1987 to 1995 were used to initialize the model (see Table 1 for an overview).

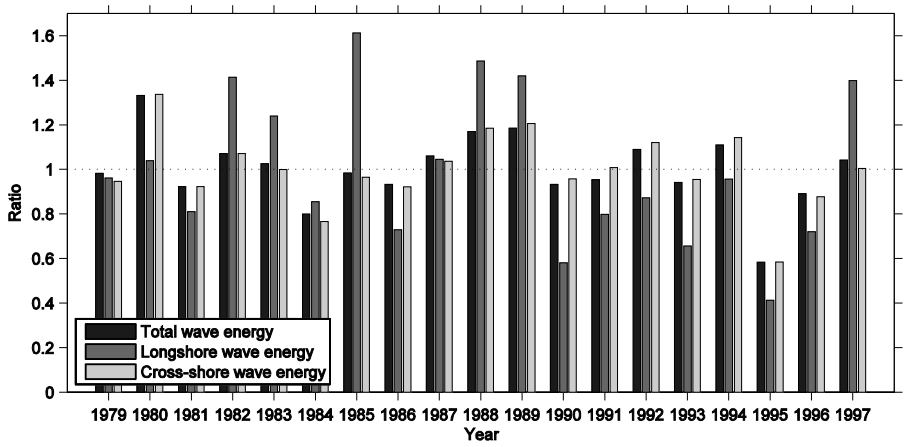

Figure 3.5 *Ratios of the annual mean total, longshore and cross-shore wave energy scaled with the 19 year means (1979-1998). Annual means are based on the period between consecutive annual survey dates.*

The resulting 1176 3-year simulations (see Table 3.1) are analyzed in Section 3.4 by inter-comparing the morphological development and indicators, introduced in Section 3.3.2, that describe alongshore variability. First, the reference simulations covering the 1987-1990 and 1989-1992 periods are evaluated; next, the relative influence of the profile initializations and the wave forcing is investigated by comparing the predicted inter-annual bar morphology for the profile and wave forcing scenarios listed in Table 3.1.

Prior to the steps outlined above we first validated the model for the 1995 to 1998 period (during which bars were alongshore continuous) for which all 24 transects were considered. The model's free parameters were set to the values determined in Walstra et al. (2012) based on a calibration on the 1984-1987 data for a single transect (y=80km) at Noordwijk. The 1995-1998 simulation at the same transect yielded a slightly better performance than was achieved by the original calibration, also classifying the validation result for this transect as "reasonable" according to Van Rijn et al. (2003). Furthermore, application of the model on all transects for the 1995-1998 period resulted in "reasonable" to "good" agreement according to the Van Rijn et al.

(2003) classification with, on average, the highest skill in the northern section of the study area.

Table 3.1 *Overview of the model simulation scenarios.*

Scenario	Profile Initialization Year[1)]	Wave forcing start year[2)]	Number of simulations[3)]
Reference	1987, 1988, 1989, 1990, 1991, 1992, 1993, 1994 , 1995	1987, 1988, 1989, 1990, 1991, 1992, 1993, 1994 , 1995	216
WF1987[4)]	1988, 1989, 1990, 1991, 1992, 1993, 1994 , 1995	1987	192
DP1987[5)]	1987	1988, 1989, 1990, 1991, 1992, 1993, 1994 , 1995	192
WF1989[4)]	1987, 1988, 1990, 1991, 1992, 1993, 1994 , 1995	1989	192
DP1989[5)]	1989	1987, 1988, 1990, 1991, 1992, 1993, 1994 , 1995	192
WF1995[4)]	1987, 1988, 1989, 1990, 1991, 1992, 1993, 1994	1995	192

[1)] All simulations cover the 3-year period between the corresponding survey dates (e.g. 1987 profile initialization represents the simulation from 3-10-1987 to 6-5-1990)

[2)] For scenarios indicated by WF, the length of the simulations is determined by the period of wave forcing time series (e.g. WF1995 was initialized with the 1987 to 1994 profiles, but were always run from 3-7-1995 to 10-8-1998)

[3)] All 24 (Δy=250 m) survey transects between y=78 and 83.75 km were considered.

[4)] WF stands for simulations in which a single wave forcing time series was combined with all the considered profiles.

[5)] DP stands for simulations in which the profiles of a specific year were combined with all considered wave forcing time series.

3.3.2 Indicators of alongshore variability

To evaluate the temporal evolution of the alongshore variability, the alongshore averaged values of the bar crest location, and the water depth above the bar crest, were considered. In case of discontinuous alongshore bars, these indicators may become unreliable or do not fully capture the morphological variability. Therefore, we also utilized the alongshore variability ratio, $\langle F_{3D} \rangle$, which is based on the variance of the profile perturbations (Plant et al., 1999):

$$\langle F_{3D} \rangle = 1 - \frac{1}{N_x} \sum_{x=x_1}^{x=x_{Nx}} \left[F_{2D}(x) \right] \tag{3.3}$$

in which N_x is the number of cross-shore grid points (assuming an equidistant cross-shore distance x). $\langle F_{3D} \rangle$ is the ratio between alongshore non-uniform and total bathymetric variability. A value of 1 implies a fully 3D bathymetry without any alongshore coherence, whereas a value of 0 represent an alongshore uniform bathymetry. In Eq. (3.4) $F_{2D}(x)$ is the cross-shore distribution of the alongshore variability ratio:

$$F_{2D}(x) = \left[\frac{s_{y,t}(x)}{S_{y,t}(x)} \right]^2 \tag{3.4}$$

in which $s^2_{y,t}(x)$ is the temporal variance of alongshore uniform component

$$s^2_{y,t}(x) = \frac{1}{3} \sum_{t=T_i}^{t=T_{i+3}} \left[Z'_y(x,t) \right]^2 \tag{3.5}$$

And $S^2_{y,t}(x)$ is the variance of the profile perturbation averaged in both time and alongshore

$$S^2_{y,t}(x) = \frac{1}{3N_y} \sum_{y=78}^{y=83.75} \sum_{t=T_i}^{t=T_{i+3}} \left[Z'_t(x,y,t) \right]^2 \tag{3.6}$$

T_{i+3} reflects the 3-year duration of the simulations.

3.4 Results

3.4.1 Initiation and decay of bar switches

We discuss two periods (1987-1990 and 1989-1992) during which a bar switch was initiated (1988) that had vanished two years later. First, the simulations starting in 1987 (and ending in 1990) are discussed. Since the bar switch is not present in the 1987 bar morphology, it can be investigated whether the cross-shore processes can initiate a bar switch from relatively alongshore uniform bars. The opposite (i.e. can the model predict the end of a bar switch when it is present in the initial bar morphology) is tested

with the simulations starting in 1989. The basis of the analysis is a comparison of the observed and predicted profile perturbations. Although the simulations at each transect were independent, we combined the predicted profile development into a top view of the perturbations of the 6 km study area.

The initial (1987) and predicted morphological development from 1988 to 1990 are compared with the observations in Figure 3.6. The offshore migration and amplitude growth of the inner bar coincided reasonably well after 1 year (year 1988, compare Figure 3.6b and e). However, the offshore migration of the outer bar was significantly over-estimated. Besides the over-estimated offshore migration of both bars in the following years, X_b (and also h_{Xb}) remained alongshore coherent, in contrast to the observations. In the southern section the outer bar is interpreted as being no longer present as it has decayed considerably, resulting in a relict feature without alongshore coherence. From 1989 to 1990, the former inner bar (which by now had become the outer bar) was predicted to gradually migrate further offshore. The predicted alongshore variability remained approximately constant. As the bar switch had disappeared by 1990 (Figure 3.6d), the final prediction (Figure 3.6g) resembled the observations (Figure 3.6d) fairly well. However, the model completely failed to predict the observed initiation and decay of the bar switch.

Interestingly, similar to the observations, the initial 1989 inner bar switch was almost removed in the predictions (compare Figure 3.7b and e). The transformation of the concave shape of the inner bar at y=81 to 84 km in 1989 to a convex shape in 1990 qualitatively agrees with the observations. In the model this change in plan shape was caused by the alongshore variability in the water depth above the 1989 bar crest, $h_{x,b}$. At the center of the convex shape (y = 82.25 km) the bar was most pronounced (i.e. small $h_{x,b}$) whereas at the distal ends $h_{x,b}$ was initially larger and therefore limited the offshore migration from 1989 to 1990. The alongshore variability of the inner bar was, however, significantly over-estimated. The alongshore variability was predicted to increase with time as the southern section of the bar migrated further offshore and decayed more than the northern section. The enhanced offshore migration in the southern section created accommodation space for a new inner bar, which in 1991 nearly attached to the outer bar at y=80.5km (Figure 3.7f). However, probably due to the absence of alongshore interaction, this connection did not occur during the following year. By 1992 a new bar switch was present in the observations which showed some similarities with the final predicted morphology.

A common finding from both simulation periods is that the model largely maintains the initial alongshore variability throughout the simulations. As a consequence the model fails to predict the observed generation and decay of bar switches. This is investigated further in the following section.

3.4.2 Relative importance of the wave forcing and the antecedent morphology

The predicted alongshore variability for the 1989-1992 period (Figure 3.7) was significantly larger than for the 1987-1990 period (Figure 3.6). Apparently, specific wave forcing combined with the alongshore fluctuations in h_{Xb} present in the initial profiles, amplified the alongshore variability of the bar migration response for the 1989-1992 period, whereas for the 1987-1990 period such a non-linear response appeared to be largely absent. Given the observed variability in both the wave climate (Figure 3.5) and the observed morphology (Figure 3.4), we investigate their relative influence on the predicted alongshore variability in this section.

We first analyze the alongshore variability $\langle F_{3D} \rangle$ for the reference cases and all the profile and wave forcing scenarios outlined in Section 3.3.1. Next, the relative importance of the profile initialization and wave forcing is further investigated by considering the bar morphology in greater detail for a number of specific scenarios.

Comparison with the observed $\langle F_{3D} \rangle$ clearly shows that the reference simulations initialized with profiles that contained bar switches (years of initialization: 1988, 1989 and 1992) persistently over-estimated the alongshore variability (compare black and red lines in Figure 3.8a). In contrast, periods that were initially relative alongshore uniform, but during which a bar switch developed within the 3-year simulation period, under-estimated $\langle F_{3D} \rangle$ (e.g. years of initialization: 1987 and 1991). For periods where the observed alongshore uniformity was approximately constant, there was mostly good agreement in $\langle F_{3D} \rangle$ (e.g. years of initialization: 1990, 1993 and 1994).

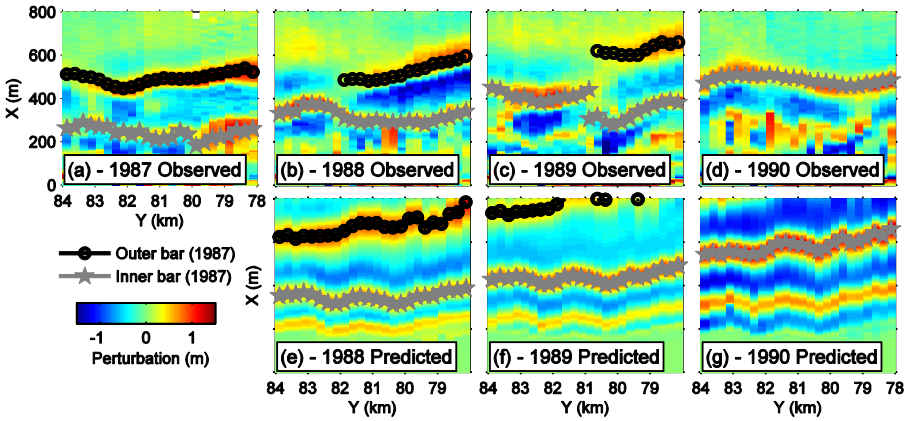

Figure 3.6 *Observed (top row) and predicted (bottom row) profile perturbations from 1987 to 1990, black (grey) line tracks the outer (inner) bar starting from 1987.*

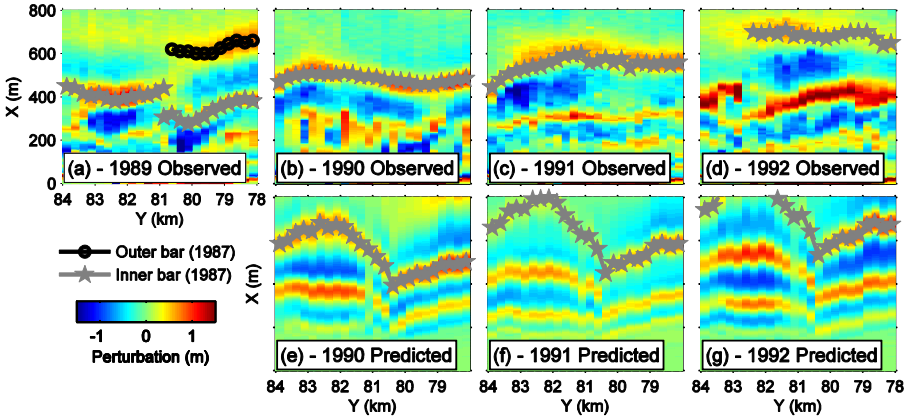

Figure 3.7 *Observed (top row) and predicted (bottom row) profile perturbations from 1989 to 1992, black (grey) line tracks the outer (inner) bar starting from 1987.*

The $\langle F_{3D} \rangle$ values resulting from the DP1987 and DP1989 scenarios (i.e. respectively initialized with the 1987 or the 1989 profiles) were approximately constant with time (blue and green lines in Figure 3.8a) and similar to their respective 1987 and 1989 reference simulations. In contrast, $\langle F_{3D} \rangle$ resulting from the WF-scenarios showed more agreement with the reference simulations (Figure 3.8b). From this we infer that the initial alongshore variability was the primary source of changes in the predicted $\langle F_{3D} \rangle$

whereas the natural temporal fluctuations in wave energy (Figure 3.8c) were of secondary importance.

These findings are investigated further by considering the bar morphology in more detail for a selected number of simulations. To this end, we compare the temporal evolution of the alongshore averaged values of X_b and h_{Xb} ($\langle \Delta X_b \rangle$ and $\langle \Delta h_{Xb} \rangle$) for four simulations of the WF1989 and WF1995 scenarios: the 1989 and 1995 starting profiles both forced with the 1989-1992 and 1995-1998 wave time series. The predicted $\langle \Delta X_b \rangle$ and $\langle \Delta h_{Xb} \rangle$ evolved very similar for identical wave forcing during the first 200 days of the simulations (Figure 3.9a,b). However, $\langle \Delta X_b \rangle$ gradually diverged after about 300 days, and even more so after 500 days. The temporal evolution of $\langle \Delta h_{Xb} \rangle$ remained very similar throughout the simulations with identical wave forcing. As the influence of the modified forcing on the bar amplitude development (not shown) was relatively small compared to the changes in h_{Xb}, the morphological response appears to be dominated by the bars migrating towards a common h_{Xb}. As a consequence, the gradually diverging $\langle \Delta X_b \rangle$ (Figure 3.9a) originated from differences in the lower regions of the 1989 and 1995 bed profiles. The more energetic 1989-1991 wave forcing time series result in a further seaward migration and increased $\langle \Delta h_{Xb} \rangle$. Consistent with Ruggiero et al. (2009) and Walstra et al. (2012), this underlines the importance of h_{Xb} in the bar response.

Despite the clear effect of the wave forcing on the alongshore averaged bar morphology, the alongshore variability of the bar crest positions appeared to be relatively unaffected for alongshore uniform initial profiles (Figure 3.10a-c). In case a bar switch is present in the initial profiles, the alongshore variability was comparable for the bar sections on either side of the bar switch (e.g. north and south of y = 81.50 km Figure 3.10d-f). However, the alongshore averaged bar morphology at each side of the bar switch responded differently to the modified wave forcing. This is further investigated in Figure 3.11, where the offshore bar migration at both sides of the bar switch had a dissimilar response to the modified wave forcing. The southern area experienced an accelerated offshore migration relative to the northern area in case of the more energetic wave forcing (WF1987 and WF1989), whereas such a response was absent for the less energetic wave forcing (WF1995).

3.5 Discussion

Because our model is reasonably accurate in the absence of bar switches, we infer that the increased model-error in the presence of bar switches (e.g. Figure 3.6 and Figure 3.7) is primarily caused by three-dimensional processes, such as flow patterns induced by the alongshore variable morphology which are not accounted for by the model. It is fair to say, however, cross-shore processes also influenced the alongshore variability even to the extent that bar switches were nearly removed when bars at either side of the switch were temporary in a similar phase (Figure 3.10d-f). The water depth above the bar crest, h_{Xb}, was found to be of primary importance as, for a given wave forcing, it largely controlled the bar amplitude and bar migration response. For example, the alongshore variations in h_{Xb} in the 1989 profiles resulted in a non-linear morphological response that considerably increased the alongshore variability of the southern section (y>81 km, see Figure 3.7).

The increased phase differences at either side of the bar switch in the 1988 bathymetry predicted by the WF1987 and WF1989 scenarios were both induced during periods with increased wave action (Figure 3.11). However, during later periods with similar wave forcing such a response was absent. These outcomes show that a specific state of the morphology subjected to a period with energetic wave forcing can result in an alongshore varying response also when only cross-shore processes are considered. Furthermore, taking into consideration that 3D effects (such as rip currents) could further enhance the alongshore variability, we suspect that the generation of bar switches, similar to the findings of Shand et al. (2001), is the outcome of a particular morphological state and wave forcing combination.

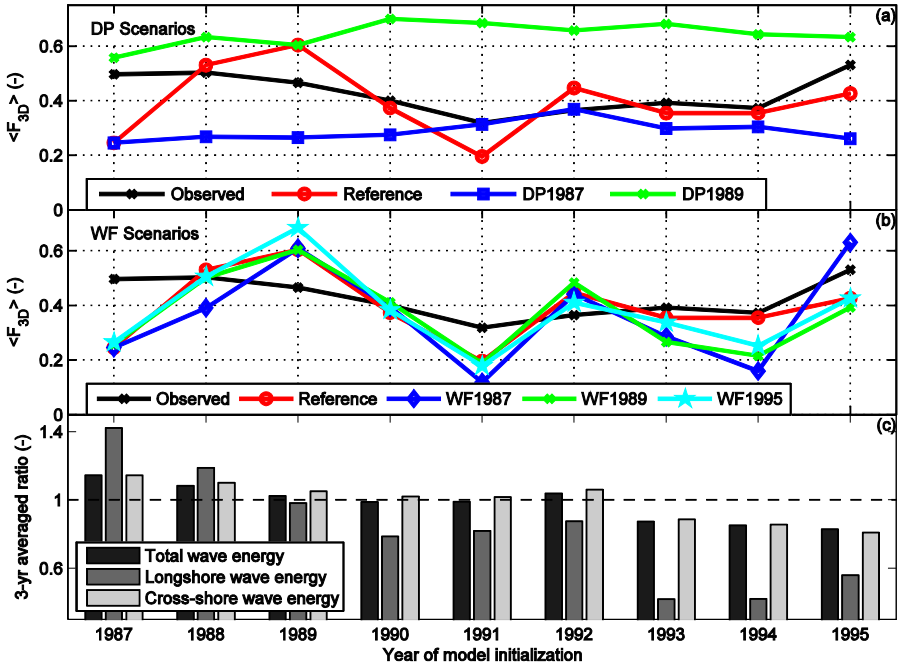

Figure 3.8 *a) Comparison of the alongshore non-uniform variance with observations (black), reference predictions (red), the DP1987 scenario (blue) and the DP1989 scenario (green, see also Table 3.1 for overview of scenarios); b) Comparison of the alongshore non-uniform variance with observations (black), reference predictions (red), the WF1987 scenario (blue), WF1989 scenario (green) and the WF1995 scenario (cyan); and c) the 3-year averaged wave energy ratios relative to the overall average.*

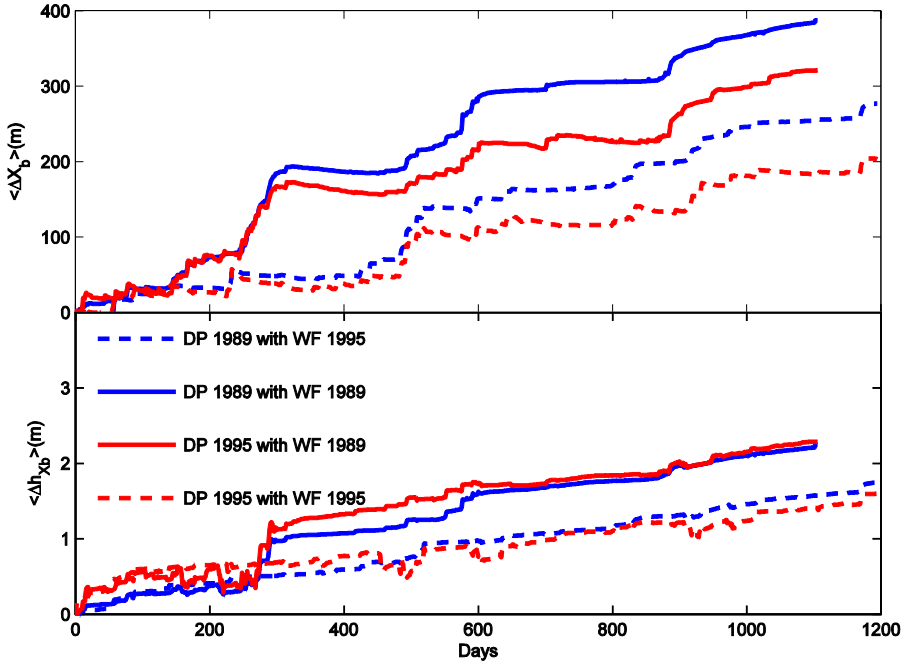

Figure 3.9 *Temporal development relative to the initial value of the longshore averaged (y=78-84 km) (a) outer bar crest positions and (b) the water depth above the bar crest for the reference simulations and simulations initialized with the 1989 and 1995 profiles and imposed with their respective wave forcing time series (WF-scenario, see Table 3.1).*

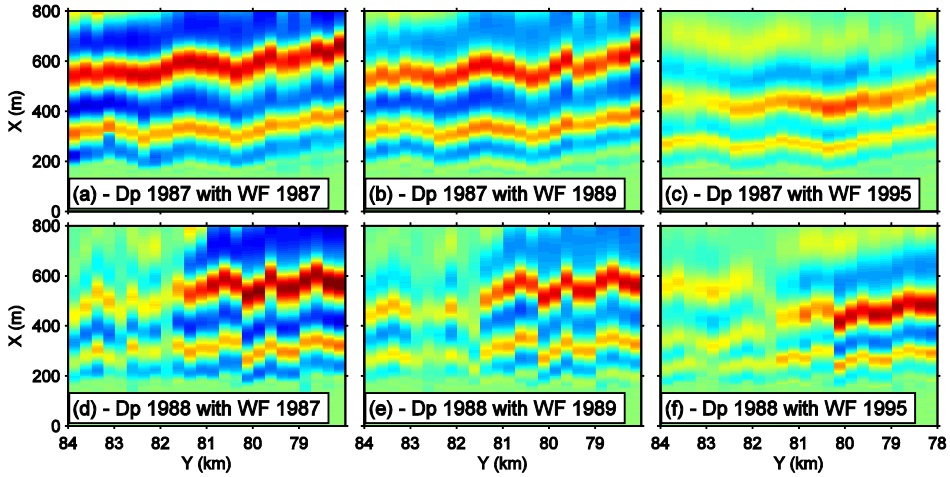

Figure 3.10 *Perturbations of the final predicted morphological development for different combinations of profile initialization and wave forcing time series. Starting from the 1987 (top row) and 1988 (bottom row) profiles imposed with 1987-1990 (left column), 1989-1992 (middle column) and 1995-1998 (right column) wave time series.*

Interestingly, the bar growth in the surf zone and bar decay further offshore deviated for identical wave forcing but different initial profiles. This was especially clear for the WF1995 scenario as the alongshore averaged temporal evolution of the outer bar amplitude (A_b) as a function of h_{Xb} clearly depended on the initial profiles (Figure 3.12c). For the reference situation (i.e. initialization of the model with the 1995 profiles) the width of the barred profile was significantly smaller as the bar decayed at smaller h_{Xb}, whereas the 1987 and 1989 profile initialisations resulted in a very similar behaviour. Also the maximum bar amplitude was about 0.5 m less for the reference case. For other wave forcing time series the differences were less pronounced, but also in these cases the bar morphology was affected for the entire simulation duration (Figure 3.12a,b). From these results it is very clear that the initial profiles in combination with specific wave forcing can result in significantly different bar migration characteristics throughout the 3-year simulation period. It is these differences in bar migration that enhance or decrease the migration characteristics at each side of a bar switch and consequently amplify or dissipate the bar switch feature.

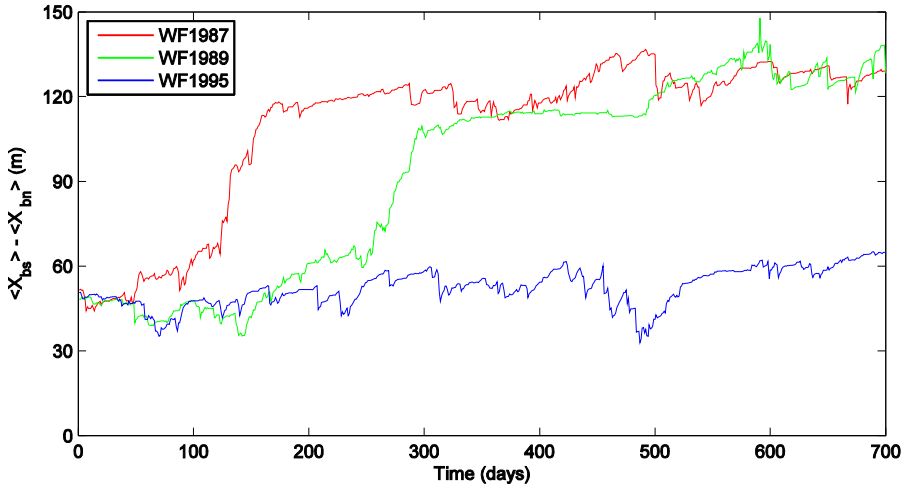

Figure 3.11 *Temporal development of the difference between the alongshore averaged bar position south, $<X_{bs}>$, and north, $<X_{bn}>$, of the bar switch at y=81.50 km for the 1987-1991, 1989-1992 and 1995-1998 wave forcing time series starting from the 1988 profiles.*

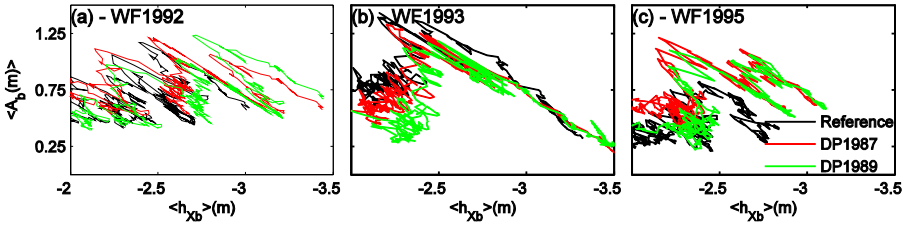

Figure 3.12 *Alongshore averaged bar amplitude, A_b, as a function of the alongshore averaged water depth above the bar crest, h_{Xb}, for various combinations of wave forcing and initial profiles.*

3.6 Conclusions

When alongshore variability is limited, the model predicts offshore migration of the bars at approximately the same rate (i.e. the bars remain in phase). Only under specific bar configurations and high wave-energy levels is an increase in alongshore variability predicted. This suggests that cross-shore processes may trigger a switch in the case of specific antecedent morphological configurations combined with storm conditions However, the model is not able to predict the dissipation of a bar switch, as in contrast to the observed bar behavior, predicted bar morphologies on either side of the switch

remain in a different phase. The alongshore variability is only temporarily reduced when the bars on either side are occasionally located in a similar cross-shore position. The data-model mismatch suggests that three-dimensional processes play a key role in the generation and decay of bar switches. Potentially 3D flow patterns are responsible for: 1) removing a switch by merging the bars when they were at a similar cross-shore position or 2) generating a switch after the alongshore variability was amplified under a specific combination of the bar morphology and energetic wave forcing.

3.7 References

Aagaard, T., Davidson-Arnott, R., Greenwood, B., Nielsen, J., 2004. Sediment supply from shoreface to dunes: linking sediment transport measurements and long-term morphological evolution. *Geomorphology* 60, 205 – 224, doi:10.1016/j.geomorph.2003.08.002

Aagaard, T., Kroon, A., Greenwood, B., Hughes, M.G., 2010. Observations of offshore bar decay: Sediment budgets and the role of lower shoreface processes. *Continental Shelf Research* 30, 1497 – 1510, doi:10.1016/j.csr.2010.05.010.

Castelle, B., Bonneton, P., Dupuis, H., Sénéchal, N., 2007. Double bar beach dynamics on the high-energy meso-macrotidal French Aquitanian Coast: A review. *Marine Geology* 245, 141-159, doi:10.1016/j.margeo.2007.06.001.

Garnier, R., Falqués, A., Calvete, D., Thiébot, J., Ribas, F., 2013. A mechanism for sandbar straightening by oblique wave incidence. *Geophysical Research Letters*, 40, 2726–2730, doi:10.1002/grl.50464.

Grunnet, N.M., Ruessink, B.G., 2005. Morphodynamic response of nearshore bars to a shoreface nourishment. *Coastal Engineering* 52(7), 119-137. http://dx.doi.org/10.1016/j.coastaleng.2004.09.006.

Grunnet, N.M., Walstra, D.J.R., Ruessink, B.G., 2004. Process-based modelling of a shoreface nourishment. *Coastal Engineering* 51(7), 581-607. doi:10.1016/j.coastaleng.2004.07.016

Holman, R.A., Symonds, G., Thornton, E.B., Ranasinghe, R., 2006. Rip spacing and persistence on an embayed beach. *Journal of Geophysical Research*, 111, C01006, doi:10.1029/2005JC002965.

Kuriyama, Y., 2002. Medium-term bar behavior and associated sediment transport at Hasaki, Japan. *Journal of Geophysical Research* 107 (C9), 3132. doi:10.1029/2001JC000899.

Lippmann, T.C, Holman, R.A., 1990. The spatial and temporal variability of sandbar morphology. *Journal of Geophysical Research* 95, 11575–11590.

Ojeda, E., Ruessink, B.G., Guillen, J., 2008. Morphodynamic response of a two-barred beach to a shoreface nourishment. *Coastal Engineering* 55(12), 1185–1196. doi:10.1016/j.coastaleng.2008.05.006

Pape, L., Kuriyama, Y. & Ruessink, B.G., 2010. Models and scales for nearshore sandbar behavior. *Journal of Geophysical Research-Earth Surface*, 115 (F03043).

Plant, N.G., Holman, R.A., Freilich, M.H., Birkemeier, W.A., 1999. A simple model for inter-annual sandbar behavior, *Journal of Geophysical Research – Oceans* 104-C7, pp 15,755–15,776.

Quartel, S., Ruessink, B.G. and Kroon, A., 2007. Daily to seasonal cross-shore behaviour of quasi-persistent intertidal beach morphology. *Earth Surface Processes and Landforms*, 32, 1293-1307. doi: 10.1002/esp.1477.

Ranasinghe, R., Symonds, G., Black, K., Holman, R., 2004. Morphodynamics of intermediate beaches: a video imaging and numerical modelling study. *Coastal Engineering* 51(7), 629–655. doi:10.1016/j.coastaleng.2004.07.018.

Reniers, A.J.H.M., Roelvink, J.A., Thornton, E.B., 2004. Morphodynamic modeling of an embayed beach under wave group forcing, *Journal of Geophysical Research*, 109, C01030, doi:10.1029/2002JC001586.

Ruessink, B.G., Kuriyama, Y., Reniers, A.J.H.M., Roelvink, J.A., Walstra, D.J.R., 2007. Modeling cross-shore sandbar behavior on the timescale of weeks. *Journal of Geophysical Research-Earth Surface* 112 (F3), 1–15. doi:10.1029/2006JF000730.

Ruessink, B.G., Kroon, A., 1994. The behaviour of a multiple bar system in the nearshore zone of Terschelling: 1965–1993. *Marine Geology* 121, 187–197. doi:10.1016/0025-3227(94)90030-2.

Ruessink, B.G., Wijnberg, K.M., Holman, R.A., Kuriyama, Y., van Enckevort, I.M.J., 2003a. Intersite comparison of inter-annual nearshore bar behavior. *Journal of Geophysical Research* 108 (C8), 3249. doi:10.1029/2002JC001505.

Ruessink, B.G., Pape, L., Turner, I.L., 2009. Daily to inter-annual cross-shore sandbar migration: observations from a multiple sandbar system. *Continental Shelf Research* 29, 1663 – 1677, doi:10.1016/j.csr.2009.05.011.

Ruggiero, P., Walstra, D.J.R., Gelfenbaum, G., van Ormondt, M., 2009. Seasonal-scale nearshore morphological evolution: Field observations and numerical modeling. *Coastal Engineering* 56, 1153–1172. doi:10.1016/j.coastaleng.2009.08.003.

Shand, R.D., 2003. Relationships between episodes of bar switching, cross-shore bar migration and outer bar degeneration at Wanganui, New Zealand. *Journal of Coastal Research* 19 (1), 157-170, ISSN 0749-0208.

Shand, R.D., Bailey, D.G., 1999. A review of net offshore bar migration with photographic illustrations from Wanganui, New Zealand. *Journal of Coastal Research* 15 (2), 365-378, ISSN 0749-0208.

Shand, R.D., Bailey, D.G., Shephard, M.J., 1999. An inter-site comparison of net offshore bar migration characteristics and environmental conditions. *Journal of Coastal Research* 15, 750–765.

Shand, R.D., Bailey, D.G., Shephard, M.J., 2001. Longshore realignment of shore-parallel sand-bars at Wanganui, New Zealand. *Marine Geology* 179, 147–161. doi: 10.1016/S0025-3227(01)00223-7.

Van Duin, M.J.P., Wiersma, N.R., Walstra, D.J.R., van Rijn, L.C., Stive, M.J.F., 2004. Nourishing the shoreface: observations and hindcasting of the Egmond case, The Netherlands. *Coastal Engineering* 51, 813-837. doi:10.1016/j.coastaleng.2004.07.011.

Van Enckevort, I.M.J., Ruessink, B.G., 2003a. Video observations of nearshore bar behavior. Part 1: alongshore uniform variability. *Continental Shelf Research* 23, 501–512. doi:10.1016/S0278-4343(02)00234-0.

Van Enckevort, I.M.J., Ruessink, B.G., 2003b. Video observations of nearshore bar behaviour. Part 2: alongshore non-uniform variability. *Continental Shelf Research* 23, 513–532. doi:10.1016/S0278-4343(02)00235-2.

Van Rijn, L.C., Walstra, D.J.R., Grasmeijer, B., Sutherland, J., Pan, S., Sierra, J.P., 2003. The predictability of cross-shore bed evolution of sandy beaches at the time scale of storms and seasons using process-based profile models. *Coastal Engineering* 47 (3), 295–327. doi:10.1016/S0378-3839(02)00120-5.

Van Rijn, L.C., Ribberink, J.S., van der Werf, J., Walstra, D.J.R., 2013. Coastal sediment dynamics: recent advances and future research needs. *Journal of Hydraulic Research* Vol. 51, No. 5, pp. 475–493. http://dx.doi.org/10.1080/00221686.2013.849297

Walstra, D.J.R., Reniers, A.J.HM., Ranasinghe, R., Roelvink, J.A., Ruessink, B.G., 2012. On bar growth and decay during inter-annual net offshore migration. *Coastal Engineering* 60, 190–200. doi:10.1016/j.coastaleng.2011.10.002.

Walstra, D.J.R., Hoekstra, R., Tonnon, P.K., Ruessink, B.G., 2013. Input reduction for long-term morphodynamic simulations in wave-dominated coastal settings. *Coastal Engineering* 77, 57-70. doi:10.1016/j.coastaleng.2013.02.001

Wijnberg, K.M., Terwindt, J.H.J., 1995. Extracting decadal morphological behavior from high-resolution, long-term bathymetric surveys along the Holland coast using eigen function analysis. *Marine Geology* 126 (1–4), 301–330. doi: 10.1016/0025-3227(95)00084-C.

Wijnberg, K.M., Wolf, F.C.J., 1994. Three-dimensional behaviour of a multiple bar system. *Proc. Coastal Dynamics Conf.*, Barcelona, Spain, 59-73.

4 Variability in the inter-annual nearshore sandbar cycles between sites

This chapter is largely based on the article:

Walstra, D.J.R., Wesselman, D.A., van der Deijl, E.C., Ruessink, B.G., 2016. On the intersite variability in inter-annual nearshore sandbar cycles. *Journal of Marine Science and Engineering*, 4(1), 15. doi:10.3390/jmse4010015.

4.1 Introduction

Alongshore sand bars are common features in shallow nearshore coastal environments (water depth typically less than 10 m) with a striking variability in the cross-shore and longshore geometry (e.g. Greenwood et al., 1979; Wijnberg and Kroon, 2002; Ruessink et al., 2003; Zenkovich, 1967). Bars are the net result of cross-shore sediment accumulation resulting from the highly non-linear morphological feedback between the bed profile and nearshore hydrodynamics (e.g. Plant et al., 1999; Walstra et al., 2015). As bars may also influence upper beach morphology (Kroon, 1990; Quartel et al., 2007; Walstra et al., 2014) and are often altered by shoreface nourishments (e.g. van Duin et al., 2004; Ojeda et al., 2008, van der Spek and Elias, 2013), their relevance for coastal managers is evident.

The behavior of (multiple) bar systems has been studied extensively over the past decades. These studies focused on bar behavior at time scales ranging from hours, days and weeks (e.g. Kroon, 1994; Quartel et al., 2007, Ruessink et al., 2007), via months and seasons (e.g. van Enckevort and Ruessink, 2003; Ruggiero et al., 2009; Dubarbier et al., 2015) to years and decades (e.g. Ruessink and Kroon, 1994; Wijnberg and Terwindt, 1995; Shand et al., 1999; Kuriyama, 2002; Walstra et al., 2012, 2014, 2015). Common findings are that bars mostly have a multi-annual lifetime and that up to 5 bars can occur simultaneously in the cross-shore. As the most seaward (outer) bar limits the amount of wave energy by enforcing waves to break, it controls the evolution of the shoreward located (inner) bars (Ruessink and Terwindt, 2000; Ruessink et al., 2003; Walstra et al., 2012). Decay of the outer bar typically initiates a cascaded response in which the next (shoreward) bar experiences amplitude growth and net

seaward migration. This in turn creates accommodation space for its shoreward neighbor and so on, eventually resulting in the generation of a new bar near the shoreline. This offshore directed cyclic character is typically measured by the period between two bar decay events, referred to as the bar cycle return period (T_r).

This T_r can vary markedly at a site and between sites, but the underlying reasons and environmental controls are not well understood (Wijnberg, 2002; Lippmann et al., 1993; Plant et al., 1999; Kuriyama, 2002; Ruessink et al. 2003). Intra-site differences in T_r are typically related to (quasi) persistent 3-dimensional bar behavior referred to as bar switching (e.g. Wijnberg and Terwindt, 1995; Shand et al., 2001). It is defined as bars being alongshore discontinuous, either in a different phase of the bar cycle (Walstra et al., 2015) or with a completely different T_r (Wijnberg and Terwindt, 1995; Plant et al. 1999). For the latter case intra-site differences in T_r can be substantial (exceeding a factor 4) and appears to be continuously present in time (e.g. Wijnberg and Terwindt, 1995), here referred to as a persistent bar switch. Bar switches that separate sections with similar T_r are usually less persistent as alongshore interactions cause bar switches to disappear when the adjacent bars temporarily are in a similar phase (Walstra et al., 2015), here referred to as a non-persistent bar switch.

Wijnberg and Terwindt (1995) were among the first to study the inter-site differences in T_r. To that end they introduced the concept of a large-scale coastal behavior (LSCB) region. It is defined as an area in which the sandbars show similar cross-shore migration (i.e. approximately constant T_r) and exhibit comparable changes in bar morphology over several decades. For the Holland coast (Figure 4.1) the annual surveys of the coastal profiles (Jarkus database) revealed that the transitions between LSCB regions were primarily persistent bar switches. In general, the transitions between LSCB regions were relatively distinct and of limited alongshore length (about 2km). One of the most prominent differences in T_r was found between the area northward of the IJmuiden harbor moles to the Petten Seawall and the area southward of IJmuiden to the harbor moles of Scheveningen (see Figure 4.1). The overall inter-annual bar cycle characteristics are similar for both areas. However, the T_r differ significantly: in the southern area the return period is much smaller (about 4 versus 15 years for the area northwards of IJmuiden). Also the alongshore coherence in offshore bar movement seems to be larger in the southern region (Wijnberg and Terwindt, 1995), that is, there are less non-persistent bar switches.

For the Holland coast Wijnberg (2002) found that changes in decadal coastal behavior were primarily coupled to large man-made structures and alongshore changes in the offshore bathymetry (ebb delta and shoreface terrace). No link could be established with any other investigated environmental variables, such as the sediment composition and wave forcing. A similar change across a man-made structure was also observed at

Duck, NC (USA), where a factor 2 difference in T_r in the areas just north and south of a pier was observed (Plant et al., 1999). Wijnberg (2002) hypothesized that structures inhibit the alongshore interaction between the intersected coastal sections causing an independent evolution that ultimately results in different equilibrium states originating from, for example, small differences in the local wave climate or bed slopes.

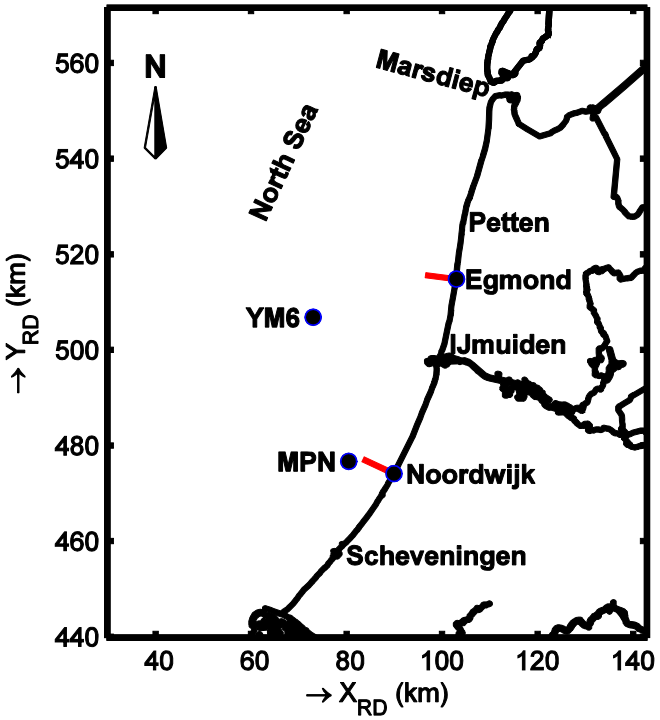

Figure 4.1 *The Holland Coast with the sites at Egmond and Noordwijk indicated, as well as the location of the wave buoys YM6 (IJmuiden Munitie Stortplaats) and MPN (MeetPost Noordwijk). Red lines indicate the considered profiles at Noordwijk and Egmond, XRD and YRD are the 'Rijksdriehoek' coordinates.*

The nearshore bar response is sensitive to initial perturbations in the bed profile and is dominated by the morphologic feedback to the wave- and current fields (e.g. Plant et al., 2001; Walstra et al., 2012; Ruggiero et al., 2009; Van Rijn et al., 2013). The inter-annual bar amplitude response is primarily governed by the water depth above the bar crest, h_{Xb}, and the incident wave angle, θ (Walstra et al., 2012; Dubarbier et al., 2015). As a consequence, the morphological developments do not only depend on the instantaneous small-scale processes; they also incorporate some degree of time history

in profile configuration. Using a process-based profile model (i.e. assuming alongshore uniformity), Walstra et al. (2015) showed that specific initial profile and wave forcing combinations could affect the bar characteristics over the entire inter-annual cycle period. This is qualitatively in line with Wijnberg and Terwindt (1995) and Wijnberg (2002) who hypothesized that regions with different large-scale coastal behavior are controlled by the combined effects of different hydrodynamic forcing, sedimentological constraints (viz. grain size, stratigraphy) and/or morphological constraints (viz. shoreline orientation, shoreface morphology, surf zone morphology). To the best of our knowledge all comprehensive data analysis studies were unable to further detail the (relative) contribution of these parameters and to identify the dominant physical processes that govern the bar cycle return period in different LSCB regions or sites.

Therefore, the present study utilizes a process-based forward model to identify the dominant environmental variables and the associated mechanisms that govern T_r. To that end, the profile model developed in Walstra et al. (2012, 2015) is applied at two locations 42 km apart (Noordwijk and Egmond, located at RSP 38 km and 80 km, respectively; RSP is the Dutch alongshore beach pole numbering system). The sites are located in the LSCB regions just South and North of the IJmuiden harbor moles (Figure 1) with distinctly different bar cycle return periods. The model is utilized to investigate the influence of various environmental parameters on T_r. To that end, a range of model simulations are evaluated by comparing the predicted bar cycle return periods for various combinations of environmental variables from the Noordwijk and Egmond sites. The considered variables comprise the wave forcing (viz. wave height and incident wave angle), sediment size, and various geometric profile properties (viz. bar size, bar location and profile steepness). Subsequently, the underlying processes that predominantly govern T_r are identified. We finalize this chapter with a discussion on the main findings and with the conclusions.

4.2 Environmental settings

Both Noordwijk and Egmond are located along the Holland coast which is enclosed by the Marsdiep inlet in the north and the Rotterdam harbor moles in the south (Figure 4.1). The Holland coast is characterized by sandy beaches and multiple barred near-shore zones (van Rijn et al., 2002). The entire Holland coast is an inlet free, sandy and wave dominated coast, with relatively small alongshore variations in offshore wave height and tide (Wijnberg, 2002). Due to the concave shape of the Holland Coast, the coastline orientation at Egmond (277 °N) and Noordwijk (298 °N) differs by about 21°. Furthermore, the sediment at Egmond is markedly coarser than at Noordwijk (see Table 4.1).

Table 4.1 *Sediment diameters for Egmond and Noordwijk expressed as the 50 and 90 percentile, D_{SS} is the estimated D_{50} of the sediment in suspension, as applied in the model, small cross-shore variations in grain size are ignored.*

Grain size	Noordwijk (μm) (Van Enckevort and Ruessink, 2003)	Egmond (μm) (Van Rijn et al., 2002)
D_{50}	180	265
D_{90}	280	380
D_{SS}	170	240

4.2.1 Cross-shore bed profile characteristics

First, in order to exclude the bar morphology, the time-averaged cross-shore bed profile characteristics are analyzed for both sites. The time-averaged profiles were derived for Noordwijk and Egmond based on the annual profile surveys of the Jarkus database (Wijnberg and Terwindt, 1995) for the period 1965 to 1998. Data from 1999 onwards were excluded because both sites were regularly nourished since that time, e.g. van Duin et al. (2004) and Ojeda et al. (2008). The shoreface (between -18 m and 0 m NAP; NAP is the Dutch datum at approximately mean sea level) is sub-divided into four sections, for each of which we compare the mean slopes in Figure 4.2: the beach section (Section 1) comprises the beachface between the dune foot (3 m NAP) and the mean water level (0m); the upper shoreface (Section 2) the profile between 0 and -8m; the middle shoreface (Section 3) is enclosed by the -8m and -15m depth contour and the lower shoreface (Section 4) is the part of the profile between -15 and -18m. The boundary between the upper and middle shoreface is defined at -8m, because it is the edge of the near-shore zone (van Rijn et al., 2002). Sandbars, and accordingly the temporal variability in sea bed elevation, are significantly reduced (Hinton and Nicholls, 1998) and bars do not occur beyond this depth. The seaward limit of the analyzed profiles is set to -18 m, which corresponds to the water depth at the location of the wave observations at Noordwijk (MPN). As indicated in Figure 4.2, the beach and lower shoreface have similar slopes whereas the upper and middle shoreface are notably steeper at Egmond.

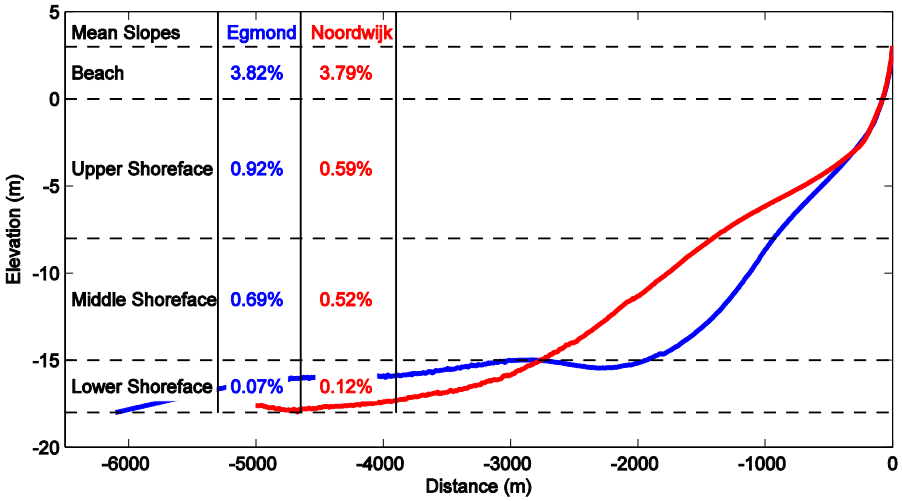

Figure 4.2 *Time-averaged profiles for Noordwijk and Egmond on the same cross-shore axis with the origin for both at NAP 0 m.*

4.2.2 Sandbar characteristics

The sandbars are studied by subtracting the time averaged profile (Figure 4.2) from the actual bed profiles; especially at the upper and middle shoreface the resulting profile perturbations result primarily from the bar morphology. Figure 4.3 shows the profile perturbations for Egmond and Noordwijk for the part of the cross-shore profile at which the bars are prevalent.

Both at Egmond and Noordwijk mostly three bars are present (Wijnberg and Terwindt, 1995; Pape et al, 2010). The positive and negative perturbations indicate the bar and trough regions, respectively. The time stack plots (Figure 4.3a,b) clearly reveal the inter-annual cyclic bar characteristics. That is, bar initiation in the inter-tidal region, gradual offshore migration and amplitude growth and finally gradual decay at the seaward limits of the surf zone. However, the difference in bar cycle return period between both sites is striking. Estimates of T_r, derived earlier with a complex EOF method are 3.9 and 15.1 years for Noordwijk and Egmond, respectively (Ruessink et al., 2003). Furthermore, the bars at Egmond are noticeably wider and higher.

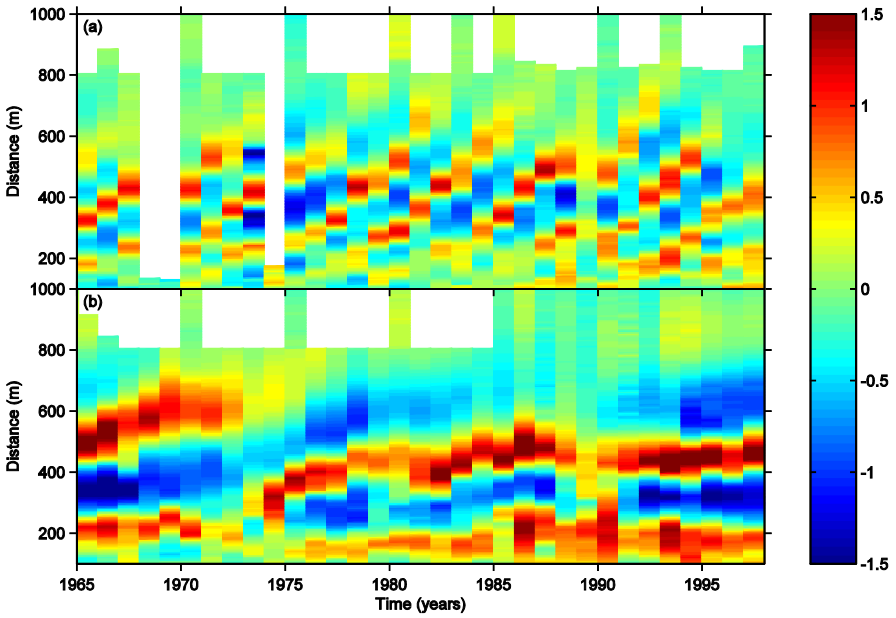

Figure 4.3 *Profile perturbations of the time averaged near-shore profile are shown for a) Noordwijk (RSP 80 km) and b) Egmond (RSP 38 km).*

4.2.3 Wave and tidal characteristics

We considered the period from 1 January 1990 to 31 December 1999 for which detailed hourly and 3-hourly wave observations (root-mean-square wave height H_{rms}, peak wave period T_p and wave direction θ) were available for Noordwijk (Meetpost Noordwijk, MPN; see Figure 4.1 and IJmuiden (about 17 km south of Egmond, Munitie stortplaats, YM6; see Figure 4.1), respectively. To ensure a consistent comparison at the same water depth, the wave conditions at YM6 were converted to the water depth at MPN (from -21 m to -18 m) using Snell's law.

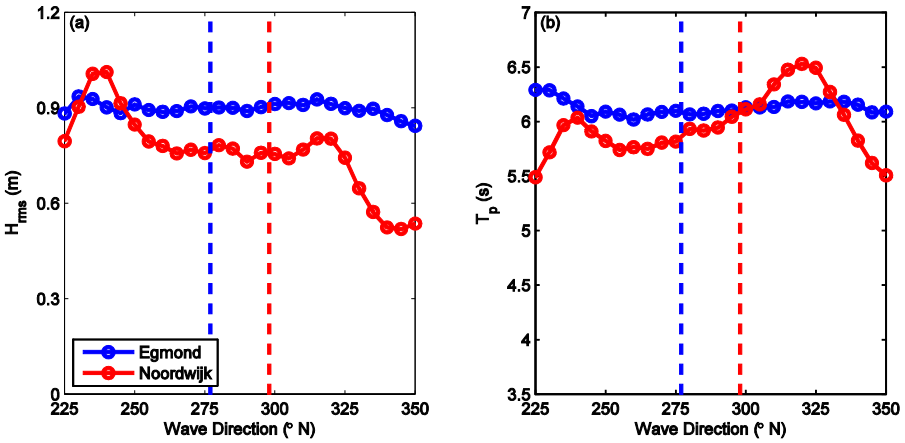

Figure 4.4 *Comparison of the root-mean-square wave height (a) and peak wave period (b) at Noordwijk and Egmond as a function of the incident wave direction, the vertical lines indicate the shore normal orientation for both sites.*

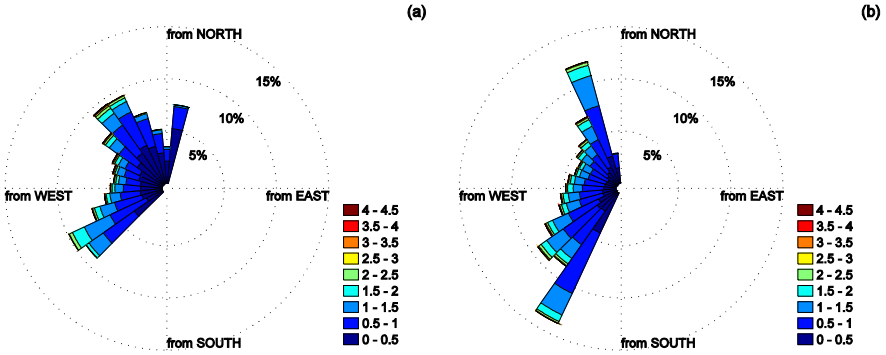

Figure 4.5 *Wave roses of the imposed wave time series at Noordwijk (a) and Egmond (b).*

Figure 4.4a compares the time-mean H_{rms} of Noordwijk and Egmond as a function of θ. Apart from the waves from the southwestern direction, the wave height at Egmond is larger. Especially for the northwestern direction this difference increases as Egmond is more exposed to the North Sea. Differences in the time-mean wave period are relatively small (Figure 4.4b). Storms (H_{rms} > 1.5 m) are predominantly obliquely incident (Figure 4.5) and occur throughout the year, although the fall and winter are usually more energetic than spring and summer (van Enckevort and Ruessink, 2003).

This gives rise to a weak seasonality in H_{rms} (Wijnberg, 2002). In addition, there is some year-to-year variability in the wave climate (Walstra et al., 2015). At Noordwijk, for example, the annual cumulative wave energy can be up to 30% higher or lower than the multi-annual mean, although the differences are usually substantially smaller (Walstra et al., 2015). Also, there is no periodicity in the year-to-year variability.

The tide along the Holland coast is micro-tidal, with a mean tidal range of about 1.6 m. The tidal range decreases slightly in northward direction, which results in a tidal range that is on average about 0.1 m smaller at Egmond than at Noordwijk (Wijnberg, 2002). Tidal currents are generally lower than 1 m/s with little alongshore variations.

4.3 Approach

The main objective is to identify which environmental parameters and processes primarily govern the bar cycle duration. To that end we apply the calibrated Noordwijk model (Walstra et al., 2012) to a profile at Egmond as well. Although profile models typically require a site-specific calibration (e.g. Ruessink et al., 2007), we maintain the Noordwijk model settings in the application at the Egmond site. Only the site specific environmental variables from Egmond are used (i.e., profile, d_{50} and time series of the waves and waterlevels). It is not our aim to achieve an optimal performance at Egmond (i.e. best agreement with the observed inter-annual profile evolution) as long as the model is able to predict a significant difference in T_r between both sites. That will allow us to generate consistent predictions for both sites in which, for example, one specific (known) variable is modified. This approach allows us to identify the influence of the main environmental parameters such as wave height, near shore profile shape and sediment size on T_r. A comparison of two separately calibrated models would hamper such a comparison. Although different model settings will not influence the overall characteristics of the simulated bar morphology (i.e., the net offshore directed cycle), it will affect the magnitude of the morphodynamic response. This will influence the subtle interdependencies between the hydrodynamic forcing and the morphodynamic response, which, in turn, will convolute the analysis of the predictions at both sites. However, as stated earlier, the primary concern is to verify that the predicted T_r at Egmond differs sufficiently (i.e. larger) than at Noordwijk in the reference simulations. Therefore, as a first step, the predictions for both sites are evaluated. Next, the main environmental variables will be interchanged to identify the relative contribution of the wave climates, profiles and sediment size to changes in the bar cycle return period (e.g. the Egmond wave climate is combined with the Noordwijk profile and vice versa). The results of these hindcast simulations and the overall effects of the Egmond and Noordwijk wave climates, profiles and sediment sizes on T_r are discussed in detail in Section 4.4. In Section 4.5 these overall effects are further examined in order to identify the mechanisms and processes that govern T_r. For this,

detailed schematic simulations are conducted and analyzed in which, for example, the influence of the profile slope on T_r is quantified.

This section continues with a description of the hindcast simulations in Section 4.3.1. Finally, the adopted analysis method is briefly discussed in Section 4.3.2.

4.3.1 Hindcast model simulations

The simulations are based on the settings according to the Noordwijk model calibrated for 1980 to 1984 period (i.e. one bar cycle period, see Walstra et al., 2012). As the calibrated model was shown to be valid for other periods at Noordwijk as well (Walstra et al., 2015) and the primary focus of the present study is to investigate the difference between the two sites, we did not perform additional calibration or validation simulations for the Noordwijk and the Egmond model application.

The hindcast simulations have a net duration of about 9.5 years (1990-1999) and were forced with the locally observed (MPN and YM6 stations, see Figure 4.1) hydrodynamic forcing time series for this period for both sites (water levels and wave characteristics). The initial bed profiles were derived from the measured 1990 Jarkus transects (Figure 4.8) and the sediment characteristics are according to Table 4.1.

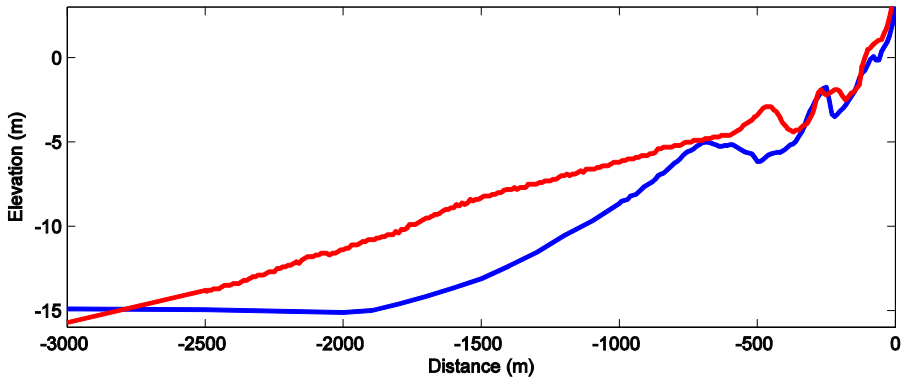

Figure 4.6 *The nearshore part of the initial profiles for Noordwijk (red) and Egmond (blue), the offshore boundary of the model is at x = -6500 m.*

Next, model simulations were performed in which the profile (and sediment diameter), wave climate (wave height, period and angle) for Noordwijk and Egmond were interchanged. Since the sediment size and the profile slope are correlated (e.g. Dean, 1977), we did not consider these separately. This implies that four combinations of wave time series and profile/D_{50} could be evaluated (Table 4.2).

Table 4.2 *Hindcast simulations for Noordwijk and Egmond with interchanged wave forcing and profiles sediment diameter.*

Scenario	Profile & Sediment	Wave Time Series
NN	Noordwijk	Noordwijk
EN	Egmond	Noordwijk
NE	Noordwijk	Egmond
EE	Egmond	Egmond

To investigate whether specific profile characteristics influenced the bar cycle period, we constructed synthetic profiles in which parts of the Noordwijk and Egmond (time-averaged) profiles and bars were combined. These profiles were subsequently used to perform hindcast simulations forced with the wave climates of both sites. We considered combinations of the upper shoreface (upper profile up to 8 m water depth), the middle shoreface (profile between 8 and 15 m water depth) and the lower shoreface (profile deeper than 15 m water depth) from both sites (see Table 4.3 and Figure 4.7). As the sediment size is assumed to be cross-shore constant in the model, it cannot be varied together with the profile sections. The choice of sediment size was therefore associated with the upper shoreface profile as in test simulations it was found that especially these required to be correlated to avoid an unstable or unrealistic profile evolution.

4.3.2 Analysis method

The bar cycle return period T_r was determined by the time it takes a bar to be at the same cross-shore position as its predecessor. Ruessink et al. (2003) showed that the complex EOF analysis is a robust method to derive T_r and it is therefore also used in this study. Complex EOF was preferred over classic EOF because it can capture the migrating sandbar pattern in a single (complex) mode and, as such, allows for a straightforward quantification of spatial and temporal sandbar characteristics, see Ruessink et al. (2003). Classic EOF is restricted to the description of standing patterns and thus requires two modes that contain approximately equal variance to describe migrating sandbars, see Wijnberg and Terwindt (1995). While these two modes can be combined into a complex pair, the technique that produces the complex mode inherently was preferred. An extensive description of complex EOF can be found in Ruessink et al. (2003) and Horel (1984).

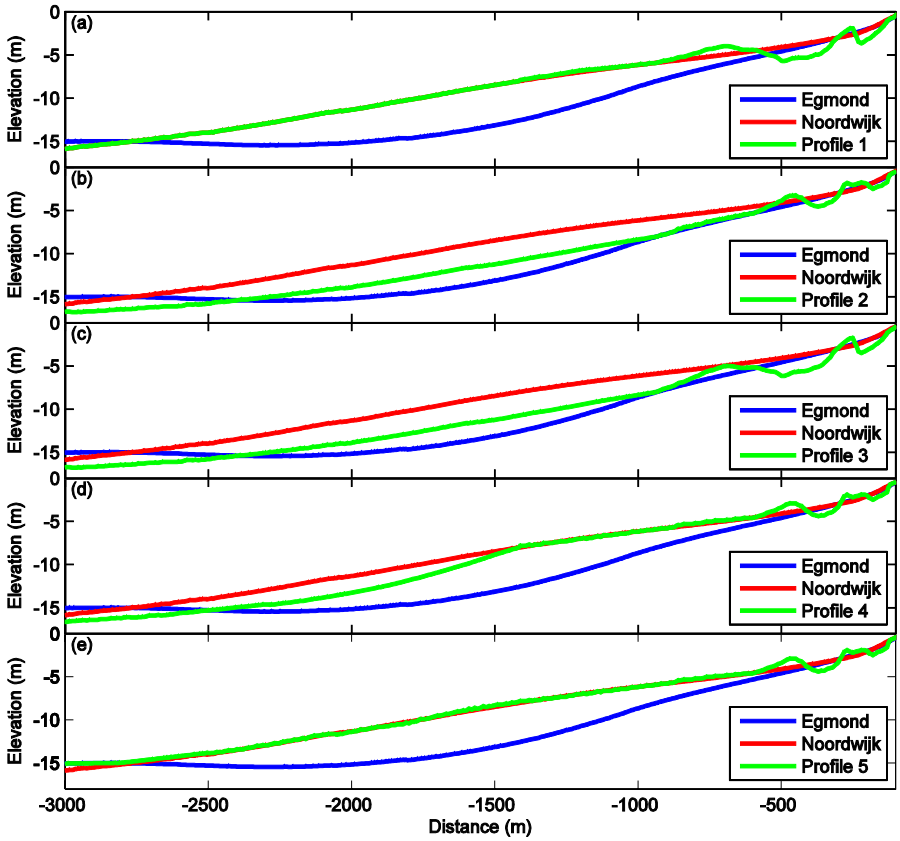

Figure 4.7 *Constructed profiles from part of the Egmond and Noordwijk profiles, see Table 4.3 for profile composition details.*

Table 4.3 *Definition of the profiles constructed from parts of the Egmond and Noordwijk profiles.*

Profile Code	Bar	Shoreface		
		Upper/Sediment	Middle	Lower
1 (ENNN)	Egmond	Noordwijk	Noordwijk	Noordwijk
2 (NENN)	Noordwijk	Egmond	Noordwijk	Noordwijk
3 (EENN)	Egmond	Egmond	Noordwijk	Noordwijk
4 (NNEN)	Noordwijk	Noordwijk	Egmond	Noordwijk
5 (NNNE)	Noordwijk	Noordwijk	Noordwijk	Egmond

4.4 Model Results

First the reference cases for Noordwijk and Egmond are presented. Subsequently, the results of the modified model set ups described in Section 4.3 are discussed by comparing these to the reference case predictions.

4.4.1 The reference cases

From the comparison of the predicted profile development (Figure 4.8) the difference in bar cycle duration stands out immediately. The bar cycle period for Noordwijk (Scenario NN) is 4.8 years which compares well to that derived from the observations for the same period (T_r = 3.9 years). For Egmond (Scenario EE) the predicted T_r of 8.7 years is significantly larger. However, it is still a significant under-estimation of the value derived from the profile surveys (T_r = 15.1 years). Ruessink et al. (2007) showed that the model required a site specific calibration effort on weekly time scales. Given the multi-annual time scales considered in the present study, relatively larger model errors are to be expected as the model was not calibrated to the Egmond site. Since we are primarily interested in identifying the causes for the difference in the bar cycle period, we consider the model performance at Egmond to be adequate since the model predicts a significant difference in T_r between both sites. Furthermore, the short-term response to periods of increased or reduced wave energy is relatively stronger for Noordwijk (i.e. short-term variations around the annual trend are larger at Noordwijk). The difference in T_r primarily originates from the combined effects of a larger annual offshore migration at Noordwijk (averaged offshore migration rate is approximately 55 m/yr compared to 40 m/yr for Egmond) and an approximately 200 m narrower cross-shore bar zone because the bars decay at a relatively shallow water depth.

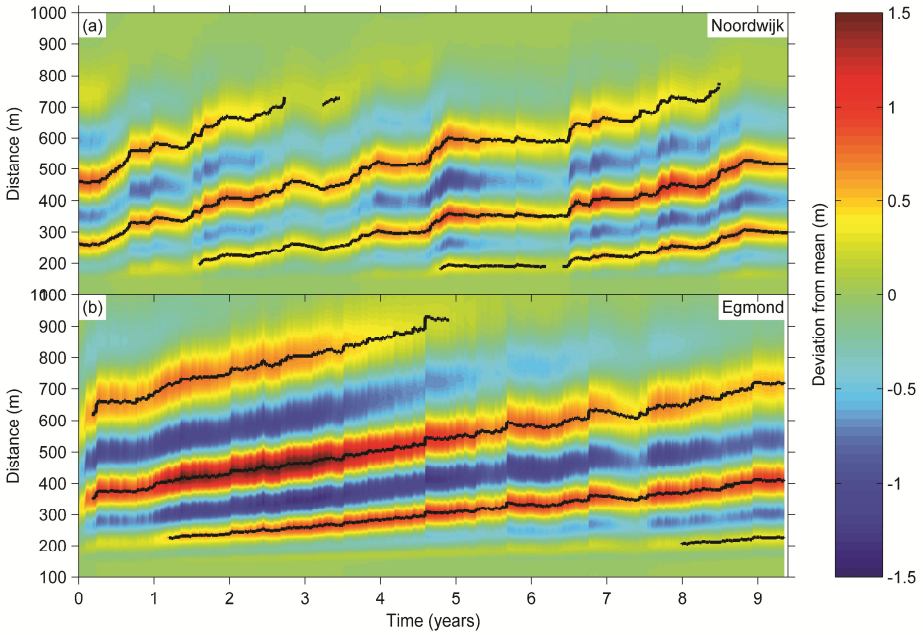

Figure 4.8 *Predicted profile perturbations for a) Noordwijk (Scenario NN) and b) Egmond (Scenario EE).*

4.4.2 Effects of wave climate vs. sediment size & profile

The initial profile and wave climate have a profound impact on the resulting profile evolution (Figure 4.9). Imposing the slightly more energetic Egmond wave climate on the Noordwijk profile (Scenario NE, see Figure 4.6a) results in a 50% reduction of the bar cycle period (Scenario NN, see Figure 4.9a). The opposite occurs when subjecting the Egmond profile to the Noordwijk wave climate (Scenario EN, see Figure 4.9b): the bar cycle period is almost doubled to 14.6 years. Although the Egmond wave climate reduced T_r, the wave climate increases the bar zone width by about 200 m and also results in slightly increased maximum bar amplitude. Due to the increased T_r, the bar zone width is difficult to determine for Scenario EN, but the results seem to suggest that it decreases by at least 100 m. Furthermore, the maximum bar amplitude in this scenario is about 0.5 m less compared to the Egmond reference case (Scenario EE, see Figure 4.6b).

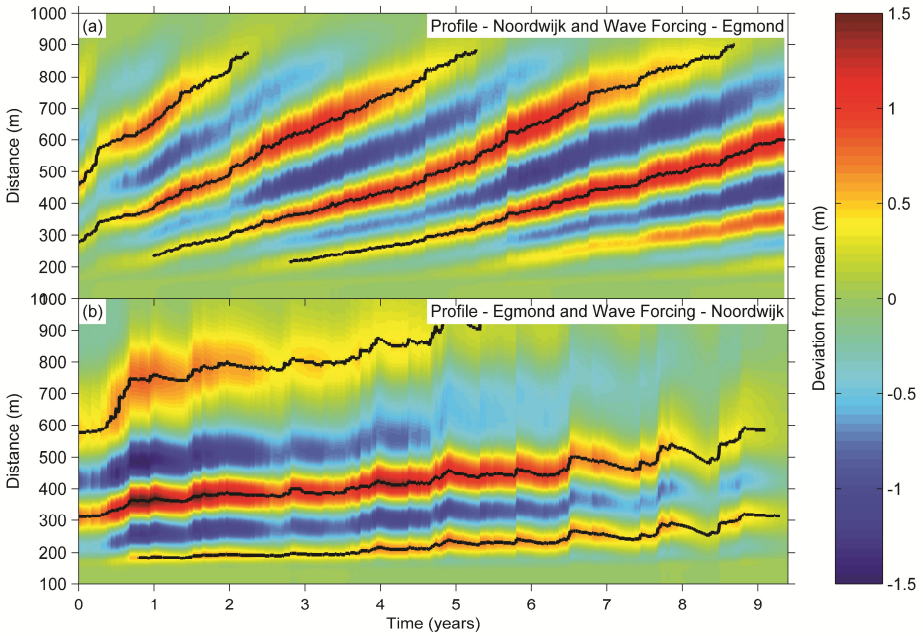

Figure 4.9 *Predicted profile perturbations for scenarios with swapped wave forcing: a) Noordwijk profile with wave forcing from Egmond (Scenario NE) and b) vice versa (Scenario EN).*

Consistent with Ruessink et al. (2003), the energy level of the wave climate appears to influence T_r significantly. However, the effect of the initial profile and bar morphology has an even larger influence. Comparing T_r for the four scenarios (summarized in Table 4.4) an indication of the relative importance of the initial profiles and wave climates can be obtained. The interchange of wave climates results in a change of T_r of about 200% (compare scenarios NN & NE and EE & EN). The influence of the initial profile, bar morphology and sediment size results in a variation T_r of about 300%. For example, the Egmond climate on the Noordwijk profile results in a T_r of 2.4 years compared to T_r = 8.7 years for the Egmond profile.

Table 4.4 *Hindcast simulations for Noordwijk and Egmond with interchanged wave forcing and profiles (and D_{50}).*

Scenario	Profile/Sediment	Wave Conditions	Cycle Period (years)
NN	Noordwijk	Noordwijk	4.8
EN	Egmond	Noordwijk	14.6
NE	Noordwijk	Egmond	2.4
EE	Egmond	Egmond	8.7

4.4.3 Effects of profile slope and bar characteristics

The various profile compositions as summarized in Section 4.3 are used as the starting point for 10 year morphodynamic simulations using the wave and water level time series of both Noordwijk and Egmond as boundary conditions. The predicted return periods are collected in Table 4.5. The table shows the return periods for the composite profiles forced with the Noordwijk and Egmond wave climates as well as the relative change compared to the appropriate hindcast simulations.

Table 4.5 *Bar cycle periods and relative change to reference simulations for the different profile compositions subjected resulting from 10 year simulations for both the Noordwijk and Egmond wave time series. Scenarios between the brackets in columns 4 and 5 are according to Table 4.4. Profile codes in first column according to Table 4.3, indicating the origin of (from left to right): the bar, the upper shoreface (and sediment), middle shoreface and lower shoreface.*

Profile Code	Bar return period, T_r (years) Wave Time Series		Relative change in T_r (-) Wave Time Series	
	Noordwijk	Egmond	Noordwijk	Egmond
1 (ENNN)	6.5	2.8	1.36 (NN)	1.17 (NE)
2 (NENN)	7.0*	6.1	1.46 (NN)*	2.55 (NE)
3 (EENN)	12.9	7.0	0.89/2.69 (EN/NN)	0.80/2.91 (EE/NE)
4 (NNEN)	4.6	2.2	0.95 (NN)	0.90 (NE)
5 (NNNE)	5.1	2.6	1.05 (NN)	1.10 (NE)

*) indicates a simulation for which bar cycle period could not be determined reliably.

Combining the Egmond bars with the Noordwijk profile (profile 1 - ENNN) clearly causes an increased T_r for both wave climates (i.e. compare T_r -values for profile 1 in Table 4.5). Compared to the original Noordwijk profile the increase is about twice as large for the Noordwijk wave climate compared to the Egmond wave climate (1.36 vs. 1.17). However, incorporating the Egmond upper shoreface in the Noordwijk profile

(i.e. bar zone; profile 2 - NENN) has a larger impact. Profile 2 combined with the Noordwijk climate results in a somewhat unrealistic profile evolution for which only a visual estimate of the bar cycle period could be made; however, a clear substantial increase in T_r was present (7 years). For the Egmond wave climate, the relatively steep slope of the Egmond upper shoreface results in a major (2.55) relative increase in T_r.

The comparison of profile 3 (i.e. Egmond bar and upper shoreface combined with the middle and lower shoreface of Noordwijk; EENN) with the original Noordwijk profile simulations shows significantly increased T_r for both wave forcing time series (changes in T_r for profile 3 are 2.69 and 2.91 compared original Noordwijk profile, see Table 4.5). This implies that the combined effect of the upper shoreface slope and bar volume (and sediment size) has the largest effect on T_r of all the considered scenarios by far. The bed slope of the upper shoreface is especially clear for the Egmond wave forcing (i.e. for NENN -only upper shoreface is taken from Egmond- T_r is 2.55 larger than for the complete Noordwijk profile, using the Egmond bar results in an T_r of 2.91). For the Noordwijk wave forcing this is less obvious (T_r respectively 1.46 and 2.69 larger). This is probably due to the unrealistic predictions starting from profile 2 subjected to the Noordwijk wave forcing.

The return periods for profile 3 were reduced by only 10 to 20% relative to original Egmond profile simulations. This implies the effect of the middle and lower shoreface are relatively limited. This is also reflected by Profiles 4 and 5. Interestingly, comparison of the perturbation time stacks revealed that the slope of the upper shoreface also influenced the bar amplitude. This was especially clear for the simulations with Profile 2 in which the bar amplitude rapidly increased to similar values as observed at Egmond (not shown).

In the simulations with the composite profiles the upper shoreface and bar volume appear to contribute about 80% to 90% of the profile induced changes on T_r. The Egmond wave climate reduces T_r by about a factor 2 - 2.5 and is approximately similar for most composite profiles (except for profile 2). The relative influence of the profile and wave climate on T_r are therefore similar as found for the reference simulations (Sections 4.4.1 and 4.4.2).

4.5 The relative influence of environmental parameters on T_r

4.5.1 Introduction

From the evaluation in the previous section it is apparent that the wave climate, profile geometry and sediment size all have a significant effect on T_r. Increased sediment size causes a decrease in sediment transport and T_r (and vice versa). A relatively energetic

wave climate results in an enhanced net bar offshore migration and consequently reduces T_r, whereas relatively large bars and steeper upper shoreface bed slopes have the opposite effect. Of the latter two, it was found in the previous section that especially the upper shoreface bed slope has a major influence on T_r. At first sight this is somewhat counter-intuitive as a steeper slope typically results in more intense wave breaking and consequently enhanced undertow and offshore sediment transport at the bar crest. This is addressed in Section 4.5.2 by comparing outcomes from morphostatic simulations (i.e. no bed updating) for profiles with identical bars in the inner surf zone, but different profile slopes. This approach is extended in Section 4.6 to investigate the influence of the water depth at the bar crest (h_{Xb}) on T_r by considering sets of simulations in which a bar with constant shape is placed at 21 equidistant locations across the barred zone.

4.5.2 Effect of the profile slope on the bar migration rate in the inner surf zone

The effect of the profile slope was further investigated by considering morphostatic simulations (i.e. no bed updating) starting from schematic profiles in which identical bars (with the crest at identical water depth) are combined with bed slopes representative for Egmond and Noordwijk (Figure 4.10) which were subjected to the full 9.5 year Noordwijk wave and water level time series. Detailed comparisons of wave height, undertow and sediment transport at the crest of the bars (location indicated in Figure 4.10) clearly confirmed that, despite the identical wave height at the top of the bar (Figure 4.11a), the undertow (depth-averaged return flow) is indeed larger due to more intense wave breaking at the bar crest for the steeper Egmond profile (Figure 4.11b). The enhanced turbulence levels due to the wave breaking and the increased return flow velocities consequently enhance the offshore sediment transports (Figure 4.11c). Potentially, this would induce an enhanced offshore bar migration.

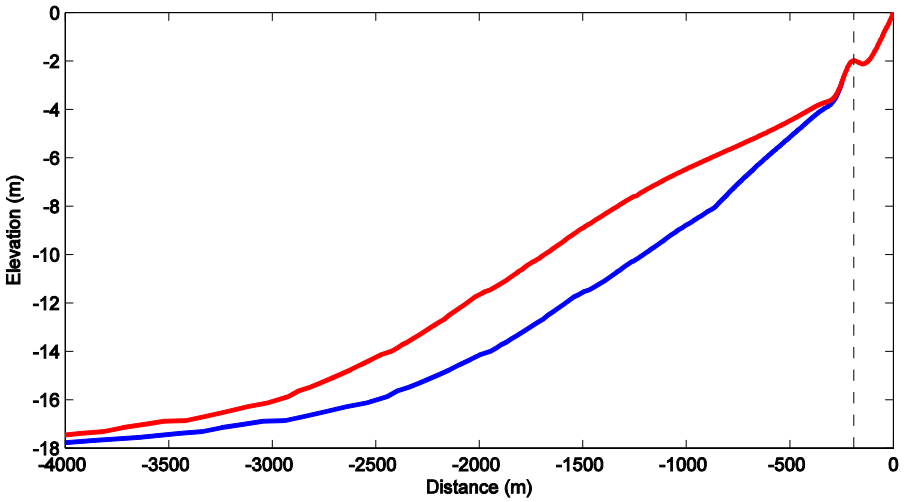

Figure 4.10 *Schematic upper shoreface profiles combined with the middle and lower shoreface profiles for Noordwijk (red) and Egmond (blue) with the same water depth at the bar crest. Vertical dashed line indicates bar crest location at which model predictions are compared in Figure 4.11.*

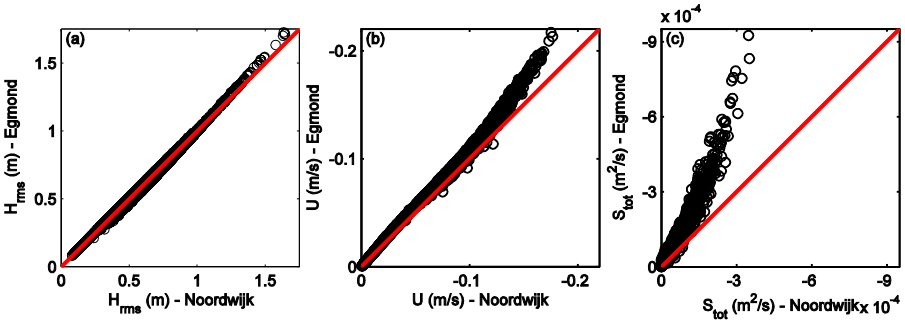

Figure 4.11 *Comparison of the root-mean-square wave height H_{rms} (a), depth-averaged return flow U (b) and total sediment transport S_{tot} (c) at the top of the bar crest Noordwijk vs. Egmond (location shown in Figure 4.10). Red line indicates equality between Egmond and Noordwijk.*

4.6 Identification of the effects of H_{rms}, θ and d_{50} on T_r

In the hindcast simulations this initial response apparently does not result in an increased T_r. Therefore, it is assumed that the cumulative effect of the morphodynamic feedback between the barred profile and the wave forcing primarily governs T_r. In Walstra et al. (2012) the water depth above the bar crest (h_{Xb}) was identified to be a

crucial parameter. Therefore, we need to investigate how h_{Xb} and the morphodynamic feedback loop affects T_r. In other words, how is the offshore migration rate affected as the bar migrates offshore and can we quantify the impact on T_r? To estimate T_r we conduct a set of 1-day simulations starting from plane profiles in which a bar is placed at 21 equidistant locations across the bar zone. In order to exclude the effect of the transient bar amplitude response (i.e. the change from growth to decay as the bar migrates across the surf zone) we considered a bar with a constant shape. For each simulation the daily migration rate and bar amplitude response are determined by considering the change in the horizontal and vertical bar crest position. Subsequently, the daily migration rates are integrated over the set of 21 simulations to estimate the time it takes for a bar to migrate across the bar zone as a proxy for T_r.

By modifying a single environmental variable in each considered set we are able to isolate its influence on T_r. We considered 10 profile slopes ranging from 0.5% to 1% (see Figure 4.12). The same single wave condition as also used in Walstra et al. (2012), viz. H_{rms} = 1.7 m, T_p = 8 s, θ = 20° was applied. Normally a single wave condition is not sufficient to represent the full wave climate (Walstra et al., 2013). However, since we are primarily interested in the relative changes in T_r, the full wave climate is not required. In addition to the profile slope, the wave height and wave direction were also varied with ranges that are representative of the difference in these parameters between Egmond and Noordwijk. The relevant Noordwijk environmental variables were used as a reference. Since in this approach T_r is derived from the initial profile response it will also allow us to isolate the effect of the sediment size (this was not possible in the morphodynamic simulations as unrealistic profiles or instabilities resulted if the upper profile and bar zone were inconsistent with the sediment size).

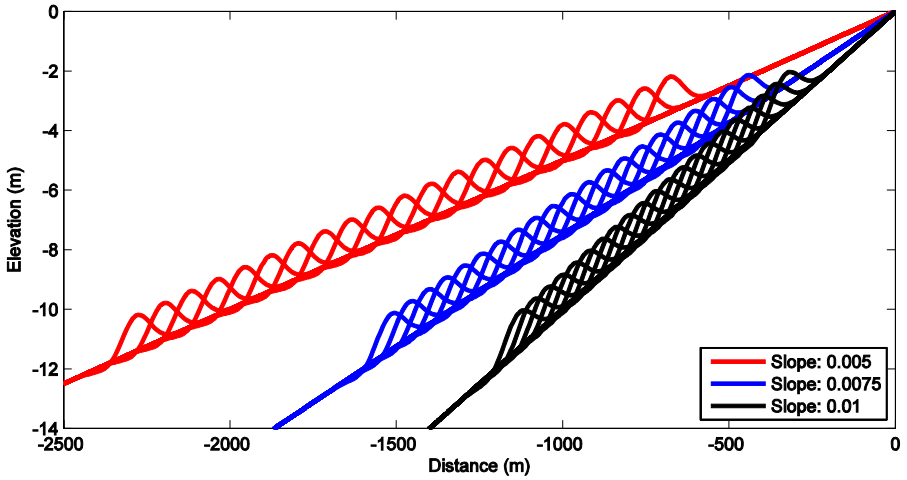

Figure 4.12 *Plane profiles with the 21 schematic bars for 3 of the 10 considered profile slopes. Each bar was subjected to a 1-day simulation with H_{rms} = 1.7 m, T_p = 8 s and θ = 20°, and various additional scenarios.*

The migration rate (dX_b/dt) and bar amplitude response (dA_b/dt) as derived for the set of reference simulations as a function of the bed slope are shown in Figure 4.13 for both h_{Xb} and x. The influence of the bed slope on both dX_b/dt and dA_b/dt is striking. A steeper profile clearly results in an offshore migration of the bar into larger water depths, but in a narrower cross-shore region (compare Figure 4.13a and Figure 4.13b). It clearly illustrates the importance of h_{Xb}: steeper slopes initially induce an increased offshore migration but it quickly reduces as the bar migrates to deeper water. As a result also the cross-shore region at which this offshore migration occurs is narrower. The bar amplitude growth is significantly larger for steeper profile slopes, extends into larger water depths, and also occurs in a relatively narrow region (Figure 4.13c,d). The integrated positive (i.e. offshore) migration rates across the surf zone are used as a proxy for T_r. In this way the varying width of the barred zone (see Figure 4.13b) is included in the analysis.

The predicted T_r are clearly influenced by the bed slope for all the considered scenarios (Figure 4.14a) with a larger T_r for a steeper slope. Despite the larger maximum offshore migration rates (as shown Figure 4.13), the cumulative result is an increased T_r for steeper bed slopes as these high rates only occur in a relatively narrow cross-shore region. This confirms our idea that the morphodynamic feedback loop primarily governs T_r. Comparing the relative change in T_r compared to the averaged value for each series ($T_r/\langle T_r \rangle$, Figure 4.14b), it can be seen that the sensitivity to the bed slope varies. The simulations with increased sediment size, wave angle and a reduced wave

height result in a relatively reduced sensitivity to the bed slope, whereas an increased wave height shows an increased sensitivity.

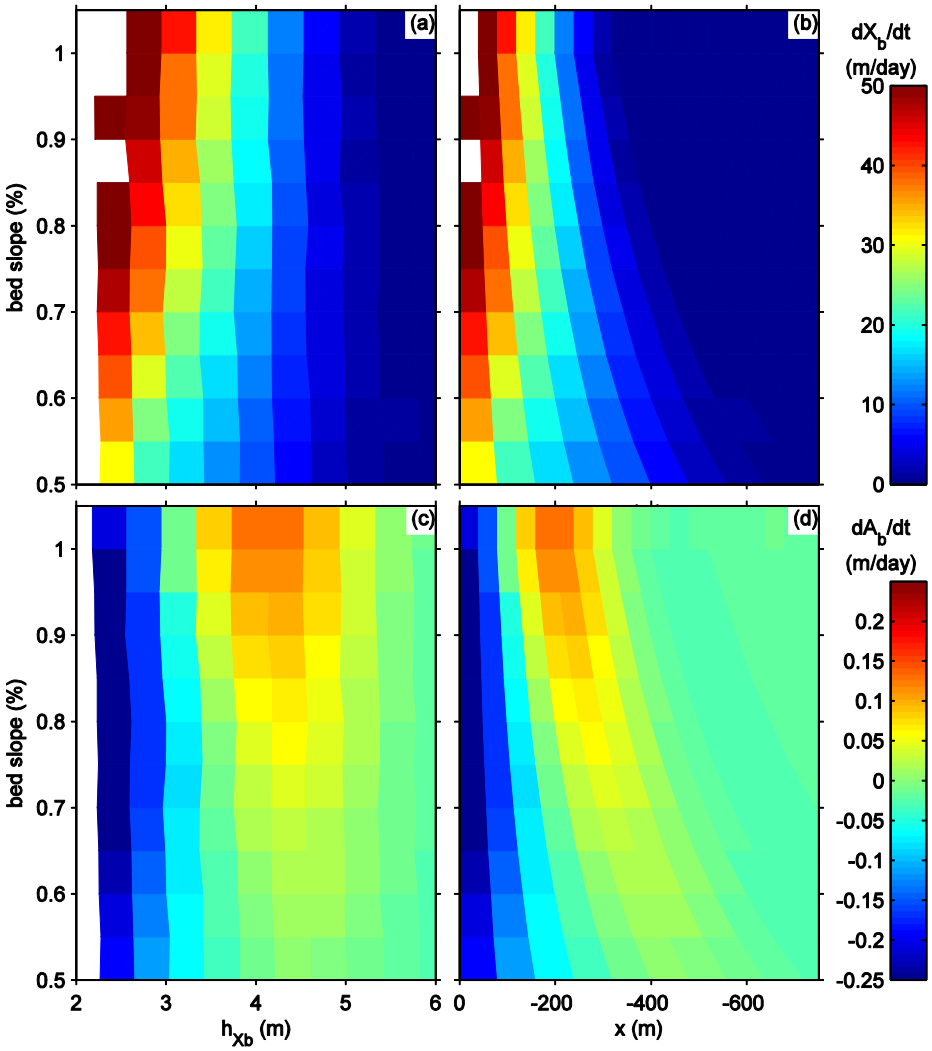

Figure 4.13 *The migration rates, dX_b/dt (a,b) and bar amplitude response, dA_b/dt (c,d) for the reference case as a function of the bed slope plotted with h_{Xb} (a,c) and x (b,d).*

The importance of the bed slope implies that h_{Xb} and the morphodynamic feedback loop primarily govern T_r. Despite more intense wave breaking and an initial enhanced

offshore migration rate, the overall effect of a steeper profile is an increased T_r as it causes:

1) A relatively larger increase in h_{Xb} as a bar gradually migrates offshore which in turn causes fewer waves to break on the bar and consequently reduces the offshore bar migration.
2) Enhanced wave breaking results in relatively larger bars (e.g. see Figure 4.13b) that will also reduce the offshore migration (e.g. compare scenarios ENNN and NN in Table 4.5; see also Shand et al., 1999). Although a larger bar amplitude implies a somewhat smaller h_{Xb} at the same cross-shore location (and T_r), the increase in h_{Xb} as a bar migrates offshore dominates the T_r response.
3) An increased water depth where bar decay sets in due to more intense wave breaking. Combined with the more energetic wave climate this increases the bar zone width at Egmond by about 200 m compared to Noordwijk (as was both observed -Figure 4.2- and predicted -Figure 4.8). Therefore it takes longer for the bars to migrate across this region (e.g. a mean offshore migration rate of 40 m/year would lead to a five year increase in T_r).

4.7 Discussion

The present study has provided a physics-based exploration of the known world-wide differences in bar cycle duration, with a focus on the Dutch sites Noordwijk and Egmond. Although the model underestimated T_r by about 30% for Egmond, the factor 2 difference in T_r relative to Noordwijk is remarkable and provided us with significant confidence to use the model as an exploratory tool. By using identical model settings, the detailed and consistent model predictions allowed us to study the contributions of individual environmental parameters in great detail. Especially the role of the morphological feedback loop in which changes in depth also affect the waves, currents and sediment transport, which in turn influence the profile evolution, could be identified clearly. Due to the importance of the water depth at the bar crest (h_{Xb}), this feedback loop proved to be of major importance to explain the effect of the bed slope on T_r. The complex and highly non-linear interaction between the forcing and the inter-annual bar behaviour can thus result in gradually diverging profile evolution at sites with seemingly very similar characteristics (e.g. profile evolution at either side of the pier at Duck or bar switch, see Plant et al. (1999) and Walstra et al. (2015). Our model results indicate that the inter-annual bar evolution should be regarded as forced behaviour. Despite the non-linearities, the dissipation of wave energy within the nearshore system and the subsequent morphological response can be attributed to the forcing. In our opinion the indications of free (i.e. non-forced) behaviour as identified in some studies (e.g. De Vriend, 1998) are due to the inability in data analysis studies

to couple the observed non-linear response behaviour to the (combined) state of a range of environmental parameters.

The identified dependences of T_r on wave climate, bar size/volume, bar zone width (and depth range) and sediment size are consistent with previous data-based studies of inter-site bar behaviour (e.g. Ruessink et al. 2003 and references therein). The importance of the bed slope on T_r has been suggested in earlier studies (e.g. Shand et al., 1999; Wijnberg, 2002) and our work unraveled the underlying physical processes. In contrast, Ruessink et al. (2003) found that the bed slope did not appear to control inter-site differences in geometric and long-term temporal bar variability. We suspect that the varying influence of the environmental parameters on T_r for different bed slopes (Figure 4.14) and the limited amount of datasets/sites that could be considered in Ruessink et al. (2003) are the primary reasons for this discrepancy.

4.8 Conclusions

Consistent with some earlier findings from field observations, our numerical model simulations illustrate that the bar cycle duration (T_r) is found to be positively correlated with sediment diameter and bar size, while T_r is negatively correlated with the wave forcing and profile slope. The simulations starting from composite profiles in which bar size, profile slope and sediment size were varied, clearly identified that the bed slope in the barred zone is the most important parameter that governs T_r. The sensitivity of T_r to this upper profile slope arises from the importance of the water depth above the bar crest (h_{Xb}) for sandbar response. As a bar migrates seaward, a steeper slope results in a relatively larger increase in h_{Xb}, which reduces wave breaking and subsequently causes a reduced offshore migration rate. Therefore we conclude that the morphodynamic feedback loop is significantly more important than the initially larger offshore bar migration due to the more intense wave breaking in case of a steeper profile slope.

The application of the Egmond instead of the Noordwijk wave climate reduces T_r by a factor 3 to 4. However, the predicted T_r at Egmond is about 2 times larger which is primarily originating from the difference in the upper profile slope and the larger sediment diameter at Egmond. These opposing effects further emphasize the importance of the upper bed slope and sediment diameter on T_r and illustrate that the net offshore bar migration is due to the highly non-linear two-way interaction between the wave forcing and the evolving profile morphology.

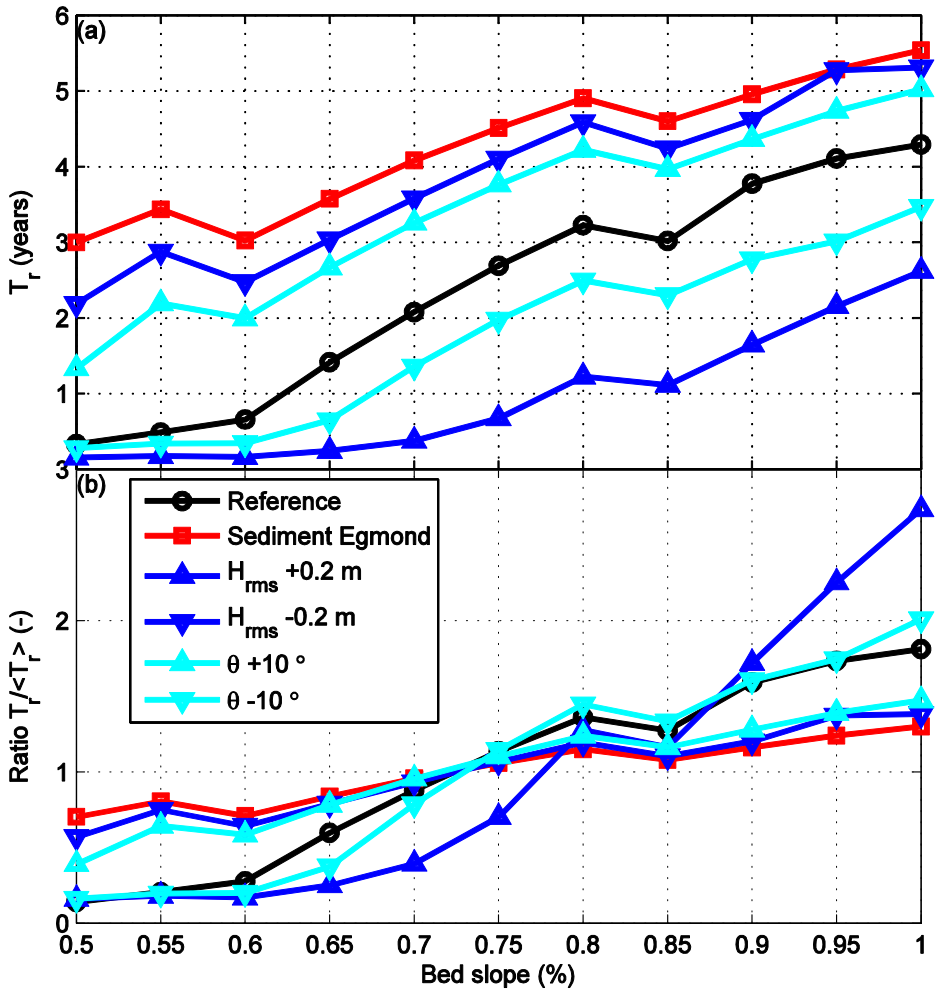

Figure 4.14 *Absolute T_r (a) and the change in T_r relative to the T_r averaged over all considered bed slopes $T_r/<T_r>$ (b) as a function of the bed slope. The reference case is based on the Noordwijk environmental parameters.*

4.9 References

Dean, R.G., 1977. Equilibrium beach profiles: U.S. Atlantic and Gulf coasts, *Technical Report No. 12*, Department of Civil Engineering, University of Delaware.

De Vriend, H.J., 1998. On the predictability of coastal morphology, paper presented at *3rd European Marine Science and Technology Conference*, Eur. Comm., Lisbon, Portugal.

Dubarbier, B., Castelle, B., Marieu, V., Ruessink, B.G., 2015. Process-based modeling of cross-shore sandbar behavior. *Coastal Engineering* 95, 35–50. doi:10.1016/j.coastaleng.2014.09.004.

Greenwood, B., Davidson-Arnott, R.G.D., 1979. Sedimentation and equilibrium in wave-formed bars: a review and case study. *Can. J. Earth Sci*. 16, 312–332.

Guillén, J., Stive, M.J.F., Capobianco, M., 1999. Shoreline evolution of the Holland coast on a decadal scale, *Earth Surface Processes and Landforms* 24, 517–536.

Hinton, C. and Nicholls., R.J., 1998. Spatial and temporal behaviour of depth of closure along the Holland coast. *26th International Coastal Engineering Conference*, ASCE, 2913–2925.

Horel, J.D.. 1984. Complex principal component analysis: theory and examples. *Journal of Climate and Applied Meteorology*, 23, 1660-1673. doi: https://dx.doi.org/10.1175/1520-0450(1984)023<1660:CPCATA>2.0.CO;2

Kroon, A., 1990. Three-dimensional morphological changes of nearshore bar system along the coast near Egmond aan Zee. Proc. of the Skagen symp., *Journal of Coastal Research*, SI 9, 430–451.

Kroon, A., 1994. Sediment transport and morphodynamics of the beach and nearshore zone near Egmond, the Netherlands. *PhD thesis*, Utrecht University, The Netherlands.

Kuriyama, Y., 2002. Medium-term bar behavior and associated sediment transport at Hasaki, Japan. *Journal of Geophysical Research* 107 (C9), 3132. doi:10.1029/2001JC000899.

Lippmann, T.C., Holman, R.A., Hathaway, K.K., 1993. Episodic, non-stationary behaviour of a double bar system at Duck, North Carolina, USA. *Journal of Coastal Research*, Special Issue 15, 49–75.

Ojeda E., Ruessink B.G., Guillen J., 2008. Morphodynamic response of a two-barred beach to a shoreface nourishment. *Coastal Engineering* 55(12): 1185–1196. doi: 10.1016/j.coastaleng.2008.05.006.

Pape, L., Plant, N.G., Ruessink, B.G. (2010). On cross-shore sandbar behavior and equilibrium states. *Journal of geophysical research-Earth surface* 115 (F03008). doi:10.1029/2009JF001644.

Plant, N.G., Holman, R.A., Freilich, M.H., Birkemeier, W.A., 1999. A simple model for inter-annual sandbar behavior, Journal *of Geophysical Research – Oceans*, 104-C7, pp 15,755–15,776.

Quartel, S., Ruessink, B.G., Kroon, A., 2007. Daily to seasonal cross-shore behaviour of quasi-persistent intertidal beach morphology. *Earth Surface Processes and Landforms*, 32, 1293–1307. doi: 10.1002/esp.1477.

Reniers, A.J.H.M., Thornton, E.B., Stanton, T.P., Roelvink, J.A., 2004. Vertical flow structure during sandy duck: observations and modeling. *Coastal Engineering* 51(3), 237–260. doi:10.1016/j.coastaleng.2004.02.001.

Ruessink, B.G., Kuriyama, Y., Reniers, A.J.H.M., Roelvink, J.A., Walstra, D.J.R., 2007. Modeling cross-shore sandbar behavior on the timescale of weeks. *Journal of Geophysical Research-Earth Surface* 112 (F3), 1–15. doi:10.1029/2006JF000730.

Ruessink, B.G., Kroon, A., 1994. The behaviour of a multiple bar system in the nearshore zone of Terschelling: 1965–1993. *Marine Geology* 121, 187–197. doi:10.1016/0025-3227(94)90030-2.

Ruessink, B.G., Terwindt, J.H.J., 2000. The behaviour of nearshore bars on the time scale of years: a conceptual model. *Marine Geology*, 163, 289 – 302. doi:10.1016/S0025-3227(99)00094-8.

Ruessink, B.G., Wijnberg, K.M., Holman, R.A., Kuriyama, Y., van Enckevort, I.M.J., 2003. Intersite comparison of inter-annual nearshore bar behavior. *Journal of Geophysical Research* 108 (C8), 3249. doi:10.1029/2002JC001505.

Ruggiero, P., Walstra, D.J.R., Gelfenbaum, G., van Ormondt, M., 2009. Seasonal-scale nearshore morphological evolution: Field observations and numerical modeling. *Coastal Engineering* 56, 1153–1172. doi:10.1016/j.coastaleng.2009.08.003.

Shand, R.D., Bailey, D.G., Shephard, M.J., 1999. An inter-site comparison of net offshore bar migration characteristics and environmental conditions. *Journal of Coastal Research* 15, 750–765.

Shand, R.D., Bailey, D.G., Shephard, M.J., 2001. Longshore realignment of shore-parallel sand-bars at Wanganui, New Zealand. *Marine Geology* 179, 147–161. doi: 10.1016/S0025-3227(01)00223-7.

Van de Spek, A.J.F., Elias, E.P.L., 2013. The effects of nourishments on autonomous coastal behavior. *Proc. Coastal Dynamics Conf.*, ASCE. 1753–1763.

Van Duin, M.J.P., Wiersma, N.R., Walstra, D.J.R., van Rijn, L.C., Stive, M.J.F., 2004. Nourishing the shoreface: observations and hindcasting of the Egmond case, The Netherlands. *Coastal Engineering* 51, 813–837. doi:10.1016/j.coastaleng.2004.07.011.

Van Enckevort, I.M.J., Ruessink, B.G., 2003. Video observations of nearshore bar behavior. Part 1: alongshore uniform variability. *Continental Shelf Research* 23, 501–512. doi:10.1016/S0278-4343(02)00234-0.

Van Rijn, L.C., Ruessink, B.G., Mulder, J.P.M., 2002. Coast3D Egmond: The Behaviour of a Straight Sandy Coast on the Time Scale of Storms and Seasons, *Aqua Publications*, Amsterdam.

Van Rijn, L.C., Ribberink, J.S., van der Werf, J., Walstra, D.J.R., 2013. Coastal sediment dynamics: recent advances and future research needs. *Journal of Hydraulic Research* Vol. 51, No. 5, pp. 475–493. http://dx.doi.org/10.1080/00221686.2013.849297

Walstra, D.J.R., Reniers, A.J.H.M., Ranasinghe, R., Roelvink, J.A., Ruessink, B.G., 2012. On bar growth and decay during inter-annual net offshore migration. *Coastal Engineering* 60, 190–200. doi:10.1016/j.coastaleng.2011.10.002.

Walstra, D.J.R., Hoekstra, R., Tonnon, P.K., Ruessink, B.G., 2013. Input reduction for long-term morphodynamic simulations in wave-dominated coastal settings. *Coastal Engineering* 77, 57-70. doi:10.1016/j.coastaleng.2013.02.001.

Walstra. D.J.R., Brière, C.D.E., Vonhögen-Peeters. L.M., 2014. Evaluating the PEM passive beach drainage system in a 4-year field experiment at Egmond (The Netherlands). *Coastal Engineering* 93, 1–14. doi:10.1016/j.coastaleng.2014.07.002.

Walstra, D.J.R., Ruessink, B.G., Reniers, A.J.H.M., Ranasinghe, R., 2015. Process-based modeling of kilometer-scale alongshore sandbar variability. *Earth Surface Processes and Landforms* 40, 995–1005. doi:10.1002/esp.3676.

Wijnberg, K.M., 2002. Environmental controls on decadal morphologic behaviour of the Holland coast. *Marine Geology* 189, 227–247. doi:10.1016/S0025-3227(02)00480-2.

Wijnberg, K.M., Terwindt, J.H.J., 1995. Extracting decadal morphological behavior from high-resolution, long-term bathymetric surveys along the Holland coast using eigen function analysis. *Marine Geology* 126 (1–4), 301–330. doi: 10.1016/0025-3227(95)00084-C.

Wijnberg, K.M., Kroon, A., 2002. Barred beaches. *Geomorphology* 40, 103–120. doi:10.1016/S0169-555X(02)00177-0.

Wijnberg, K.M., Wolf, F.C.J., 1994. Three-dimensional behaviour of a multiple bar system. *Proc. Coastal Dynamics Conf., Barcelona*, Spain, 59–73.

Zenkovich, V.P., 1967. Processes of Coastal Development, *Oliver and Boyd*, White Plains, N.Y.

5 Input reduction for long-term morphodynamic simulations in wave-dominated coastal settings

This chapter is largely based on the article:

Walstra, D.J.R., Hoekstra, R., Tonnon, P.K., Ruessink, B.G., 2013. Input reduction for long-term morphodynamic simulations in wave-dominated coastal settings. *Coastal Engineering*, 77, 57–70. doi:10.1016/j.coastaleng.2013.02.001.

5.1 Introduction

Over the last decades process-based models have shown the capability to predict realistic evolution of coastal morphology in applications covering time scales ranging from years (e.g. Jones et al., 2007; Elias et al., 2006; Brown and Davies, 2009; Ruggiero et al., 2009; Tung et al., 2012; Walstra et al., 2012), decades (e.g. Lesser, 2009; Hibma et al., 2005) to centuries and even millenia (e.g. van der Wegen and Roelvink, 2008; Dastgheib et al., 2008). In such models morphology evolves because of the feedback between the hydrodynamics (waves and currents), sediment transport and the morphology itself. Most of these studies have considered a limited number of forcing conditions to avoid excessive computation times. The influence of the adopted input reduction method (i.e. derivation of a reduced set of representative conditions that accurately approximates the long-term morphological evolution, De Vriend et al., 1993) was usually not addressed. Input reduction tends to be based on the representation of a specific target such as the annual transports along a coast or through an inlet (e.g. Van Duin et al., 2004; Lesser, 2009), or on the direct simplification of forcing times series whilst maintaining its relevant statistical properties (e.g. Southgate, 1995; Chesher and Miles, 1990; Brown and Davies, 2009). Clearly, any input reduction involves a number of choices, but their effect on the predicted morphological evolution is often not considered.

The ultimate evaluation of an applied input reduction method should be based on a comparison of the long-term predicted morphology using the reduced and the full set of

conditions. Southgate (1995) was among the first to systematically study the effect of modified forcing by systematically varying the wave forcing time series in process-based profile model simulations covering a four month period, in this way focusing on wave chronology effects. Interestingly, he found that the order in which sequences with high waves were incorporated in the time series did not significantly affect the model predictions; whether this was also the case in a reduced wave climate was not investigated. Based on medium-term brute forcing simulations (i.e. simulations forced with measured time series) for an inlet system covering 5 years with various reduced wave and tidal climates, Lesser (2009) concluded that wave-climate reduction was the largest source of error. Curiously, Lesser (2009) found a cruder wave climate (i.e. based on less wave conditions) to yield the best results (i.e. closest to brute forcing prediction). Although Lesser's (2009) study covered multiple years, the considered 5-year length was relatively short given the cycle duration inherent to such inlets of typically several decades to centuries. To our knowledge input reduction aiming to reproduce coastal morphology on time scales similar to an inherent (quasi)-cyclic variation has not yet been performed and is the topic of this paper.

The objective of the present study is to investigate the influence of input reduction techniques on the wave-driven morphological evolution of nearshore sandbars on the time scale of years, i.e. on the time scale of their quasi-cyclic offshore-directed behavior. For this we utilize the process-based cross-shore model Unibest-TC (Ruessink et al., 2007) on two sites (Noordwijk, The Netherlands and Hasaki, Japan) for which calibrated long-term brute force models are available (Walstra et al., 2012; Pape et al., 2010) that can act as a reference to evaluate the predictions using reduced wave forcing. We start off by introducing an input reduction framework (Section 5.2). The framework is then applied to both sites to evaluate the impact of the input reduction derived from morphological predictions generated by a range of reduced wave climates (Section 5.3). Section 5.4 discusses the results and the implications for long-term modeling. Finally, conclusions can be found in Section 5.5.

5.2 Approach to input reduction

5.2.1 Concepts of input reduction and implications for long-term modeling

Two basic choices are available to derive the reduced set of forcing conditions that enable deterministic long-term predictions. The first option is to reconstruct (or aggregate) time series of measured wave forcing with a limited number of representative conditions to maintain the same pattern of wave chronology (e.g. Brown and Davies, 2009). The second option becomes available if wave chronology can be ignored, implying the selected representative conditions can be combined in ascending,

descending or arbitrary order into a synthetic time series (e.g. Van Duin et al., 2004, Grunnet et al., 2004, 2005).

Besides chronology effects, the choice between reconstructed or synthetic time series is also governed by the morphological modeling approach. Brown and Davies (2009) utilized a model that simulates the morphology directly from the divergence in sediment transports originating from the hydrodynamic forcing. However, to increase the computational efficiency, a number of techniques have been developed which accelerate or upscale the morphology (Roelvink, 2006). The so-called "online" or "MorFac"-approach (Lesser et al., 2004 and Ranasinghe et al., 2011) is now one of the most commonly applied methods (e.g. Geleynse et al., 2010, 2011; Edmonds and Slingerland, 2010; van der Wegen and Roelvink, 2008; Dastgheib et al., 2008; Jones et al., 2007). This method directly scales the calculated depth change by a constant (*MF*) factor, so that after a simulation over a hydrodynamic period *T* we have in fact modeled the morphological changes over *MF***T*. Here we also use the MorFac-concept to illustrate the implications input reduction may have on the morphodynamic modeling approach.

Reconstructed time series are appropriate for simulations using a constant *MF*-value; however, the maximum allowable *MF* is typically governed by the high-energy events in the time series (Jones et al., 2007), as these induce the largest morphological response. For storm conditions, *MF* is typically set to 10-20, but for moderate conditions *MF* can be O(100) without affecting the quality of the predictions (Ranasinghe et al., 2011). Because moderate and low conditions occupy the majority of time, the application of a varying *MF* significantly reduces the computational time. However, the transition between conditions with a different *MF* requires the settling of all suspended sediment to the bed prior to the activation of the next condition followed by a spin-up to let the hydrodynamics (and sediment transports) re-adjust to the next condition before bed-updating can be re-activated in order to avoid mass balance errors. Therefore, a straightforward application of reconstructed time series with varying *MF* is typically less efficient than the application of a constant *MF*.

Synthetic time series do not require the selected conditions to be split up into short duration events. This can significantly reduce the number of transitions between conditions (*NoT*), therefore making synthetic time series more appropriate for varying *MF* applications. Application of synthetic time series (with reduced *NoT*) combined with varying *MF* has the potential to significantly increase the computational efficiency (typically, a varying *MF* -combined with a synthetic time series- reduces the computation time by at least a factor 2 compared to synthetic forcing with constant *MF*).

5.2.2 Input reduction framework

Input reduction essentially aims at selecting a limited number of conditions with which the morphological prediction obtained with the original time series is accurately reproduced (de Vriend et al., 1993). Therefore, it is not our aim to reproduce or maintain the statistical properties of the full wave climate since an accurate reproduction of the coastal morphology is the primary objective. Here a framework is introduced in which all the issues related to input reduction are addressed in a number of analysis steps:

1. Selection of the input reduction period,
2. Selection of the representative wave conditions,
3. Sequencing of the selected conditions,
4. Determine the wave climate duration.

For reconstructed time series only steps 1 and 2 are relevant (e.g. sufficient for constant *MF* applications); all four steps need to be applied for synthetic time series (required for varying *MF* applications). We now further explain each step in more detail, applications are found in Section 3.

Step 1. Selection of the reduction period.

The reduction period is defined as the length of the measured brute forcing time series that is used to reduce the input. The upper limit of the reduction period, T_R, is primarily governed by the time scales related to the inherent morphological (quasi)-cyclic variation. The annual time scale is typically the lower limit to ensure that the seasonal variations in the wave climate are included. In general T_R should be multiples of one year to avoid seasonal bias; however, if variability on smaller time scales need to be maintained (e.g. if a seasonal response dominates the long-term morphology), shorter reduction periods are appropriate. Following Southgate (1995) this could result in a forcing time series in which several reduced wave climates with shorter T_R are sequentially combined.

Step 2. Selection of the representative wave conditions.

The selection of the representative wave conditions is usually based on a weighted average of the frequency of occurrence aggregated over the observed wave conditions

$$F_{rep,j} = \frac{\sum_{i=1}^{n} f_i F}{\sum_{i=1}^{n} f_i} \tag{5.1}$$

where F represents the wave height, period or direction, f is the frequency of occurrence of the wave conditions i and n is the number of wave conditions within the aggregated wave height, period and/or direction bin. The wave period can also be related to the wave height (if a strong correlation exists) to reduce the number of independent parameters (Roelvink and Reniers, 2011).

The representative conditions are determined by grouping the observed wave conditions (i = 1, 2, .., n) enclosed by the bin boundaries (e.g. $F_{rep,j}$ is based on all wave conditions within each bin j, indicated by the squares in Figure 5.1b). The representative wave condition $F_{rep,j}$ is weighted with the cumulative frequency of occurrence, $f_{rep,j} = \sum_{i=1}^{n} f_i$.

To account for non-linear effects (i.e. the non-linear dependence of sediment transport on wave height), the representative root-mean-square wave height, H_{rms}, conditions can also be determined as

$$H_{rms,rep,j} = \left(\frac{\sum_{i=1}^{n} f_i H_{rms,i}^{p}}{\sum_{i=1}^{n} f_i} \right)^{\frac{1}{p}} \tag{5.2}$$

where p is the power to which the sediment transports are assumed to be related to the wave height. Typically p is set to 2 to 3 (see e.g. Roelvink and Reniers, 2011).

Both equidistant (i.e. constant bin-size) and non-equidistant binning (varying bin-size) of the wave conditions were considered. In the non-equidistant binning method, bin sizes are chosen such that weights of the representative conditions are similar (Benedet et al., 2016). First, the direction bins are chosen such that the weighted wave conditions are evenly distributed, next the same procedure is followed for the wave height within each direction bin. Here, we use p=1 for the equidistant binning and p=2 for the non-equidistant binning.

The difference between equidistant and non-equidistant binning is illustrated in Figure 5.1. Equidistant binning, in Figure 5.1b with intervals of 1 m and 30º for H_{rms} and θ (the offshore incident wave angle with respect to the shore-normal), respectively, results in non-equal representative weights $f_{rep,j}$ (indicated by the colors of the bins). By varying the bin sizes such that the representative weights are approximately equal (notice the more evenly distributed weighting colors in Figure 5.1c compared to Figure 5.1b), small bin sizes result for levels where wave

conditions are frequent (and vice versa). Notice, furthermore, that the representative wave conditions (indicated by the red circles) are not in the bin centers as the wave selected wave conditions are not evenly distributed over the bins. The reconstructed time series are rebuilt observed time series in which each observation is converted to the representative condition of the bin that it falls within. In Section 5.3 the optimum bin sizes are iteratively established by evaluating morphological predictions forced with time series reconstructed from the observations based on the reduced wave climates.

Step 3. Sequencing of the selected conditions.

As the morphological response to time-varying forcing is usually non-linear, the sequence in which the wave conditions are imposed potentially influences or may even dominate long-term predictions. In the case of synthetic time series it is therefore essential to investigate to what extent wave chronology influences the long-term morphological evolution. This is also related to step 1 as chronology effects smaller than the reduction period are destroyed in synthetic time series (e.g. seasonal fluctuations are removed in synthetic time series based on T_R=1 yr). Therefore, a range of predictions resulting from synthetic time series with different sequencing options are evaluated in Section 3. To that end, a reduced wave climate resulting from step 2 is systematically and randomly sequenced into a number of synthetic forcing time series. The systematically sequenced time series are constructed by arranging the representative wave conditions in ascending or descending H_{rms} and arranging θ in positive or negative directions. This results in 8 possible combinations (schematically shown in Figure 5.1b), the wave height sequence is indicated by A (ascending) and D (descending) whereas the wave direction sequence is indicated by P (positive direction) and N (negative direction). For example wave sequence DP implies that first the wave heights are sequenced by starting at the top row and then ordering θ within this row from left to right, whereas for wave sequence PD the conditions are sequenced by starting at the left column and subsequently ordering H_{rms} within this column from top to bottom. Furthermore, five randomly sequenced time series are considered in Section 5.3.

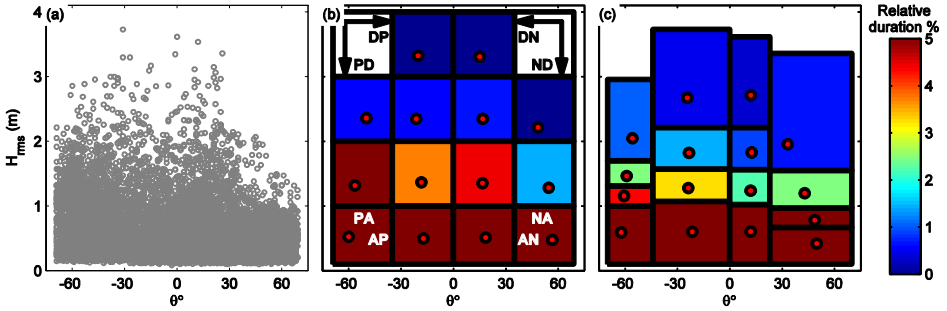

Figure 5.1 *Comparison of (b) equidistant and (c) non-equidistant binning based on (a) the measured conditions; colors indicate the relative duration; red circles represent the representative wave conditions.*

Step 4. Determine the wave climate duration.

The wave climate duration, T_{wc}, is defined as the length of the synthetic time series containing all the selected conditions:

$$T_{wc} = \sum_{j=1}^{N} f_{rep,j} \frac{T_R}{N_R} \tag{5.3}$$

in which N is the total number of selected conditions that comprise the reduced wave climate and N_R is the number of times the reduced wave climate is repeated. Thus N_R equals 1 in case the representative wave climate is applied on the same time scale as the observed time series it was based on.

As was highlighted in Section 5.2.1, the computational efficiency increases significantly if the synthetic time series can be lengthened and coupled to increased *MF* as this reduces *NoT*. However, T_{wc} can affect the morphological prediction as the morphological response depends on both the magnitude and the duration of the forcing. For example, increasing T_{wc} could result in an over-estimated storm response for infrequent storm events (or vice versa). Conceptually, this imposes both upper and lower limits to T_{wc}. An indication of the lower limit is estimated by applying the randomized time series approach (Southgate, 1995). It is determined by evaluating morphodynamic simulations forced with time series in which the observed conditions are randomly re-arranged. These random time series are generated by splitting the observed time series into a number of segments of constant length, and randomly re-ordering these segments. T_{wc} is compared to the segment length by considering the condition with the lowest frequency of occurrence of the reduced wave climate: $f_{rep,\min} * T_{wc}$ The lower

limit of T_{wc} is based on the shortest segment length for which still an acceptable prediction (skill) results. The upper limit of T_{wc} is iteratively established by evaluating the morphological predictions resulting from synthetic time series composed with a range of T_{wc} (i.e. evaluation of multiple synthetic time series in which N_R is varied).

Because the randomized time series approach preserves the wave properties of the original time series (i.e. all wave conditions of the full sequence are still considered) it can also be used to assess the applicability of synthetic time series (i.e. model performance of synthetic time series simulations cannot exceed the maximum skill of the randomized time series approach).

Conceptually, a limited reduction in the number of wave conditions (step 2) makes the sequencing of the conditions (step 3) less critical and vice versa and also affects the optimal climate duration (step 4). Because cyclic morphodynamic sandbar behavior is governed by the interplay between episodic storms and prolonged calm periods (e.g. Walstra et al., 2012), it is essential that a reduced wave climate preserves the associated response mechanisms. It is especially challenging to preserve the storm response in a reduced wave climate due to its intermittent character. Above considerations and the non-linear response of the coastal morphology to the magnitude and duration of the forcing are of major importance in all input reduction steps and therefore inhibit a straightforward step by step application of the input reduction framework. Instead, it is envisaged that the input reduction steps should be repeated a number of times to establish an optimal wave climate. The optimal wave climate implies a minimization of *NoT* which is determined by the number of conditions (*NoC*) from step 2 and T_{wc} (identified by N_R, see Eq. (5.3)) from step 4 as

$$NoT = NoC * N_R - 1 . \tag{5.4}$$

The optimal reduced wave climate should result in a prediction that still agrees well with the brute forcing based simulation.

To evaluate the effect of input reduction we compare the resulting model predictions (z_{red}) with the reduced wave forcing to the model prediction based on the brute forcing time series (z_{full}). Following Lesser (2009) and Ranasinghe et al. (2011) we define the performance of the reduced set of wave conditions by using a cumulative skill score *R* (Ruessink et al., 2007) and employing z_{full} as reference

$$R(t) = 1 - \frac{\varepsilon_{red}^2(t)}{\varepsilon_{full}^2(t)} \tag{5.5}$$

with

$$\varepsilon_{red}^2(t) = \sum_{x=x_1,t=0}^{x=x_{end},t=t} \left(z_{red}(x,t) - z_{full}(x,t) \right)^2 \tag{5.6}$$

and

$$\varepsilon_{full}^2(t) = \sum_{x=x_1,t=0}^{x=x_{end},t=t} \left(z_{full}(x,t) - z_{full}(x,t=0) \right)^2 . \tag{5.7}$$

An R of 1 implies a perfect match in predicted morphological evolution between the reduced and full set of wave conditions. An R less than 1 indicates a difference between both simulations. In Eqs. (5.6) and (5.7) x refers to cross-shore distance, and the $x_1 - x_{end}$ range is the barred part of the profile.

5.2.3 Test cases

We apply the input reduction framework on two sites (Noordwijk, The Netherlands and the Hasaki Oceanographic Research Station (HORS), Japan) for which calibrated long-term brute force predictions were available (Walstra et al., 2012; Pape et al., 2010) that act as a reference to evaluate $z_{red}(x,t)$ found by the reduced wave climates. In both studies the calibrated model predictions compared favorably to the observed morphological evolution. To enable a consistent comparison we applied the same model (Unibest-TC, Ruessink et al., 2007) as in the brute force predictions using identical model settings without morphodynamic upscaling (i.e. MF = 1). The brute forcing for Noordwijk contains 3 hourly observations for wave height, period and direction, whereas for Hasaki daily observations of wave height and period were available. However, no wave direction was measured at Hasaki; therefore Pape et al. (2010) used a constant direction of 30º relative to the coast normal which was also applied in the present study in both the brute forcing and the reduced wave climates.

Both Noordwijk and Hasaki are characterized by a double sandbar system that propagates offshore on the time scale of years (Wijnberg and Terwindt, 1995; Kuriyama et al., 2008). At Noordwijk the cycle from bar inception in the swash zone to bar decay in the outer surf zone region takes about 3 - 4 years (Figures 2a,c). There appears to be no direct link between specific wave events and the bar cycle duration, see also Ruessink et al. (2009). Storms cause a noticeable offshore migration, but the magnitude of the response is small relative to the width of the barred part of the cross-shore profile. The bars at Hasaki exhibit similar behavior, but with a cycle period in the

range of 1 to 4 years it is substantially more variable than at Noordwijk (Figures 2b,d). This is primarily caused by the fact that outer-bar decay (i.e. the end of a cycle) usually sets in after a storm event (Kuriyama et al., 2008; Pape et al., 2010). From Figures 2b,d it can be seen that two distinct bar cycles were present in the considered period. After about 200 days the initial outer-bar decayed followed by a period of about 250 days during which a new bar developed whilst gradually moving offshore. After 450 days a stormy period caused the outer bar to migrate beyond the location where the previous bar decayed. Following Ruessink et al. (2009), we classify bar dynamics at Hasaki as episodic net offshore migration (NOM) and the Noordwijk bar dynamics as inter-annual NOM. The contrasting sensitivity to individual wave events and hence chronology was our main motivation to include both sites in this study.

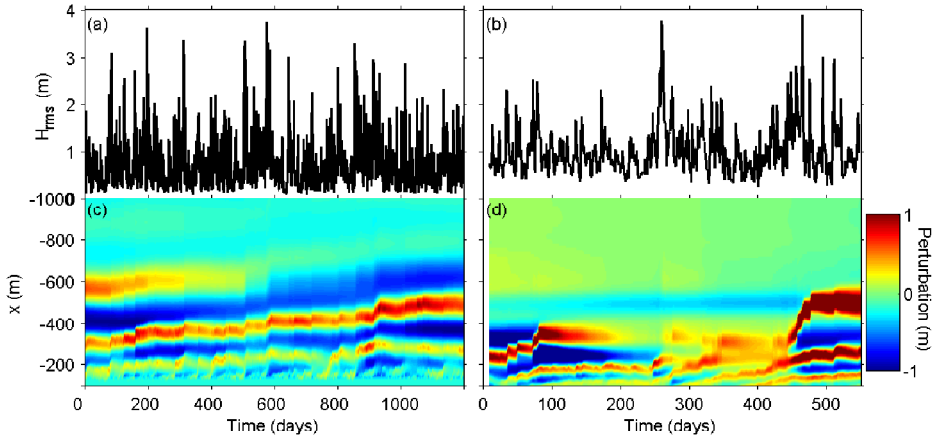

Figure 5.2 *Time series of (a,b) offshore root-mean-square wave height H_{rms} and (c,d) time stacks of brute forcing based predictions of the profile perturbations (i.e. deviations from the time mean profile) at Noordwijk (left) and Hasaki (right). In (c,d) warm colors correspond to sandbars, cold colors to troughs.*

5.3 Application

5.3.1 Step 1. Selection of the reduction period

Based on the observed cycle periods we used ~4 years at Noordwijk and ~1.5 years at Hasaki as reduction periods. This corresponds to the length of the time series in the brute force simulations for both sites.

5.3.2 Step 2. Selection of the representative wave conditions

For Noordwijk, representative H_{rms}, T_p and θ were determined by applying Eq. (5.1) with equidistant bins for all combinations of 2, 4, 8 and 16 H_{rms}-bins (respectively ΔH_{rms} = 2, 1, 0.5 and 0.25 m) with 2, 4, 7 and 14 θ-bins (respectively Δθ= 70°, 35°, 20° and 10°). Two non-equidistant wave climates were also evaluated: 4 and 8 H_{rms}-bins combined with 4 non-equidistant θ-bins (Figure 5.3). All the reduced wave climates were subsequently converted to reconstructed time series. Figure 5.4 compares some of the reconstructed H_{rms} time series with the observations and reveals that ΔH_{rms}=1.0 m still represented the high energy events fairly well; however, the moderate wave conditions were poorly represented when ΔH_{rms} was larger than 1 m. This was confirmed by the correlation coefficient, *r*, between the reconstructed and observed H_{rms}, T_p and θ time series (Table 5.1). ΔH_{rms}=2.0 m resulted in a significantly reduced correlation compared to ΔH_{rms}=1.0 m. For θ, *r* seemed to be fairly insensitive to bin size which was probably caused by the fact that the time series only contained wave directions within ±70° relative to the shore normal. The non-equidistant binning resulted in a comparable *r* for both 4 and 8 H_{rms}-bins.

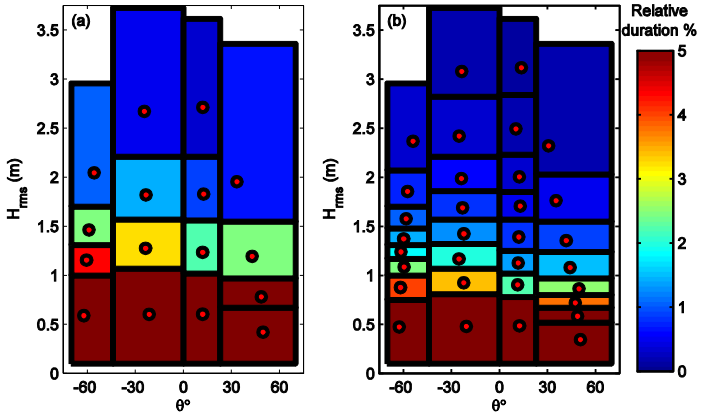

Figure 5.3 *The non-equidistant (a) 4x4$_{NEQ}$ and (b) 8x4$_{NEQ}$ wave climates for Noordwijk. Colors indicate the relative duration (%); red circles represent the selected wave condition in each bin.*

The model performance appeared to be rather insensitive to the chosen bin sizes (Table 5.2), above certain bin size thresholds. The skill *R* was high for all combinations of $\Delta H_{rms} \leq 1$ m and $\Delta\theta \leq 35°$. For ΔH_{rms}=2.0 m the final profile did not contain any bars and the inter-tidal area had accreted unrealistically, see Figure 5.5a and Figure 5.7b. While ΔH_{rms}=0.25 and 0.5 m resulted in near perfect agreement with the reference run (*R*=0.99, see Table 5.2), ΔH_{rms}=1.0 m maintained the bars, but slightly underestimated

offshore bar migration (R=0.92, see Figure 5.7a). Varying $\Delta\theta$ hardly influenced the predictions for $\Delta\theta \leq 35°$ (Figure 5.5b), but with $\Delta\theta=70°$ the outer bar migrated too far offshore. The temporal evolution of the R-values (Figures 6a,b) reveals that the model performance was high throughout the simulation period for ΔH_{rms}<1m. The largest bin size (ΔH_{rms}=2 m and $\Delta\theta$ =70°) had considerably lower R throughout the simulation (see Figure 5.6b). For ΔH_{rms}=2 m and $\Delta\theta=70°$ R was low irrespective of the bin size for $\Delta\theta$ and ΔH_{rms}, respectively. Non-equidistant binning only improved R for 4 H_{rms}-bins (Table 5.2), while for 8 H_{rms}-bins R was high for both types of binning.

For Hasaki we considered 4 and 8 H_{rms} equidistant and non-equidistant bins, respectively. The correlation between the reconstructed H_{rms} time series and the observations was approximately similar to Noordwijk (compare Table 5.3 with Table 5.1). The reconstructed T_p time series had much lower correlations, primarily caused by the presence of swell (high T_p) and sea waves (low T_p) at Hasaki. Therefore, we also analyzed 2 and 4 T_p-bins (ΔT_p resp. 5 and 2.5 s) with the equidistant 4 H_{rms}-bins. This improved the correlation between the reconstructed T_p time series and the observations considerably (see Table 5.3). Despite the improved correlation, the morphological predictions only improved slightly (R increased from 0.83 to 0.86, see Table 5.4). Apparently our model was only weakly sensitive to a more detailed T_p forcing. On the whole, the skill for Hasaki was lower compared to Noordwijk, which was also confirmed by a comparison of the predicted profiles (Figure 5.5c). The temporal evolution of R (Figure 5.6c) was comparable for the first 250 days (i.e. during the first bar cycle). The model performance then gradually reduced for the remainder of the simulation with a distinct further reduction after about 420 days, related to a series of storm events causing a major offshore migration of the outer bar which was not captured by the reconstructed time series simulations (compare Figure 5.2b with Figure 5.7c, which is consistent with findings from Ruessink and Kuriyama, 2008). With all reconstructed time series the model underestimated this migration causing the overall low R.

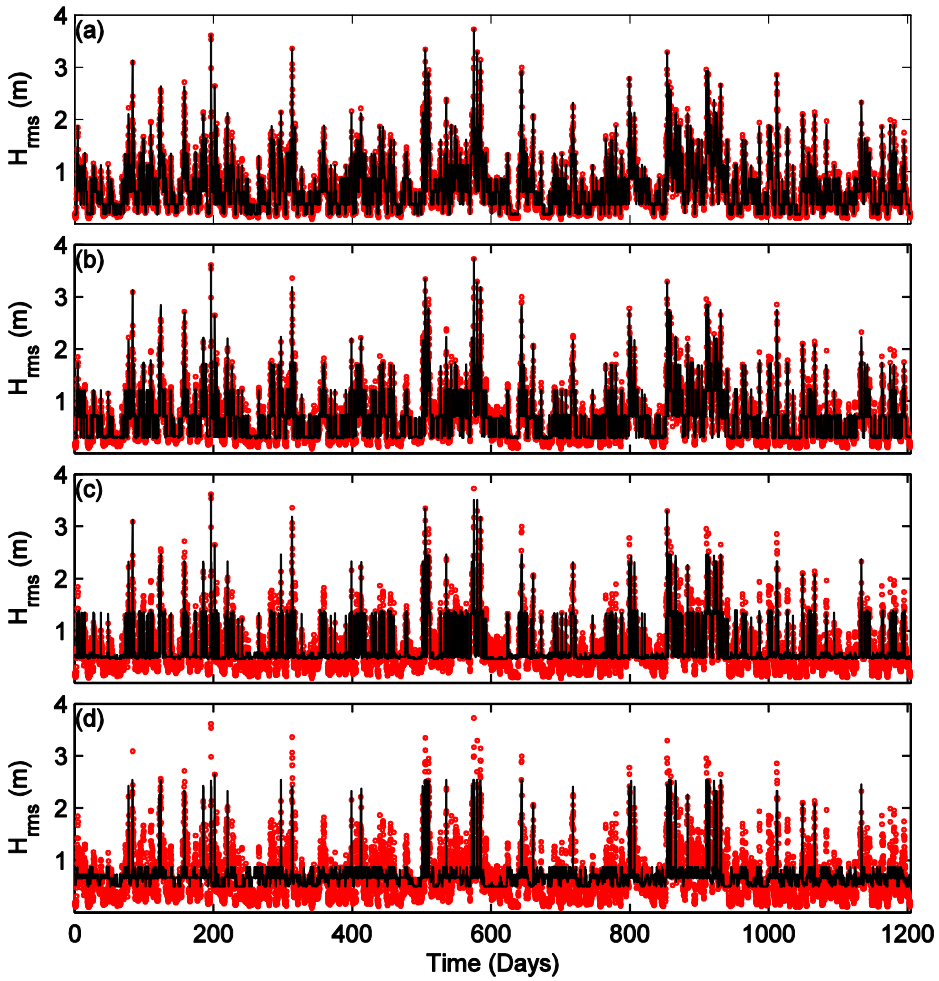

Figure 5.4 *Measured (red dots) and reconstructed time series (lines) for various wave height bin sizes (a) ΔH_{rms} = 0.25 m (16 bins), (b) ΔH_{rms} = 0.50 m (8 bins), (c) ΔH_{rms} = 1.0 m (bins), (d) ΔH_{rms} = 2.0 m (2 bins) with $\Delta\theta$=10º.*

Table 5.1 *Correlation coefficients r between the reconstructed H_{rms}, θ and T_p time series and the measurements at Noordwijk.*

Number of bins (equidistant and non-equidistant)	2 (Δθ=70°)			4 (Δθ=35°,Non-Equidistant)			7 (Δθ=20°)			14 (Δθ=10°)		
	H_{rms}	θ	T_p	H_{rms}	θ	T_p	H_{rms}	θ	T_p	H_{rms}	θ	T_p
2 (ΔH_{rms}=2.0 m)	0.53	0.2	0.36	0.54	0.87	0.48	0.55	0.96	0.51	0.56	0.99	0.53
4 (ΔH_{rms}=1.0 m, Non-Equidistant)	0.86	0.2	0.62	0.86 0.90	0.87 0.84	0.67 0.66	0.86	0.97	0.69	0.86	0.99	0.70
8 (ΔH_{rms}=0.5 m, Non-Equidistant)	0.96	0.2	0.70	0.96 0.96	0.87 0.84	0.74 0.71	0.96	0.97	0.76	0.96	0.99	0.77
16 (ΔH_{rms}=0.25)	0.99	0.2	0.72	0.99	0.87	0.76	0.99	0.97	0.78	0.99	0.99	0.79

Table 5.2 *Skill R for simulations forced with reconstructed time series for the considered aggregation levels at Noordwijk.*

Number of bins (equidistant and non-equidistant)	2 (Δθ=70°)	4 (Δθ=35°, non-equidistant)	7 (Δθ=20°)	14 (Δθ=10°)
2 (ΔH_{rms}=2.0 m)	0.03	0.06	0.08	0.08
4 (ΔH_{rms}=1.0 m)	0.50	0.92	0.92	0.92
4 (non-equidistant)	-	0.98	-	-
8 (ΔH_{rms}=0.5 m)	0.54	0.99	0.98	0.99
8 (non-equidistant)	-	0.99	-	-
16 (ΔH_{rms}=0.25)	0.34	0.99	0.99	1.00

Table 5.3 *Correlation coefficients r between the reconstructed H_{rms} and T_p time series and the measurements at Hasaki.*

Number of bins (equidistant and non-equidistant)	1		2 (ΔT_p=5 s)		4 (ΔT_p=2.5 s)	
	H_{rms}	T_p	H_{rms}	T_p	H_{rms}	T_p
4 (ΔH_{rms}=1.0 m)	0.91	0.36	0.91	0.71	0.91	0.89
4 (non-equidistant)	0.92	0.39	-	-	-	-
8 (ΔH_{rms} =0.5 m)	0.97	0.40	-	-	-	-
8 (non-equidistant)	0.97	0.40	-	-	-	-

Table 5.4 *Skill R for simulations forced with reconstructed time series for the considered aggregation levels at Hasaki.*

Number of bins (equidistant and non-equidistant)	1	2 (ΔT_p=5 s)	4 (ΔT_p =2.5 s)
4 (ΔH_{rms} =1.0 m)	0.83	0.83	0.86
4 (non-equidistant)	0.81	-	-
8 (ΔH_{rms} =0.5 m)	0.89	-	-
8 (non-equidistant)	0.78	-	-

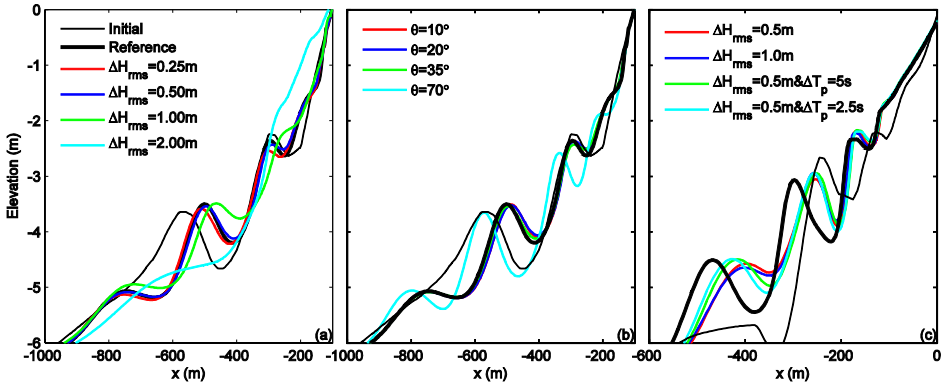

Figure 5.5 *Initial and final profile using equidistant binning: (a) all considered ΔH_{rms} combined with $\Delta\theta$=35° (Noordwijk), (b) all considered $\Delta\theta$ combined with ΔH_{rms}=0.50m (Noordwijk) and (c) all combinations of ΔH_{rms} and ΔT_p considered for Hasaki.*

5.3.3 Steps 3 and 4: Sequencing and Duration of the reduced wave climate

The construction of a synthetic time series is governed by the sequence in which the conditions (step 3) are imposed as well as by the duration of the wave climate (step 4). In this section both steps are jointly investigated for a number of the reduced wave climates derived in step 2 for Noordwijk and Hasaki.

First, we apply the randomized waves approach (Southgate, 1995) to establish the lower limit of T_{wc}. This involves the application of re-ordered time series which are generated by splitting up the observed time series into segments of constant length and then randomly re-ordering these segments. For Noordwijk, time series based on segment lengths of 3 hrs, 12 hrs, 1, 2, 7, 28 and 92 days were considered. For Hasaki the segment lengths of 1 day and larger were applied due to the 1-day resolution of the observations. For each segment length 5 randomly sequenced time series are imposed

on the model. The lower limit of T_{wc} was therefore defined as the minimum segment length at which the model outcomes become insensitive and are in good agreement with the brute force simulations.

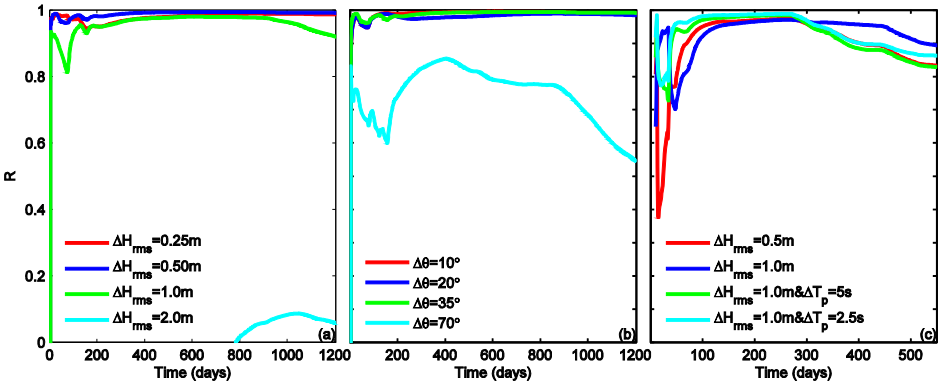

Figure 5.6 *Temporal evolution of the skill R: (a) equidistant ΔH_{rms} bins for $\Delta\theta$=35° (Noordwijk), (b) equidistant $\Delta\theta$ bins for ΔH_{rms}=0.50m (Noordwijk) and (c) equidistant ΔH_{rms} and ΔT_p bins (Hasaki).*

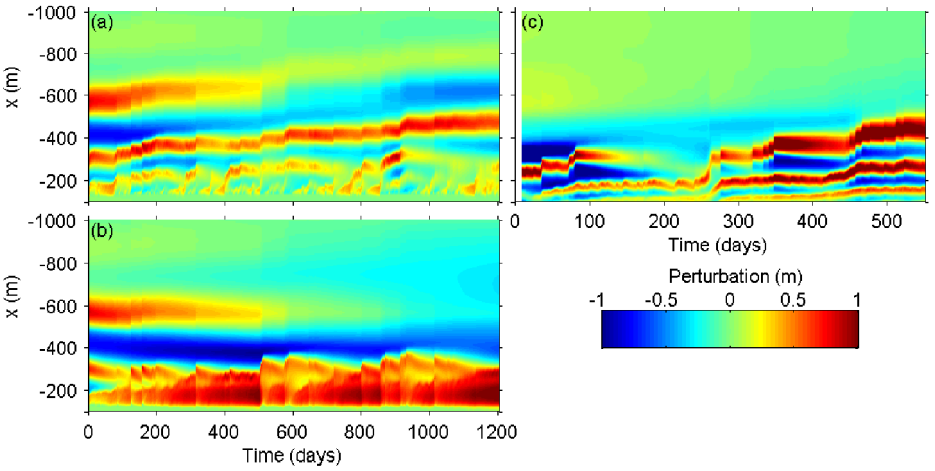

Figure 5.7 *Time stacks of the profile perturbation based on reconstructed time series: (a) Noordwijk with ΔH_{rms}=1.0m & $\Delta\theta$=35°, (b) Noordwijk with ΔH_{rms}=2.0m & $\Delta\theta$=35° and (c) Hasaki with ΔH_{rms}=1.0m & ΔT_p=2.5s.*

For Noordwijk the model predictions for 3-hour segments length all deviated from the reference run results (Figure 5.8a). The decay of the initial outer bar (x=-550m) was still well represented, but the middle bar (x=-320m) no longer migrated offshore and grew. In contrast, model predictions resulting from the 28 days segment length in general agreed well with the reference run (Figure 5.8b); only one of the time series (Random02) deviated more than the other time series. This difference was caused by the presence of several high-wave events near the end of the simulation. On the whole, a segment length of 12 hours caused the predictions to agree fairly well with the reference run (R>0.8); model performance was found to be relatively insensitive to longer segment lengths (Figure 5.9). For Hasaki the performance of the considered segment lengths was comparable but with considerable scatter. Compared to Noordwijk, the overall performance was significantly lower for all segment lengths (Figure 5.9). This was predominantly due to errors in bar migration rate rather than in bar height or width. The most detailed considered representative wave climates (Table 5.1 and Table 5.3) result in lower limits for T_{wc} of about 10 to 20 days (assuming the minimum segment lengths of 12 hrs and 1 day equals $f_{rep,\min} * T_{wc}$, see Section 5.2.2, for Noordwijk and Hasaki respectively).

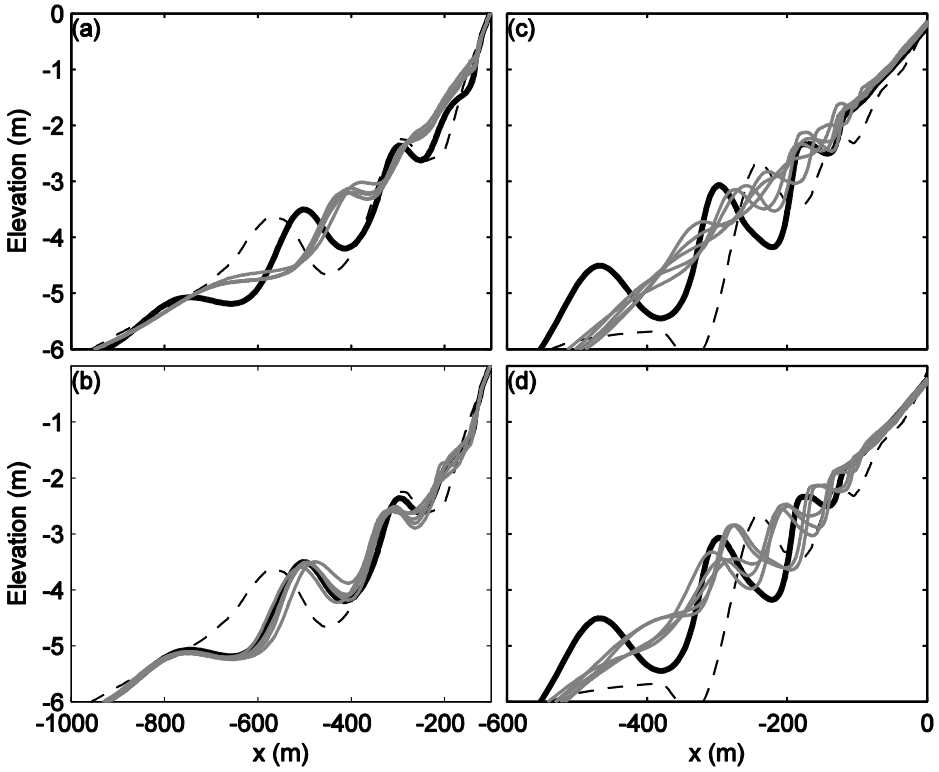

Figure 5.8 *Initial (dashed line), final brute-forcing prediction (solid line) and final profile prediction for the 5 randomly re-arranged time series (grey) for Noordwijk (a,b) and Hasaki (c,d); a) segment length is 3 hrs, b) segment length is 28 days, c) segment length is 1 day and d) segment length is 28 days.*

Conceptually, the model performance using reconstructed time series (Table 5.2 and Table 5.4) constitutes the best possible performance given a reduced set of input conditions and therefore acts as the upper performance limit for synthetic time series. The randomized time series approach therefore acts as an indicator to what extent synthetic time series are an appropriate way to simulate long-term profile evolution (tested in the next section). Consequently, an accurate reproduction of the brute forcing prediction based on synthetic time series may be achievable for Noordwijk, while this is unlikely for Hasaki. Instead, for the latter focus could be on more aggregated bar cycle characteristics such as averaged cycle period and the transient bar amplitude response which are still predicted using the randomized time series; therefore, the efficacy of synthetic time series was also considered for Hasaki.

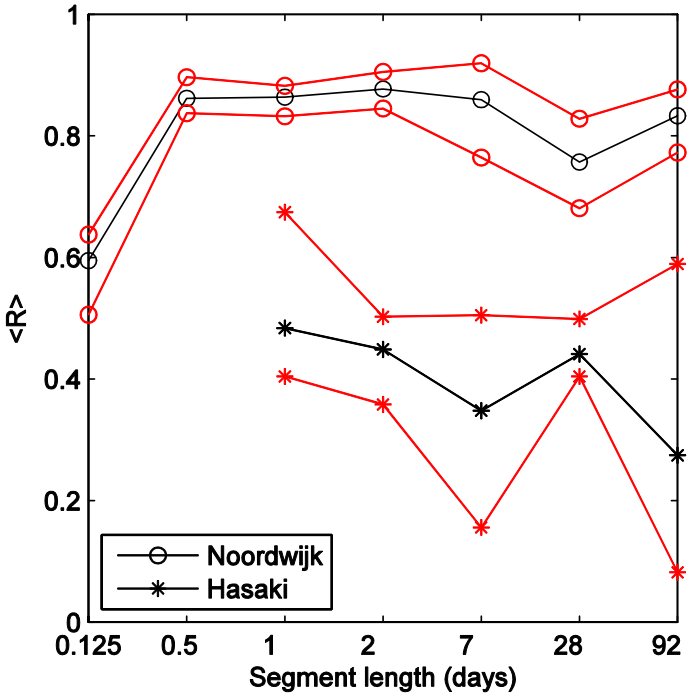

Figure 5.9 *Skill R (black) averaged over the 5 random simulations as a function of the segment length, red lines are the maximum and minimum R.*

Next, we identify the effect of sequencing and the wave climate duration. As an example, Figure 5.10 compares the synthetic forcing time series for the combination of descending wave heights and the wave directions subsequently sequenced in negative direction (labeled DN) with the same sequencing but starting with the wave directions and subsequently the wave heights (labeled ND, see also Figure 5.1a). Interestingly, for the randomized time series in Figure 5.10 H_{rms} and θ have similar characteristics (e.g. temporal distribution of the storm wave conditions over the time series) when sequenced second (i.e. H_{rms} resulting from the ND sequence and θ from the DN sequence, respectively).

The Noordwijk case was used to jointly investigate the influence of sequencing and varying T_{wc} for the $8x4_{EQ}$ wave climate (i.e wave climate resulting from equidistant binning of the observed H_{rms} and θ into 8 and 4 bins, respectively). To that end, the model performance for six wave climate durations (T_{wc} =1205, 603, 402, 301, 241, 114 days (all well above the lower limit) which implies the conditions in the reduced wave climate are repeated 1, 2, 3, 4, 5 and 9 times, respectively, see also Eq. (5.3)) combined

with all the sequencing options is summarized in Figure 5.11. Interestingly, a wave climate duration equal to the reduction period (i.e. T_{wc}=1205 days) resulted in negative R for most of the sequencing options (dark blue colors in Figure 5.11a), while T_{wc} < 401 days only marginally increased R (Figure 5.11b). For all synthetic time series, R increased for shorter wave climate durations. This is due to the reduced duration of the individual conditions and the repetition of the wave conditions, causing a better resemblance to the brute forcing time series.

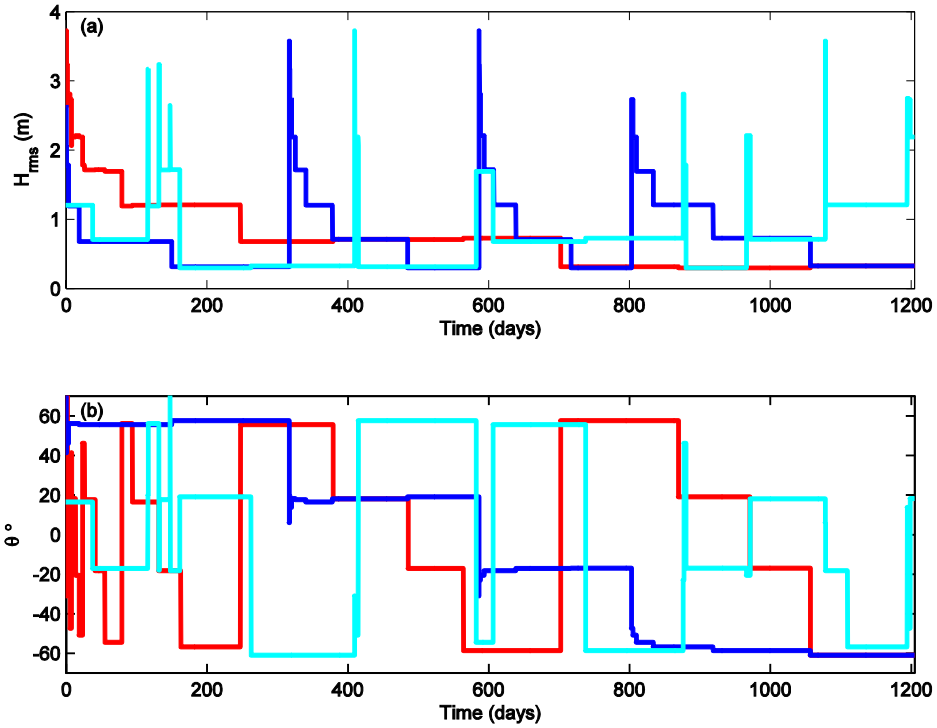

Figure 5.10 *Synthetic time series of (a) offshore root-mean-square wave height H_{rms} and (b) angle of incidence θ for descending H_{rms} and θ in negative direction (DN, red), vice versa (ND, blue) and random time series (R1, cyan) for T_{wc} = 3.5 yrs at Noordwijk.*

The presented results indicate that systematic sequencing of wave conditions consistently resulted in lower skills compared to the randomly ordered time series (Figure 5.11b), even though R2 consistently resulted in relatively low skill for most T_{wc} (Figure 5.11a). The fairly large range of skills for the randomly sequenced time series (mainly caused by the R2 sequence) reduced for shorter T_{wc}. In fact, for T_{wc} = 114 days

all sequences (systematic and random) resulted in a comparable skill. Especially for the longer T_{wc} differences in skill emerged. For T_{wc}>301 still a substantial part of the inaccuracies originated from T_{wc}, but the sequencing had an increased influence on the skill. The primary sequencing of H_{rms} (indicated by DN, AN, DP and AP in Figure 5.11a) dominated the model performance as these sequences had the lowest skill. Primary sequencing of θ (indicated by PD, PA, ND, NA in Figure 5.11a) causes the associated H_{rms} (sequenced second) to be more randomly ordered (see Figure 5.10) and consequently resulted in skills that approach the performance of the randomly sequenced time series. Since the random sequences resulted in the highest skill, these are considered to evaluate the effects of bin size and the binning method (equidistant and non-equidistant) for synthetic time series.

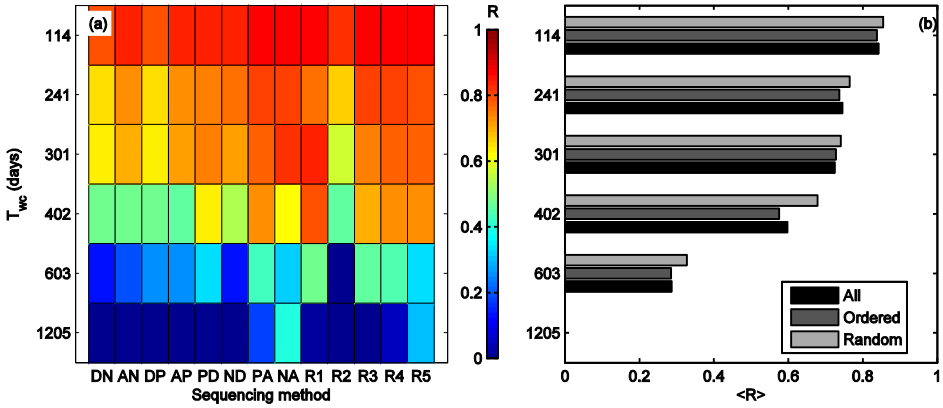

Figure 5.11 *Summary of model performance at Noordwijk; a) skill R for all sequencing options and considered wave climate durations and b) averaged over the sequencing methods (wave climate: 8x4$_{EQ}$; systematic sequences labeled by A/D and N/P, random sequences by R1 – R5).*

5.3.4 Influence of bin size and binning method on synthetic time series

We extend the analysis from the previous section to also include the 4x4 and 8x4 wave climates for Noordwijk and the 4x1 and 8x1wave climates for Hasaki considering both equidistant (EQ) and non-equidistant binning (NEQ).

At Noordwijk the use of the more detailed 8x4 wave climates generally improved *R* (Figure 5.12). Non-equidistant binning had a similar or larger positive impact on *R* for most of the 4x4 based synthetic time series; compare *R* for 4x4$_{EQ}$ and 4x4$_{NEQ}$ in Figures 12a,b. For the 8x4 wave climates, non-equidistant binning improved results to a lesser extent (consistent with Benedet et al., 2016). In general, *R* converged at about 0.85 for all wave climates with T_{wc}=114 days. The influence of *N* (number of

conditions in the reduced wave climate) is limited for non-equidistant binning (i.e. compare R of $4x4_{NEQ}$ with $8x4_{NEQ}$ wave climates). For the equidistant binning method, the influence of N is somewhat larger.

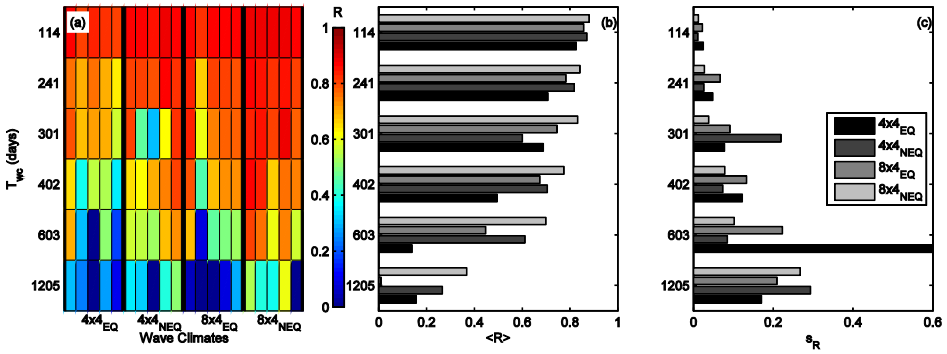

Figure 5.12 *Model performance at Noordwijk for the reduced wave climates: a) skill R resulting from the 5 randomly sequenced synthetic time series; b) and c) shows average R and its standard deviation* s_R*, respectively.*

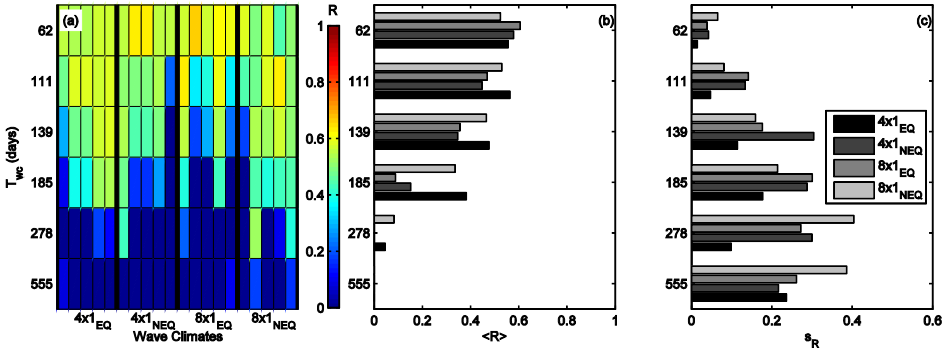

Figure 5.13 *Model performance at Hasaki for the reduced wave climates: a) skill R resulting from the 5 randomly sequenced synthetic time series; b) and c) shows average R and its standard deviation* s_R*, respectively.*

For Hasaki it appears that the wave climate duration and especially the sequencing were even more critical (i.e. relatively increased standard deviation of the skills, s_R, compare Figure 5.12c and Figure 5.13c). The 4x1 and 8x1 wave climates and the non-equidistant binning did not influence R as consistently as for Noordwijk (Figure 5.12). Compared to $4x1_{EQ}$, the $4x1_{NEQ}$ wave climate had relatively larger bin sizes for the higher wave conditions which negatively impact the predictions, whereas this was not

the case for the $8x1_{NEQ}$ wave climate. The influence of N appeared to be less critical non-equidistant binning (i.e. compare R for $4x1_{NEQ}$ and $8x1_{NEQ}$ in Figure 5.13c).

As suggested in the previous section, the randomized waves approach is a good indicator for the validaty of synthetic time series (e.g. for Noordwijk the skills for the shorter wave climate durations was very similar to the skills for the randomized waves approach with the longer segment lengths, compare Figure 5.12 and Figure 5.9). Interestingly, the synthetic time series resulted in somewhat higher R than the randomized waves approach for Hasaki (Figure 5.13 and Figure 5.9). The large influence of the sequencing at Hasaki was caused by the fact that the morphological response strongly depends on the phase of the bar cycle at the time of high wave events.

For both sites it can be concluded that sequencing, the aggregation level (i.e. number of conditions in the reduced wave climate) and the binning method (equidistant vs non-equidistant) are less critical for low T_{wc} as $\langle R \rangle$ and s_R converge (Figures 12b,c and Figures 13b,c) for T_{wc}<301 and T_{wc}<139 days respectively. For the remaining T_{wc} these input reduction parameters are of similar importance.

5.4 Discussion

The investigated aspects of input reduction (selection of conditions, wave climate duration and sequencing) were shown to influence model predictions. For Noordwijk the aggregation level and the type of binning influenced the results in a consistent way (e.g. more conditions improved the predictions). As the bar cycle characteristics in Noordwijk were not directly coupled to individual storm events, a reduced set of input conditions combined in a synthetic time series still results in reliable predictions provided T_{wc}<301 days. In contrast, the bar cycle characteristics at Hasaki were dominated by storm events as these had the ability to reset the bar cycle (i.e. offshore migration and decay of outer bar). As a consequence, lower R were found for all considered synthetic time series.

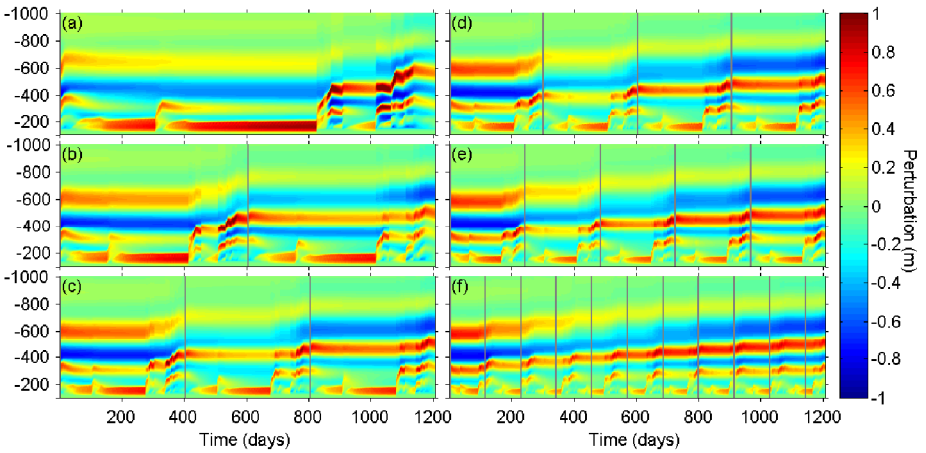

Figure 5.14 *Time stack of the predicted profile perturbations at Noordwijk for the 4x4$_{EQ}$ wave climate with randomized time series (R3) with T_{wc}= (a) 1205, (b) 602, (c) 401, (d) 301, (e) 241 and (f) 114 days. T_{wc} is indicated by the vertical grey lines.*

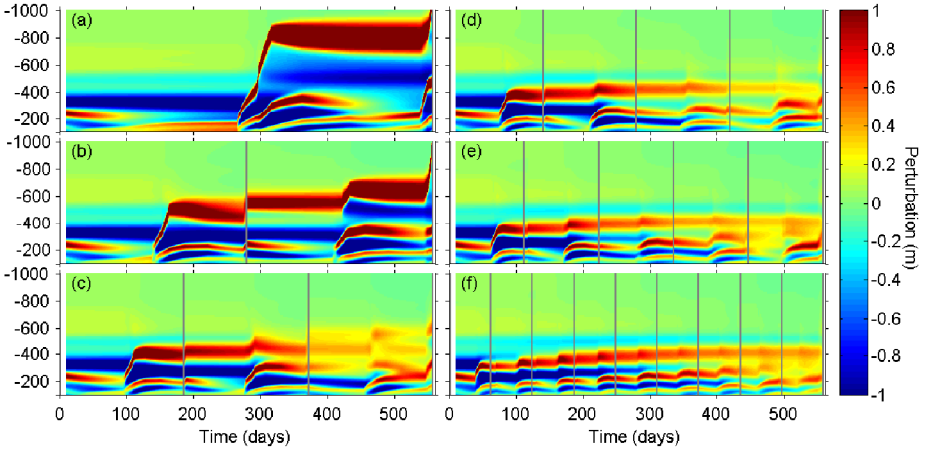

Figure 5.15 *Time stack of the predicted profile perturbations at Hasaki for the 4x4$_{EQ}$ wave climate with randomized time series (R3) with T_{wc}= (a) 555, (b) 278, (c) 185, (d) 139, (e) 111 and (f) 62 days. T_{wc} is indicated by the vertical grey lines.*

The influence of T_{wc} was illustrated by comparing time stacks of the profile perturbations for Noordwijk and Hasaki for all six considered T_{wc} with the brute force predictions (Figures 14 and 15, respectively with Figure 5.1). At Noordwijk the outer and middle bars characteristics were already fairly well reproduced with T_{wc} =602 days (Figure 5.14b). However, the inner bars (x=-400 m) only started to converge for

$T_{wc} \leq 401$ days (Figures 14c-f). On the bar cycle time scale, the middle and inner bars were coupled to the dynamics of the outer bars. However, near the water line (x>-200 m) bar generation, decay and/or merging with the inner bar occurred at a much higher frequency as it was directly coupled to the wave forcing. At Hasaki T_{wc} had an even large influence, for $T_{wc} \geq 277$ days (Figures 15a,b) the initial outer bar rapidly decayed which was the onset for strong bar growth and offshore migration of the former inner bar. With shorter T_{wc} (Figures 15c-f) the offshore migration and bar growth of the inner bar was less pronounced. As a result this bar only gradually moved offshore and slowly decayed for the remainder of the simulation. Although the predictions converge, the model failed to reproduce the bar characteristics of the brute force prediction for all the considered wave climates. The predicted gradual offshore migration, decay and merging of the inner and outer bars contrast with the episodic nature of the bar dynamics in the brute forcing prediction. Therefore, input reduction at Hasaki was only feasible by applying reconstructed time series. The R resulting from the reconstructed time series were fairly similar for all considered wave climates (Table 5.4). This implies that a reconstructed time series with $4x1_{EQ}$ will suffice. The morphological response to extreme wave events was so strong that this will be an important aspect for the interpretation of the model predictions. This could be addressed by considering a number of reconstructed time series for different time periods to obtain further insight in the variability in the model predictions.

For Noordwijk, the performance of the synthetic time series were further examined for the lower and upper parts of the profile, Figures 16a,b. The differences in R between the upper and lower parts of the profile confirmed the sensitivity of the upper part of the profile to T_{wc}. R converged for shorter T_{wc}, but was relatively low for the upper part of the profile. The lower part of the profile was less sensitive to T_{wc}, the aggregation level and the type of binning. Therefore, sensitivity in R for the entire profile (Figure 5.11a) was clearly dominated by the morphology of the upper part of the profile.

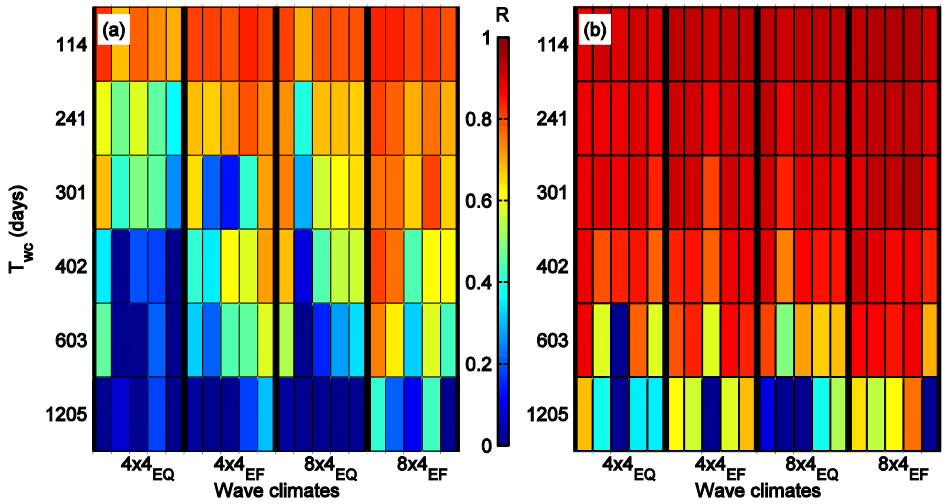

Figure 5.16 *Skill R at Noordwijk for the reduced wave climates resulting from the 5 randomly sequenced synthetic time series: a) upper part of profile (x=[-400m:-100m]) and b) lower part of profile (x=[-1000m:-400m]).*

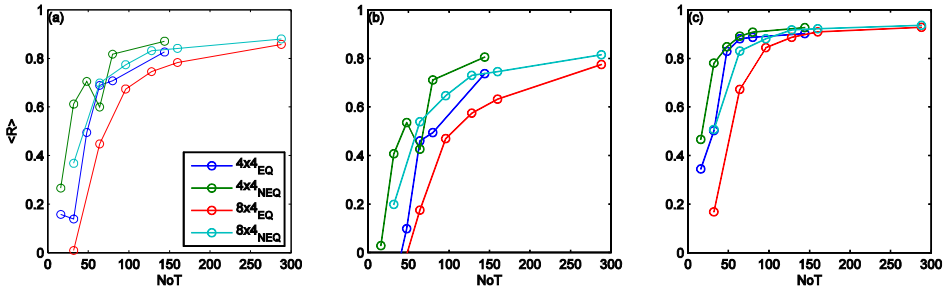

Figure 5.17 *Averaged skill R for a) the complete profile, b) the upper part of the profile (x=[-400m:-100m]) and c) the lower part of the profile (x=[-1000m:-400m]) as a function of the number of condition transitions (NoT) in the synthetic time series at Noordwijk.*

Because the computational efficiency of a reduced wave climate (imposed as synthetic time series required for upscaled morphodynamic simulation with varying *MF*, see also Section 5.2.1) is governed by *NoT* it should be used as the primary selection criterion. Therefore, the considered wave climates were evaluated for Noordwijk by comparing *R* averaged over the 5 random simulations as a function of *NoT* for the entire profile and for the upper and lower parts of the profile (Figure). It is evident that the number of conditions and binning method (step 2) were of similar importance as the wave climate

duration (step 4). Although, the $4x4_{NEQ}$ wave climate was the optimal climate (largest R for a given NoT), the $8x4_{NEQ}$ wave climate resulted in a comparable model performance with a nearly similar efficiency. Given the comparable performance of the $4x4_{NEQ}$ and $8x4_{NEQ}$ wave climates, a final selection could also be based on a more detailed inspection of the predictions and other aspects such as robustness of the predictions. For example, the standard deviation s_R shown in Figure 5.12c and Figure 5.13c is mostly lower for $8x4_{NEQ}$, suggesting that $8x4_{NEQ}$ is to be preferred over $4x4_{NEQ}$.

Furthermore, the variability in R for the 5 random synthetic time series appeared to be an indicator for overall agreement at both sites (compare $\langle R \rangle$ and the standard deviation S_R in Figure 5.12b, c and Figure 5.13b,c). Despite the differences between both sites, R showed similar trends for changes in T_{wc} and the type of wave climate. For the considered wave climates both $\langle R \rangle$ and S_R converge for decreasing T_{wc}. This could be used as an a-priori quality indicator in a relative comparison of wave climates (and T_{wc}): optimal choice of T_{wc} where $\langle R \rangle$ has sufficiently converged and in case different wave climates have similar $\langle R \rangle$, the minimum S_R could be the secondary selection criteria.

In this paper we used brute force simulations that reproduced observed bar behavior as reference. We realize this is a rare reference, as such simulations would often require unfeasibly long run times or general wave characteristics (e.g. a wave rose) are available only. In fact, if a brute force simulation is feasible, there is no need for any input reduction. Does this invalidate our framework? We believe it does not as the input reduction framework can also be applied to evaluate reduced wave climates by using the observed morphology as reference. In other words, by (qualitatively) exploring whether the model with reduced input reproduces the essential characteristics of the morphological evolution. Alternatively, one could use a detailed model prediction (i.e. with the smallest feasible bin sizes) as reference. In the latter case, the input reduction framework will at least provide a relative comparison based on which the level and method of input reduction can be established objectively. Furthermore, insight is obtained into the errors input reduction may introduce. Given the relatively large influence of input reduction at the sites studied in the paper, we expect that such insight is also highly relevant in other applications.

The considered wave climates were relatively detailed (16 to 32 wave conditions) compared to commonly applied wave climates in multi-annual morphodynamic simulations (typically about 10 wave conditions, see, for example van Duin et al., 2004 and Grunnet et al., 2004). This further reduction was partly achieved by ignoring the

low to moderate wave conditions. To test whether exclusion of low conditions is justified we excluded $H_{rms} < 1$ m wave conditions from the $8x4_{EQ}$ and $8x4_{NEQ}$ wave climates for all wave climate durations for the Noordwijk case. This resulted in significantly increased bar amplitudes and enhanced offshore bar migration, causing negative skill for all considered wave climates and T_{wc}. It proves that, although storms strongly influence profile evolution, the interplay between such episodic events and prolonged periods of low to moderate waves cannot be ignored.

5.5 Conclusions

Input reduction can have a major impact on model simulations, even to such an extent that major characteristics of cyclic behavior of sub tidal sandbars are no longer reproduced. This is particularly true when long-term evolution is steered by episodic storm events, such as at Hasaki. Therefore, the characteristics of the bar cycle response (e.g. episodic or inter-annual net offshore migration of bars) should be accounted for when applying input reduction. Synthetic time series of wave conditions are only appropriate if the bar-cycle dynamics are not directly linked to individual storm events. If such a coupling does exist, reconstructed time series that retain the original chronology should be applied (also implying that constant *MF*-values should be used in case morphodynamic upscaling is utilized).

The effect of input reduction is not steered by a single choice. In our application, the aggregation level, the binning methods and the wave climate duration T_{wc} affected skill to a similar degree. Since the efficiency of long-term process-based morphodynamic models (with varying *MF*) is governed by the number of transitions *NoT*, the optimal wave climate should also consider T_{wc}. This could result in the selection of an optimal reduced wave climate containing a larger number of conditions but with a longer T_{wc}.

Given its potentially major influence, the type of input reduction, including associated choices, should be well-motivated and investigated. In other words, it should be an intrinsic part of model set-up, calibration and validation procedures.

5.6 References

Benedet, L., Dobrochinski, J.P.F., Walstra, D.J.R., Klein, A.H.F., Ranasinghe, R., 2016. A morphological modeling study to compare different methods of wave climate schematization and evaluate strategies to reduce erosion losses from a beach nourishment project. *Coastal Engineering*, 112, pp 69–86. doi:10.1016/j.coastaleng.2016.02.005

Brown, J.M. and Davies, A.G., 2009. Methods for medium-term prediction of the net sediment transport by waves and currents in complex coastal regions. *Continental Shelf Research* (29), pp 1502-1514. doi:10.1016/j.csr.2009.03.018.

Chesher, T.J. and Miles, G.V., 1990. The concept of a single representative wave for use in numerical models of long term sediment transport predictions. *Proc. 2nd intl. conf. on hydraulic and environmental modelling of coastal, estuarine and rivers waters*. Eds. Falconer, R.A., Chandler-Wilde, S.N. and Liu, S.Q.

Dastgheib, A., Roelvink, J.A. and Wang, Z.B., 2008. Long-term process-based morphological modeling of the Marsdiep Tidal Basin. *Marine Geology* 256 (1-4), pp 90-100. doi:10.1016/j.margeo.2008.10.003.

De Vriend, H.J., Capobianco, M., Chesher, T., de Swart, H.J., Latteux, B. and Stive, M.J.F., 1993. Approaches to long-term modelling of coastal morphology: a review. *Coastal Engineering* 21, 225-26. doi:10.1016/0378-3839(93)90051-9.

Edmonds, D.A., Slingerland, R.L., 2010. Significant effect of sediment cohesion on delta morphology. *Nature Geoscience* 3, 105–109. doi:10.1038/ngeo730

Elias, E.P.L., Cleveringa, J., Buijsman, M.C., Roelvink, J.A., Stive, M.J.F., 2006. Field and model data analysis of sand transport patterns in Texel tidal inlet. *Coastal Engineering* 53(5–6), pp 505–529. doi: 10.1016/j.coastaleng.2005.11.006.

Geleynse, N., Storms, J.E.A., Stive, M.J.F., Jagers, H.R.A., Walstra, D.J.R., 2010. Modeling of a mixed load fluvio-deltaic system. *Geophysical Research Letters*, Vol. 37, L05402, doi:10.1029/2009GL042000.

Geleynse, N., Storms, J.E.A., Walstra, D.J.R., Jagers, H.R.A., Wang, Z.B., and Stive, M.J.F. 2011. Controls on river delta formation; insights from numerical modeling, *Earth and Planetary Science Letters*, Vol 302, pp 217–226, doi: 10.1016/j.epsl.2010.12.013.

Grunnet, N.M., Walstra, D.J.R., Ruessink, B.G., 2004. Process-based modelling of a shoreface nourishment. *Coastal Engineering* 51 (7), 581–607. doi:10.1016/j.coastaleng.2004.07.016.

Grunnet, N.M., Ruessink, B.G., Walstra, D.J.R, 2005. The influence of tides, wind and waves on the redistribution of nourished sediment at Terschelling, The Netherlands. *Coastal Engineering* 52, 617–631. doi:10.1016/j.coastaleng.2005.04.001.

Hibma, A.; de Vriend, H.J.; Stive, M.J.F., 2005. Numerical modelling of shoal pattern formation in well-mixed elongated estuaries, *Estuarine Coastal and Shelf Science*, Vol. 57 (5-6), pp 981-991. doi:10.1016/S0272-7714(03)00004-0.

Jones, O.P., Petersen, O.S., Kofoed-Hansen, H., 2007. Modelling of complex coastal environments: Some considerations for best practice. *Coastal Engineering* 54, 717–733. doi:10.1016/j.coastaleng.2007.02.004.

Kuriyama, Y., Ito, Y., Yanagishima, S., 2008. Medium-term variations of bar properties and their linkages with environmental factors at Hasaki, Japan. *Marine Geology*, Vol. 248 (1-2), pp1-10. doi:10.1016/j.margeo.2007.10.006.

Lesser, G.R., Roelvink, J.A., van Kester, J.A.T.M., Stelling, G.S., 2004. Development and validation of a three-dimensional morphological model. *Coastal Engineering* 51 (8-9), 883-915. doi:10.1016/j.coastaleng.2004.07.014.

Lesser, G.R., 2009. An approach to medium-term coastal morphological modeling. *Phd-thesis*, Delft University of Technology, CRC Press/Balkema. ISBN 978-0-415-55668-2.

Pape, L., Kuriyama, Y., Ruessink, B.G., 2010. Models and scales for nearshore sandbar behavior. *Journal of Geophysical Research — Earth Surface* 115, F03043. doi:10.1029/2009JF001644.

Ranasinghe, R., Swinkels, C., Luijendijk, A., Roelvink, J.A., Bosboom, J., Stive, M.J.F., Walstra, D.J.R, 2011. Morphodynamic upscaling with the MorFac approach: dependencies and sensitivities. *Coastal Engineering* 58, 806–811, doi:10.1016/j.coastaleng.2011.03.010.

Roelvink, J.A., 2006. Coastal morphodynamic evolution techniques. *Coastal Engineering* 53, 277–287. doi:10.1016/j.coastaleng.2005.10.015.

Roelvink, J.A., Reniers, A.J.H.M., 2011. A guide to modelling coastal morphology. *Advances in Coastal and Ocean Engineering*. World Scientific Pub. Co. Inc.

Ruessink, B.G., Kuriyama, Y., Reniers, A.J.H.M., Roelvink, J.A., Walstra, D.J.R., 2007. Modeling cross-shore sandbar behavior on the timescale of weeks. *Journal of Geophysical Research-Earth Surface* 112 (F3), 1–15. doi:10.1029/2006JF000730.

Ruessink, B.G., Kuriyama, Y., 2008. Numerical predictability experiments of cross-shore sandbar migration. *Geophysical Research Letters* 35, L01603, doi:10.1029/2007GL032530.

Ruessink, B.G., Pape, L. and Turner, I.L., 2009. Daily to inter-annual cross-shore sandbar migration: observations from a multiple sandbar system. *Continental Shelf Research*, 29, 1663-1677. doi:10.1016/j.csr.2009.05.011.

Ruggiero, P., Walstra, D.J.R., Gelfenbaum, G., van Ormondt, M., 2009. Seasonal-scale nearshore morphological evolution: field observations and numerical modeling. *Coastal Engineering* 56 (11–12), 1153–1172. doi:10.1016/j.coastaleng.2009.08.003.

Southgate, H., 1995. The effects of wave chronology on medium and long term coastal morphology. *Coastal Engineering* 26, 251-270. doi:10.1016/0378-3839(95)00028-3

Sutherland, J., Peet, A.H., Soulsby, R.L., 2004. Evaluating the performance of morphological models. *Coastal Engineering* 51 (8–9), 917–939. doi:10.1016/j.coastaleng.2004.07.015.

Tung, T.T., van der Kreeke, J., Stive, M.J.F., Walstra, D.J.R, 2012. Cross-sectional stability of tidal inlets: A comparison between numerical and empirical approaches. *Coastal Engineering* 60, 21–29. doi:10.1016/j.coastaleng.2011.08.005.

Van der Wegen, M., Roelvink, J.A., 2008. Long-term morphodynamic evolution of a tidal embayment using a two-dimensional, process-based model. *Journal of Geophysical Research-Oceans* 113 (C3016). Doi:10.1029/2006JC003983.

Van Duin, M.J.P.,Wiersma, N.R.,Walstra, D.J.R., van Rijn, L.C., Stive, M.J.F., 2004. Nourishing the shoreface: observations and hindcasting of the Egmond case, The Netherlands. *Coastal Engineering* 51 (8–9), 813–837. doi:10.1016/j.coastaleng.2004.07.011.

Van Enckevort, I.M.J., Ruessink, B.G., 2003. Video observations of nearshore bar behavior. Part 1: alongshore uniform variability. *Continental Shelf Research* 23, 501–512. doi:10.1016/S0278-4343(02)00234-0.

Walstra, D.J.R., Reniers, A.J.HM., Ranasinghe, R., Roelvink, J.A., Ruessink, B.G., 2012. On bar growth and decay during inter-annual net offshore migration. *Coastal Engineering* 60, 190-200. doi:10.1016/j.coastaleng.2011.10.002.

Wijnberg, K.M., Terwindt, J.H.J., 1995. Extracting decadal morphological behavior from high-resolution, long-term bathymetric surveys along the Holland coast using eigen function analysis. *Marine Geology* 126 (1–4), 301–330. doi: 10.1016/0025-3227(95)00084-C.

6 Conclusions

The overarching objective of this study was to elucidate the anatomy of the inter-annual bar morphology. This overarching objective is in turn devolved into three objectives aiming to understand the key features of bar morphology. A further objective is defined to enable a comprehensive modelling approach based on the acquired insights. In Chapters 2 to 5 these objectives were investigated and addressed in great detail. In this final chapter the research questions are successively answered together with a short recapitulation of the adopted approach to address each of the four objectives.

Objective I:

To elucidate the morphodynamic processes that result in cross-shore transient sandbar amplitude responses, that is, the transition from bar growth in the intertidal and across surf zone to sandbar decay at the seaward edge of the surf zone.

With a relatively simple wave-averaged cross-shore profile model the observed bar growth and decay during inter-annual net offshore bar migration at Noordwijk (Netherlands) could be reproduced by tuning only three free model parameters. This calibrated model was used to answer Research Questions 1 and 2.

Research Question 1: *Why does a bar experience amplitude growth when it migrates from the inner to the middle surf zone regions?*

A linear regression analysis between the bar amplitude response and wave characteristics (both offshore and at the bar crest) resulted in relatively low correlations ($r < 0.5$). The highest correlation was found with the longshore component of the local surface shear stress due to wave breaking, $\tau_{sw,y}$. Detailed inspection of the model results indicate that the enhanced sediment stirring on the landward bar slope and trough by the breaking-induced longshore current can shift the cross-shore transport peak landward of the bar crest. This forces bar amplitude growth during offshore migration. During onshore bar migration the enhanced sediment stirring by the longshore current results in increased transport from the landward trough toward the bar crest, promoting bar amplitude growth. The water depth at the bar crest, h_{Xb}, and the angle of wave incidence, θ, control the generation of the longshore current. For bars in shallow water

the bar amplitude response and θ are strongly related, due to the relatively strong longshore current that waves breaking under an angle generate. This highlights the hitherto largely ignored importance of the wave angle on cross-shore bar dynamics.

Research Question 2: *Why does a bar decay at the seaward boundary of the surf zone and does the offshore migration stop?*

The reduction of the number of breaking waves decreases the relevance of the associated longshore currents at bars in deeper water. This causes the undertow to dominate the cross-shore sediment transports. Consequently the transport peaks will coincide with the bar crest location which results in net bar amplitude decay at larger water depths. The strong dependency on the longshore current also explains the observed transient bar amplitude response during the net inter-annual offshore migration. For bars in relatively shallow water wave breaking is more frequent, promoting net bar amplitude growth in case of oblique wave incidence, whereas in deeper water wave breaking on the bars is limited, leading to net bar amplitude decay.

Objective II:

To establish the role of cross-shore processes in non-persistent bar switches.

The reference model is applied on the 24 transects measured at a 250 m interval surrounding the transect considered for Objective I. The model predictions were combined into plan view to evaluate potential changes in alongshore variability of the cross-shore bar location and bar amplitude. Comparison of the predictions starting from years with large and limited alongshore variability were compared with observed bed changes to answer Research Questions 3 and 4.

Research Question 3: *To what extent can cross-shore processes initiate, amplify or dampen the km-scale alongshore sandbar variability?*

The model is not able to predict the dissipation of a bar switch, as in contrast to the observed bar behavior, predicted bar morphologies on either side of the switch remain in a different phase. The alongshore variability is only temporarily reduced when the bars on either side are occasionally located in a similar cross-shore position. The data-model mismatch suggests that three-dimensional processes play a key role in the generation and decay of bar switches. Potentially 3D flow patterns are responsible for: 1) removing a switch by merging the bars when they are at a similar cross-shore position or 2) generating a switch after the alongshore variability is amplified under a specific combination of the bar morphology and energetic wave forcing.

Research Question 4: *What is the relative importance of the wave forcing and the antecedent morphology on the predicted alongshore bar variability?*

When alongshore variability is limited, the model predicts offshore migration of the bars at approximately the same rate (i.e. the bars remain in phase). Only under specific bar configurations and high wave-energy levels an increase in alongshore variability is predicted. This suggests that cross-shore processes may trigger a switch in the case of specific antecedent morphological configurations combined with storm conditions.

Objective III:

Identify the dominant environmental variables and the associated mechanisms that govern the bar cycle return period.

The reference model at Noordwijk is compared to predictions made at Egmond, a site with a distinctly different (larger) bar cycle return period, T_r. Systematic variations of model settings and environmental conditions allowed for a detailed analysis to identify relevant environmental parameters and subsequently the physical processes that govern T_r were used to address Research Questions 5 and 6.

Research Question 5: *Which environmental parameters (e.g. wave forcing, sediment size, profile slope) primarily influence the bar evolution and consequently the bar cycle return period?*

Consistent with earlier findings from field observations, our numerical model simulations illustrate that T_r is found to be positively correlated with sediment diameter and bar size, while T_r is negatively correlated with the wave forcing and profile slope. The simulations starting from composite profiles in which bar size, profile slope and sediment size were varied, clearly identified the bed slope in the barred zone to be the most important parameter that governs T_r. The application of the Egmond instead of the Noordwijk wave climate reduces T_r by a factor 3 to 4. However, the predicted T_r at Egmond is about twice as large, which is primarily originating from the difference in the upper profile slope and the larger sediment diameter at Egmond.

Research Question 6: *What are the dominant mechanisms that govern the bar cycle return period?*

The sensitivity of T_r to the upper profile slope arises from the importance of the water depth above the bar crest (h_{Xb}) for sandbar response. As a bar migrates seaward, a steeper slope results in a relatively larger increase in h_{Xb}, which reduces wave breaking and subsequently causes a reduced offshore migration rate (and hence an increase in T_r). Therefore, we conclude that the morphodynamic feedback loop is significantly

more important than the initially larger offshore bar migration due to the more intense wave breaking in case of a steeper profile slope (as was the case for the Egmond profile). Given the significantly larger T_r at Egmond, the opposing effects of the increased wave climate and the upper profile slope further emphasize the importance of the upper bed slope and sediment diameter on T_r. As the upper profile slope and sediment size are highly correlated it was not possible to independently vary these parameters. Therefore sets of one-day schematic simulations were used to assess their relative importance. This clearly revealed the dominance of the upper profile slope. This illustrates that the net offshore bar migration rate (and therefore T_r) is very sensitive to the highly non-linear two-way interaction between the wave forcing and the evolving profile morphology.

Objective IV:

To develop an input-reduction framework to enable the application of state-of-the-art process based forward area models to simulate the multi-annual bar behaviour and nearshore morphology.

Comparison of predictions resulting from a reduced set of forcing conditions and brute forcing is the ultimate verification of any input reduction method. The brute forcing models developed for Noordwijk (The Netherlands) and Hasaki (Japan) were used to perform such a verification and to develop a generic input reduction framework for long-term morphodynamic predictions. The framework was used to answer the associated Research Questions 7 and 8.

Research Question 7: *Can the inter-annual bar evolution be predicted with a reduced set of wave conditions?*

Input reduction can have a major impact on model simulations, even to such an extent that major characteristics of cyclic behavior of sandbars are no longer reproduced. This is particularly true when long-term evolution is steered by episodic storm events, such as at Hasaki. Therefore, the characteristics of the bar cycle response (e.g. episodic or inter-annual net offshore migration of bars) should be accounted for when applying input reduction. Synthetic time series of wave conditions are only appropriate if the bar-cycle dynamics are not directly linked to individual storm events. If such a coupling does exist, reconstructed time series that retain the original chronology should be applied. Given its potentially major influence, the type of input reduction, including associated choices, should be well-motivated and investigated. In other words, it should be an intrinsic part of model set-up, calibration and validation procedures. Although a reduced set of input conditions will always introduce errors, appropriate application of the input reduction framework will result in high-quality model predictions (i.e. with limited deviations from the brute forcing predictions).

Research Question 8: *Which aspects influence the predictability of the bar evolution?*

The effect of input reduction is not steered by a single choice. In our application, the number of selected representative wave conditions, the binning method and how often the selected conditions are repeated in the forcing time series affected skill to a similar degree. The efficiency of a representative time series for long-term process-based morphodynamic models is primarily governed by the number of transitions between wave conditions which in turn is governed by the number of wave conditions and how often these are repeated. Therefore, an efficient reduced wave climate should be based on an optimal combination of these variables. This implies that the most efficient wave forcing time series could be based on a reduced wave climate with a relatively large number of representative wave conditions which, however, is relatively less frequently repeated. The binning method utilizing a varying bin size could reduce the number of representative conditions by as much as 50% compared to a reduction based on a constant bin size without adversely affecting the predictive skill.

Concluding Remarks

The results clearly indicate that a relatively simple cross-shore model can be utilized to study the highly non-linear interaction between the nearshore hydrodynamics and morphology in great detail. This was achieved through carefully designed numerical experiments in which the influence of a specific process or environmental variable could be isolated and identified. Although the model only considers cross-shore processes, the numerical experiments also generated new insights into the importance of 3D processes under particular morphological conditions of the nearshore barred profiles. Even though the model was successfully calibrated at Noordwijk, the application at Egmond showed a significantly reduced predictive capacity. The model was able to reproduce the main characteristics of the inter-annual bar morphodynamics, but the bar cycle return period was under-estimated by about 30%. This suggests that the model can capture trends fairly well, but is unable to produce accurate absolute predictions - a finding that has broader implications. Namely, accurate predictions of the long-term evolution of the nearshore barred profiles are generally considered indicative of the quality of the modelling for the entire nearshore coastal system. The ability to perform reliable and robust a-priori, long-term predictions has broad societal relevance in view of anticipated adverse impacts of climate change and sea level rise on the stability of coasts worldwide. Consequently, further improvement of morphodynamic process-based models, particularly for the nearshore zone, constitutes a major research priority.

Acknowledgements

The initial idea for this thesis dates from as early as 2003, when it was first mentioned on Marcel Stive's homepage! However, it only became a serious research endeavour when I was subjected to a mandatory 'self development' course at Deltares in 2010. My grateful thanks are extended to Wiel Tilmans and Klaas Jan Bos, my unit manager and department head at the time, for supporting me in this venture. Marcel, your faith in me over the whole period is gratefully acknowledged.

From the early days, Gerben Ruessink has been closely involved with the research. Gerben, I remember our discussions vividly. The years that you spent at Delft Hydraulics marked the start of an inspiring working relationship. I consider it special that our initial ideas on investigating the intra-site differences in the bar cycle period are developed and fully addressed in this thesis. Without your support, this would not have been possible. In particular, your reviews of my draft manuscripts were incredibly detailed and sometimes brutal, but you were always right! I regard the fact that the later papers made it past your "red pen" in one or two revisions as a major achievement.

Many people have contributed to this thesis. Rosh Ranasinghe and Ad Reniers were closely involved in the method development, and provided valuable input on the interpretation of results. Guys, thank you very much for your help and support in the difficult moments, particularly on the intra-site variability paper of Chapter 3. Rosh, after a beer at Moodz it all seemed achievable again! I wish to extend my thanks to my Deltares colleagues, Pieter Koen Tonnon and Roderik Hoekstra, who were closely involved in the input reduction paper of Chapter 5. I'm also grateful to Daan Wesselman and Eveline van der Deyl from Utrecht University, who contributed to the bar cycle variability paper of Chapter 4, as part of their internship at Deltares. They form part of a larger group of students that I have supervised over the years; I hope they learned as much from me as I did from them.

I am fortunate to work in a field with a very open and informal culture and am much indebted to Dano Roelvink for introducing me to this field and for hiring me at Delft Hydraulics all those years ago. I have been exposed to an inspiring group of morphologists, including Leo van Rijn, Marcel Stive, Ad Reniers, Zheng Bing Wang

and Dano Roelvink. You were great mentors and role models, always sharing your experience and knowledge with me. Thank you!

At Deltares, sharing an office has become a concept from the past. However, I benefitted from a series of fun and inspiring officemates. My thanks go first to Hans de Vroeg, for all the discussions and laughs we have shared. I hope we can soon arrange for a game of pool, ending up in the "Witte Aap". My first officemate at Delft Hydraulics was Stefan Aarninkhof, joined a few years later by Mark van Koningsveld. I can't believe that it's more than 10 years since we shared an office! Our adventures have already been captured in the acknowledgements of both of your theses, so I won't repeat them here. Nevertheless, it feels good that I can do my bit to close the circle. It is a privilege to have both of you as my paranymphs and it was great to discuss my propositions during an old-fashioned session with all of you: Stefan, Mark and Marcel. Among good friends years don't count!

Besides my PhD, one of the most exciting recent projects I have worked on is the development of Delft3D-GeoTool. This is the result of a collaboration of more than 10 years with Joep Storms, during which we've gradually bridged the gap between geology and morphology. Joep, it's great to see this research field expanding to include Nathanaël, Liang and Helena. I hope we can continue our alliance for many years to come.

My job satisfaction is largely determined by interactions with immediate colleagues. Therefore, a special thank you to the Harbour, Coasts and Offshore (HCO), and the Applied Morphology (AMO) departments at Deltares. I could not have wished for better colleagues to work with! In addition, since I became department head two years ago, I have the pleasure of working closely with the ZKS management team: Ankie Bruens, Annette Zijderveld, Bianca Peters, Sharon Tatman and Frank Hoozemans. Last but not least, a big thank you to my neighbours at TU Delft: Jaap van Thiel de Vries, Kees den Heijer, Fedor Baart and Arjen Luijendijk, for the stimulating discussions at the (first!) coffee in the morning. A hearty thanks to Melissa Ruts who assisted with the formatting of my thesis. I also wish to acknowledge the members of my PhD committee. Special thanks are owed to Peter Ruggiero and Hans Hanson for their willingness to participate.

Lieve papa en mama (Ype en Ans), juist op momenten als deze besef ik hoe groot jullie rol is geweest in mijn leven. Jullie hebben ons (Ernst, Saskia en mij) met een geweldige mix van veel vrijheid en vertrouwen opgevoed. Natuurlijk waren er grenzen, maar wat kon er veel! Wie kan zeggen dat hij al op z'n twaalfde in een afgedankte auto mocht rondcrossen in de tuin? Om nog maar te zwijgen van de semi-professionele discotheek die we tijdens onze tienerjaren konden uitbaten in de schuur en het illegale

radiostation op zolder met een razende reporter op pad met de autotelefoon van papa! De afgelopen jaren hebben jullie het echter zwaar gehad. Het is heel bijzonder hoe jullie omgaan met de vele tegenslagen in papa's gezondheid. Wat er ook gebeurt, papa's onverwoestbare optimisme en positivisme komen altijd weer bovendrijven.

Lieve Anna, Ryan en Alasdair, geweldig om jullie te hebben zien opgroeien tot wie jullie nu al zijn, vol vertrouwen kijk ik uit naar jullie overgang van pubers naar jong volwassenen en verder. My dearest Jill, thank you for your unconditional support throughout the years. I think you are the only person that never asked me when the thesis would be finished, thank you for your patience! You've always been very supportive both in (sometimes grudgingly) accepting that I had to work yet another evening/weekend and in editing the English in this thesis, in the papers, and even in these acknowledgements!

Dirk-Jan Walstra
Delft, May 2016

Curriculum Vitae

Dirk-Jan Walstra is op 5 september 1968 geboren in Sneek. Het grootste deel van zijn jeugd bracht hij echter door op het Friese platteland in Hennaard. Van 1980 tot 1984 doorliep hij de MAVO 'Nij Walpert' in Wommels, om daarna van 1984 tot 1986 de HAVO en vervolgens van 1986 tot 1988 het VWO te doorlopen aan het 'Magister Alvinus' in Sneek. Hierna koos hij voor de studie Civiele Techniek aan de Technische Universiteit Delft. In Augustus 1994 studeerde hij binnen een gezamenlijk onderzoek met de faculteit Toegepaste Wiskunde onder begeleiding van prof.dr.ir. Dano Roelvink, prof.dr.ir. Guus Stelling, prof.dr.ir. Pieter Wesseling en ir. Guus Segal af bij de sectie Waterbouwkunde. Het afstudeeronderzoek, uitgevoerd bij het Waterloopkundig Laboratorium in de Voorst, getiteld 'The influence of breaking waves on the vertical velocity distribution in the surf zone' markeerde het begin van zijn fascinatie met zandbanken in de brandingszone welke tot op de dag van vandaag voortduurt en (uiteindelijk) heeft geresulteerd in het voorliggende proefschrift.

Na een kort tijdelijk dienstverband bij het Waterloopkundig Laboratorium aansluitend op zijn afstudeeronderzoek is hij van januari 1995 tot juni 1996 werkzaam geweest bij CSIR in Stellenbosch, Zuid Afrika. Sinds juni 1996 heeft hij een aanstelling als kust-morfoloog bij het Waterloopkundig Laboratorium wat in 2008 is opgegaan in het onderzoeksinstituut Deltares. Vanaf augustus 2005 heeft hij een deeltijdaanstelling als Toegevoegd Onderzoeker bij de sectie Waterbouwkunde van de Faculteit Civiele Techniek en Geowetenschappen aan de Technische Universiteit Delft. Hij is gastdocent bij de Universiteit Utrecht (vanaf 2004) en Universiteit Twente (vanaf 2008). Sinds mei 2014 is hij hoofd van de afdeling 'Applied Morphodynamics', onderdeel van de unit 'Zee en Kust Systemen' bij Deltares.

Peer reviewed articles:

33. Benedet, L., Dobrochinski, J.P.F., **Walstra, D.J.R.**, Klein, A.H.F., Ranasinghe, R., 2016. A morphological modeling study to compare different methods of wave climate schematization and evaluate strategies to reduce erosion losses from a

beach nourishment project. Coastal Engineering, 112, pp 69–86. doi:10.1016/j.coastaleng.2016.02.005

32. **Walstra, D.J.R.**, Wesselman, D.A., van der Deijl, E.C., Ruessink, B.G., 2016. On the intersite variability in inter-annual nearshore sandbar cycles. *Journal of Marine Science and Engineering*, 4(1), 15. doi:10.3390/jmse4010015.
31. Duong, T.M., Ranasinghe, R., **Walstra, D.J.R.**, Roelvink, J.A., 2015. Assessing climate change impacts on the stability of small tidal inlet systems: Why and how? *Earth Science Reviews*. dx.doi.org/10.1016/j.earscirev.2015.12.001.
30. **Walstra, D.J.R.**, Ruessink, B.G., Reniers, A.J.H.M. and Ranasinghe, R., 2015. Process-based modeling of kilometer-scale alongshore sandbar variability. *Earth Surface Processes and Landforms*, 40, 995–1005. doi: 10.1002/esp.3676.
29. Monecke, K., Templeton, C.K., Finger, W., Houston, B., Luthi, S., McAdoo, B.G., Meilianda, E., Storms, J.E.A., **Walstra, D.J.R.**, Amna, R., Hood, N., Karmanocky, F.J., Nurjanah, Rusydy, I., Unggul, S., Sudrajat, U.S., 2015. Beach ridge patterns in West Aceh, Indonesia, and their response to large earthquakes along the northern Sunda trench. *Quaternary Science Reviews*, 113, 159–170. doi: 10.1016/j.quascirev.2014.10.014.
28. Li, L., **Walstra, D.J.R.**, Storms, J.E.A., 2015. The impact of wave-induced longshore transport on a delta-shoreface system. *Journal of Sedimentary Research*, 85, 6–20. doi: dx.doi.org/10.2110/jsr.2014.95.
27. **Walstra, D.J.R.**, Brière, C.D.E. and Vonhögen-Peeters, L.M., 2014. Evaluating the PEM passive beach drainage system in a 4-year field experiment at Egmond (The Netherlands). *Coastal Engineering*, 93, 1–14. doi: 10.1016/j.coastaleng.2014.07.002.
26. **Walstra, D.J.R.**, Hoekstra, R., Tonnon, P.K., Ruessink, B.G., 2013. Input reduction for long-term morphodynamic simulations in wave-dominated coastal settings. *Coastal Engineering*, 77, 57–70. doi: 10.1016/j.coastaleng.2013.02.001.
25. Van Rijn, L.C., Ribberink, J.S., van der Werf, J., **Walstra, D.J.R.,** 2013. Coastal sediment dynamics: recent advances and future research needs (vision paper). *Journal of Hydraulic Research*, 51, 5, 75–493. dx.doi.org/10.1080/00221686.2013.849297.
24. Hillen, M.M., Geleynse, N., Storms, J.E.A., **Walstra, D.J.R.**, Groenenberg, R.M., 2013. Morphodynamic modelling of wave reworking of an alluvial delta and application of results in the standard reservoir modelling workflow. In: *From Depositional Systems to Sedimentary Successions on the Norwegian Continental Margin*. IAS Special Publication 46, Wiley-Blackwell, ISBN: 978-1-118-92046-6.
23. **Walstra, D.J.R.**, Reniers, A.J.H.M., Ranasinghe, R., Roelvink, J.A., Ruessink, B.G., 2012. On bar growth and decay during inter-annual net offshore migration. *Coastal Engineering*, 60, 190–200. doi: 10.1016/j.coastaleng.2011.10.002.

22. Tung, T.T., van der Kreeke, J., Stive, M.J.F., **Walstra, D.J.R.**, 2012. Cross-sectional stability of tidal inlets: A comparison between numerical and empirical approaches. *Coastal Engineering*, 60, 21–29. doi: 10.1016/j.coastaleng.2011.08.005.
21. Geleynse, N., Storms, J.E.A., **Walstra, D.J.R.**, Jagers, H.R.A., Wang, Z.B., and Stive, M.J.F. 2011. Controls on river delta formation; insights from numerical modeling, *Earth and Planetary Science Letters*, 302, 217–226, doi: 10.1016/j.epsl.2010.12.013.
20. Dan, S., **Walstra, D.J.R.**, Stive, M.J.F., Panin, N., 2011. Processes controlling the development of a river mouth spit, *Marine Geology*, 280, 116–129. doi: 10.1016/j.margeo.2010.12.005.
19. Ranasinghe, R., Swinkels, C., Luijendijk, A., Roelvink, J.A., Bosboom, J., Stive, M.J.F., **Walstra, D.J.R.**, 2011. Morphodynamic upscaling with the MorFac approach: dependencies and sensitivities. *Coastal Engineering*, 58, 806–811. doi: 10.1016/j.coastaleng.2011.03.010.
18. van Rijn, L.C., Tonnon, P.K., **Walstra, D.J.R.**, 2011. Numerical modelling of erosion and accretion of plane sloping beaches at different scales, *Coastal Engineering*, 58, 637–655. doi: 10.1016/j.coastaleng.2011.01.009.
17. Geleynse, N., Storms, J.E.A., Stive, M.J.F., Jagers, H.R.A., **Walstra**, **D.J.R.**, 2010. Modeling of a mixed-load fluvio-deltaic system. *Geophysical Research Letters*, 37, L05402, doi: 10.1029/2009GL042000.
16. Idier, D., Hommes, S., Brière, C., Roos, P.C., **Walstra, D.J.R.**, Knaapen, M.A.F. and Hulscher, S.J.M.H., 2010. Review of morphodynamic models to study the impact of offshore aggregate extraction. *Journal of Coastal Research*, 51, 39–52. doi: 10.2112/SI51-004.1.
15. Dan, S., Stive, M.J.F., **Walstra, D.J.R.**, Panin, N., 2009. Wave climate, coastal sediment budget and shoreline changes for the Danube Delta. *Marine Geology*, 262, 39–49, doi: 10.1016/j.margeo.2009.03.003.
14. Ruggiero, P., **Walstra, D.J.R.**, Gelfenbaum, G., van Ormondt, M., 2009. Seasonal-scale nearshore morphological evolution: Field observations and numerical modeling. *Coastal Engineering*, 56, 1153–1172, doi: 10.1016/j.coastaleng.2009.08.003.
13. van Thiel de Vries, J.S.M., van Gent, M.R.A., **Walstra, D.J.R.**, Reniers, A.J.H.M., 2008. Analysis of dune erosion processes in large-scale flume experiments, *Coastal Engineering*, 55, 1028–1040. doi: 10.1016/j.coastaleng.2008.04.004.
12. Hartog, W.M., Benedet, L., **Walstra, D.J.R.**, Van Koningsveld, M., Stive, M.J.F., Finkl, C.W., 2008. Mechanisms that influence the performance of beach nourishment: a case study in Delray Beach, Florida, U.S.A. *Journal of Coastal Research*, 24, 1304–1319. doi: 10.2112/06-0749.1.

11. Ruessink, B.G., Kuriyama, Y., Reniers, A.J.H.M., Roelvink, J.A., **Walstra, D.J.R.**, 2007. Modeling cross-shore sandbar behavior on the time scale of weeks. *Journal of Geophysical Research*, 112, F03010. doi: 10.1029/2006JF000730.
10. Van Rijn, L.C., **Walstra, D.J.R.**, van Ormondt, M., 2007. Unified view of sediment transport by currents and waves. IV: Application of morphodynamic model. *Journal of Hydraulic Engineering-ASCE*, 133, 776–793. doi: 10.1061/(ASCE)0733-9429(2007)133:7(776).
9. Tonnon, P.K., van Rijn, L.C., **Walstra, D.J.R.**, 2006. The Modelling of sand ridges on the shoreface. *Coastal Engineering*, 54, 279–296. doi: 10.1016/j.coastaleng.2006.08.005.
8. Grunnet, N.M., Ruessink, B.G., **Walstra, D.J.R.**, 2005. The influence of tides, wind and waves on the redistribution of nourished sediment at Terschelling, The Netherlands. *Coastal Engineering*, 52, 617–631. doi: 10.1016/j.coastaleng.2005.04.001.
7. Van Duin, M.J.P., Wiersma, N.R., **Walstra, D.J.R.**, van Rijn, L.C., Stive, M.J.F., 2004. Nourishing the shoreface: observations and hindcasting of the Egmond case, The Netherlands. *Coastal Engineering*, 51, 813–837. doi: 10.1016/j.coastaleng.2004.07.011.
6. Grunnet, N.M., **Walstra, D.J.R.**, Ruessink, B.G., 2004. Process-based modelling of a shoreface nourishment. *Coastal Engineering*, 51, 581–607. doi: 10.1016/j.coastaleng.2004.07.016.
5. Sutherland, J., **Walstra, D.J.R.**, Chesher, T.J., van Rijn, L.C., Southgate, H.N., 2004. Evaluation of coastal area modelling systems at an estuary mouth. *Coastal Engineering*, 51, 119–142. doi: 10.1016/j.coastaleng.2003.12.003.
4. Christensen, E., **Walstra, D.J.R.,** Emarat, N., 2004. Reply to Discussion of "Vertical variation of the flow across the surf zone" [*Coastal Engineering*, 45, 169–198]. *Coastal Engineering*, 50, 165–166. doi: 10.1016/j.coastaleng.2003.09.003.
3. Van Rijn, L.C., **Walstra, D.J.R.,** Grasmeijer, B., Sutherland, J., Pan, S., Sierra, J.P., 2003. The predictability of cross-shore bed evolution of sandy beaches at the time scale of storms and seasons using process-based Profile models. *Coastal Engineering*, 47, 295–327. doi: 10.1016/S0378-3839(02)00120-5.
2. Ruessink, B.G., **Walstra, D.J.R.,** Southgate, H.N., 2003. Calibration and verification of a parametric wave model on barred beaches. *Coastal Engineering*, 48, 139–149. doi: 10.1016/S0378-3839(03)00023-1.
1. Christensen, E., **Walstra, D.J.R.,** Emarat, N., 2002. Vertical variation of the flow across the surf zone. *Coastal Engineering*, 45, 169–198. doi: 10.1016/S0378-3839(02)00033-9.

STELLINGEN

behorende bij het proefschrift

The Anatomy of Nearshore Sandbars - A systematic exposition of inter-annual sandbar dynamics

van

Dirk-Jan Walstra

Delft, 17 juni 2016

1. Kustlangse processen zijn essentieel voor het kustdwarse cyclisch bankgedrag.

2. Kustdwarse processen veroorzaken langsvariabiliteit in bankgedrag maar nemen deze niet weg.

3. Chronologie tikt door in bankgedrag.

4. De langjarige helling van het actieve profiel bepaalt de bankcyclus periode.

5. Verstandig kustbeheer houdt rekening met de stand van de bank.

6. De complexiteit van modellen staat op gespannen voet met inzicht in systeemgedrag.

7. Het achteraf succesvol valideren van een model volgens een vooraf vastgestelde methode is een bijzondere prestatie.

8. Een goede modelleur kiest het model bij de toepassing en niet de toepassing bij het model.

9. Kantoortuinen: grenzen open, luiken dicht!

10. Cultuurverandering vraagt voorbeeldig leiderschap.

Deze stellingen worden opponeerbaar en verdedigbaar geacht en zijn als zodanig goedgekeurd door de promotoren:
Prof.dr.ir. M.J.F. Stive en Prof.dr. B.G. Ruessink

PROPOSITIONS

Pertaining to the thesis

The Anatomy of Nearshore Sandbars - A systematic exposition of inter-annual sandbar dynamics

of

Dirk-Jan Walstra

Delft, 17 June 2016

1. Longshore processes are fundamental to cross-shore cyclic bar behavior.

2. Cross-shore processes generate, yet do not dissipate, longshore sandbar variability.

3. Sequencing of events and states over time holds implications for sandbar behavior.

4. The bar cycle period is determined by the time-averaged slope of the active profile

5. Responsible coastal management takes the state of the [sand]bank into account

6. There is an inherent tension between model complexity and system understanding.

7. Successful ex-post validation of a model using ex-ante prescribed methods is a noteworthy achievement

8. A good modeller matches the model to the application and not the application to the model.

9. Open offices: batten down the hatches!

10. Changing organisational culture requires exemplary management.

These propositions are regarded as opposable and defendable, and have been approved as such by the promotors:
Prof.dr.ir. M.J.F. Stive and Prof.dr. B.G. Ruessink